

©2010

Nicole M Iverson

ALL RIGHTS RESERVED

**MULTIFUNCTIONAL POLYMERS FOR INHIBITION OF OXIDIZED LIPOPROTEIN
ACCUMULATION AND INFLAMMATION IN MACROPHAGE CELLS**

By

NICOLE M IVERSON

A Dissertation submitted to the

Graduate School-New Brunswick

Rutgers, The State University of New Jersey

and

The Graduate School of Biomedical Sciences

University of Medicine and Dentistry of New Jersey

in partial fulfillment of the requirements

for the degree of

Doctor of Philosophy

Graduate Program in Biomedical Engineering

written under the direction of

Prabhas V. Moghe

and approved by:

New Brunswick, New Jersey

May 2010

ABSTRACT OF THE DISSERTATION

MULTIFUNCTIONAL POLYMERS FOR INHIBITION OF OXIDIZED LIPOPROTEIN ACCUMULATION AND INFLAMMATION IN MACROPHAGES

By **NICOLE M IVERSON**

Dissertation Director: Prabhas V Moghe

A major cause of cardiovascular disease is atherosclerosis, the progressive accumulation and modification of low density lipoproteins (LDL) within the vascular wall associated with a non-reversible inflammatory cascade. Current treatments attempt to inhibit systemic LDL levels, and thus can only secondarily de-escalate the progression of atherosclerosis. This thesis investigates the mechanisms of an alternative approach based on the use of amphiphilic polymers to directly inhibit highly oxidized LDL (hoxLDL) internalization by macrophage cells, thereby retarding foam cell formation and inflammatory cytokine secretion. First the architecture of the polymers is systematically investigated to elucidate the important design facets for hoxLDL uptake inhibition by THP-1 human macrophage cells in serum and serum free media. The optimal polymer structure is found to be comprised of one, rotationally restricted carboxylic acid conjugated to the hydrophobic end of each polymer chain. Through the

administration of carboxy-terminated amphiphilic polymers (AMs) the total concentration of hoxLDL within macrophage cells is lowered by 73% and when an encapsulated Liver-X Receptor (LXR) ligand is also delivered the hoxLDL accumulation is further lowered, decreased by 88%. The delivery of the AMs and drug encapsulated AMs *in vivo* shows a significant inhibition in cholesterol accumulation and macrophage recruitment in an injured carotid artery rat model. The AMs also inhibit inflammatory responses *in vitro*, significantly decreasing matrix metalloproteinase (57%) and cytokine secretion (TNF α 47% and IL-1 β 59%) compared to non-treated cells. Through the inhibition of hoxLDL internalization and inflammation progression these AMs show the potential to be a new and multi-faceted cardiovascular treatment modality.

TABLE OF CONTENTS

ABSTRACT OF THE DISSERTATION	ii
TABLE OF CONTENTS	iv
LIST OF FIGURES, SCHEMES AND TABLES.....	xi
Introduction	1
1.1 Cardiovascular Disease.....	1
1.2 Role of Cholesterol in Atherosclerosis Progression.....	1
1.3 Current Preventative Treatment Options.....	5
1.4 Surgical Treatment Options	6
1.5 Nanoscale Biomaterials for Treatment of Atherosclerosis	7
1.6 Intracellular Cholesterol Metabolism.....	11
Controllable Inhibition of Cellular Uptake of Oxidized Low Density Lipoproteins: .	14
2.1 Abstract.....	14
2.2 Introduction.....	16
2.3 Materials and Methods.....	17
2.3.1 <i>Synthetic Materials</i>	17
2.3.2 <i>Polymer Characterization Methods</i>	18
2.3.3 <i>Polymer Synthesis</i>	19
2.3.4 <i>Cell Culture</i>	25
2.3.5 <i>LDL Oxidation to hoxLDL</i>	26
2.3.6 <i>hoxLDL Internalization</i>	26
2.3.7 <i>Statistical Analysis</i>	27

2.4	Results and Discussion	27
2.4.1	<i>Synthesis and Characterization of AMs</i>	27
2.4.2	<i>AM Inhibition of hoxLDL Uptake.....</i>	28
2.4.3	<i>Amphiphilicity.....</i>	30
2.4.4	<i>Branching of the Hydrophobic Region.....</i>	31
2.4.5	<i>Length of the PEG Chain</i>	31
2.4.6	<i>Carboxylic Acid Location</i>	32
2.4.7	<i>Type of Anionic Charge</i>	33
2.4.8	<i>Number of Anionic Charges.....</i>	34
2.4.9	<i>Rotational Motion of the Anionic Group</i>	35
2.4.10	<i>PEG Architecture: Shorter Chain PEGs from a Branch Point.....</i>	36
2.5	Conclusions	37
2.6	Figures, Schemes, and Tables	39
2.7	Supplemental Material	50
	Anti-Atherogenic Polymers for Coordinated Rescue of Cholesterol Dynamics	53
3.1	Abstract.....	53
3.2	Introduction.....	55
3.3	Materials and Methods.....	57
3.3.1	<i>Cell Culture</i>	57
3.3.2	<i>LDL Oxidation</i>	58
3.3.3	<i>Polymer Synthesis</i>	58
3.3.4	<i>Polymer Attachment.....</i>	59

3.3.5	<i>Encapsulation of LXR Agonist</i>	60
3.3.6	<i>Cellular Internalization of LXR Agonist</i>	61
3.3.7	<i>Biological Activity of LXRA Delivery: Gene Expression Studies</i>	61
3.3.8	<i>LDL Influx.....</i>	62
3.3.9	<i>Rescue of Cholesterol Pre-loaded Cells</i>	62
3.3.10	<i>In vivo Studies of Efficacy of LXRA and AAP</i>	63
3.3.11	<i>Statistical Analysis</i>	64
3.4	Results.....	64
3.4.1	<i>Polymers Bind Preferentially to Activated Macrophage Cells</i>	64
3.4.2	<i>Drug Agonist Encapsulation by Polymer Carriers</i>	65
3.4.3	<i>Polymer Vehicles Enhance Cellular Uptake of Drug Agonist via SR-A ..</i>	65
3.4.4	<i>Expression of Key Atherosclerotic Genes is Altered by LXRA Delivery ..</i>	66
3.4.5	<i>Oxidized LDL Accumulation in Activated Macrophages is Prevented by LXRA Delivery</i>	67
3.4.6	<i>Total Cholesterol Content in OxLDL Pre-loaded Macrophages is Reduced through LXRA Delivery</i>	67
3.4.7	<i>Total Cholesterol Content in Injured Rat Carotid Artery Model is Reduced through LXRA Delivery</i>	68
3.4.8	<i>Macrophage Recruitment in Injured Rat Carotid Artery Model is Reduced through LXRA Delivery</i>	69
3.5	Discussion	69
3.6	Figures.....	74

3.7	Supplemental Material	80
3.7.1	<i>Supplemental Methods</i>	80
3.7.2	<i>Supplemental Results</i>	81
3.7.3	<i>Supplemental Figures</i>	83
	Role of Amphiphilic Macromolecules in the Inhibition	88
4.1	Abstract.....	88
4.2	Introduction.....	89
4.3	Materials and Methods.....	90
4.3.1	<i>Polymer Synthesis and Characterization</i>	90
4.3.2	<i>Cell Culture</i>	92
4.3.3	<i>LDL Oxidation to hoxLDL</i>	93
4.3.4	<i>TNFα Cytokine Secretion</i>	93
4.3.5	<i>IL-1β Cytokine Secretion</i>	93
4.3.6	<i>Matrix Metalloproteinase Secretion</i>	94
4.3.7	<i>Gene Expression</i>	94
4.3.8	<i>Statistical Analysis</i>	95
4.4	Results.....	95
4.4.1	<i>TNFα Cytokine Secretion</i>	95
4.4.2	<i>IL-1β Cytokine Secretion</i>	95
4.4.3	<i>Matrix Metalloproteinase Secretion</i>	96
4.4.4	<i>Gene Expression</i>	96
4.5	Discussion	96

4.6	Future Work	99
4.7	Figures.....	100
	Conclusions and Future Directions	104
5.1	Conclusions	104
5.2	Future Directions	105
5.2.1	<i>Polymer Mechanism of Action</i>	105
5.2.2	<i>Polymer and Drug Delivery</i>	106
5.2.3	<i>Polymer Treatment of Multiple Disease Models</i>	107
	Appendix	109
	Nanoscale Amphiphilic Macromolecules as Lipoprotein Inhibitors	110
A.1	Abstract.....	110
A.2	Introduction.....	112
A.3	Methods	114
A.3.1	<i>Chemical reagents for synthesis</i>	114
A.3.2	<i>Macromolecules 1CM, oCM and 1CP</i>	115
A.3.3	<i>Chemical characterization</i>	115
A.3.4	<i>Synthesis of 1CM1CP</i>	116
A.3.5	<i>Synthesis of 1BM</i>	117
A.3.6	<i>Synthesis of 2CM</i>	118
A.3.7	<i>Synthesis of oBM</i>	119
A.3.8	<i>Dynamic light scattering study</i>	120
A.3.9	<i>Fluorescence spectroscopy</i>	120

A.3.10	<i>Zeta potential</i>	121
A.3.11	<i>Preparation of micelles for in vitro testing</i>	121
A.3.12	<i>Lipoprotein model: LDL oxidation</i>	121
A.3.13	<i>LDL internalization</i>	122
A.3.14	<i>Cell culture</i>	122
A.4	Results.....	123
A.4.1	<i>Synthesis of the macromolecules</i>	123
A.4.2	<i>Physical properties of the AScMs</i>	124
A.4.3	<i>Highly-oxidized LDL uptake inhibition studies</i>	124
A.5	Discussion	125
A.5.1	<i>Synthesis and solution-based properties</i>	125
A.5.2	<i>Inhibition of hoxLDL uptake by amphiphilic nanoparticles</i>	126
A.6	Conclusion.....	128
A.7	Tables and Figures.....	129
Convergence of Nanotechnology and Cardiovascular Medicine		134
B.1	Abstract.....	134
B.2	Introduction.....	135
B.3	Nanotechnology as an analytical platform	136
B.3.1	<i>Atomic Force Microscopy (AFM)</i>	137
B.3.2	<i>Near-Field Scanning Optical Microscopy (NSOM)</i>	138
B.3.3	<i>Resonance Energy Transfer (FRET and BRET)</i>	138
B.4	Nanotechnology as a diagnostic modality.....	139

B.4.1	<i>Imaging/detection using nanotechnology</i>	139
B.4.2	<i>Biosensors</i>	141
B.4.3	<i>DNA sequencing</i>	142
B.5	Nanotechnology as a therapeutic modality	143
B.5.1	<i>Established cardiovascular therapies enabled via nanotechnology</i>	144
B.5.1.1	<i>Carbon Nanotubes</i>	144
B.5.1.2	<i>Cardiovascular Stents</i>	144
B.5.1.3	<i>Drug delivery</i>	146
B.5.2	<i>Novel nano technologies as potential therapies</i>	146
B.5.2.1	<i>Sonothrombolysis</i>	147
B.5.2.2	<i>Nanolipoblockers (NLBs)</i>	148
B.6	Conclusion	150
B.7	Figures	151
	References	157
	CURRICULUM VITA	176

LIST OF FIGURES, SCHEMES AND TABLES

CHAPTER 1	1
Figure 1.1:.....	4
Figure 1.2:	10
Figure 1.3:.....	11
Figure 1.4:	13
CHAPTER 2	14
Scheme 2.1:.....	39
Table 2.1:.....	41
Figure 2.1:	42
Figure 2.2:	44
Figure 2.3:	45
Figure 2.4:	46
Figure 2.5:	47
Figure 2.6:	48
Figure 2.7:	49
Table 2.2:	52
Chapter 3	53
Figure 3.1.....	74
Figure 3.2	76
Figure 3.3.....	77
Figure 3.4	78

Figure 3.5	83
Figure 3.6	84
Figure 3.7.....	85
Figure 3.8	86
Chapter 4	88
Figure 4.1	100
Figure 4.2	101
Figure 4.3	102
Figure 4.4	103
Chapter 5	104
Appendix A	110
Table A.1:	129
Figure A.1:	130
Figure A.2:.....	131
Figure A.3:	132
Figure A.4:.....	133
Appendix B	134
Figure B.1:	151
Figure B.2:	153
Figure B.3:	155
Figure B.4:	156

CHAPTER 1

Introduction

1.1 Cardiovascular Disease

Seventy-five percent of deaths caused by cardiovascular disease, the leading cause of death in America and the rest of the developed world, are caused by atherosclerosis. (1, 2) The onset of atherosclerosis causes anatomical and physiological changes in arteries, vessel hardening due to elasticity loss and luminal narrowing from plaque formation, significantly impeding vessel function. The major cause for atherosclerosis is the accumulation of cholesterol, in the form of low density lipoproteins (LDL), within arterial walls. (3) For example, in men, an increase of total cholesterol from 200 to 240 mg DL⁻¹ correlates with a three-fold increase in cardiac mortality. (4) Due to the established link between circulating cholesterol profiles and cardiac health, the main focus of cardiac disease prevention involves lowering cholesterol, and specifically LDL cholesterol, concentrations. (5)

1.2 Role of Cholesterol in Atherosclerosis Progression

Cholesterol, necessary for maintaining cell viability and function, is accumulated in two major ways; synthesis in the endoplasmic reticulum and endocytosis of cholesterol containing ligands. (6) Early atherosclerotic studies determined that cholesterol entering the vessel wall, not synthesis inside the vessel, is responsible for

plaque formation; hence low density lipoprotein (LDL), the major cholesterol carrier in the blood stream, is frequently the focus of anti-atherosclerotic treatments. (7-9)

Excessive cholesterol accumulation leads to macrophage foam cell formation, an integral step in forming atherosclerotic plaques. This process is not triggered by native LDL internalization, which has a feedback control mechanism, but instead by non-regulated, scavenger receptor-mediated uptake of highly oxidized LDL (hoxLDL).

(9) Oxidation of LDL occurs through both direct matrix association and hydrolytic and proteolytic enzymatic modifications, both of which extend intimal residency; this paradigm is known as the 'response-to-retention hypothesis'. (10) Intimal retention of LDL is governed by proteoglycan (PG) matrix binding to LDL, mediated primarily by charge-charge interactions of the negatively charged sulfate and carboxyl groups of the glycosaminoglycan (GAG) disaccharides with positively charged LDL regions, rich in arginine and lysine residues. (11) Notably, areas of atherosclerotic lesions exhibit PGs with longer GAG chains, suggesting that GAG chain length, and thus, the negative charge density, can be a determinant of atherogenic dynamics (12). The positive charge of native LDL is lowered through oxidation, thus lowering the affinity of LDL for proteoglycans. (13) Recent studies show that the oxidized LDL molecules released from PG's can be retained by other extracellular matrix components (14) and lipoprotein lipase, (15) contributing to prolonged accumulation of oxidized LDL within the intima. (16) The extended intimal exposure to reactive oxygen species magnifies the slow alteration of LDL components; cholesteryl esters, phospholipids, triglycerides, and apoB-100; leading to extensive particle modifications and native LDL receptor

incompatibility, resulting in scavenger receptor binding and uptake. (17, 18) Excessive scavenger receptor internalization of oxLDL is believed to be integral to foam cell formation and alterations in lipid metabolism, gene expression, cell migration and motility, and local immune response. (19)

Two major atherosclerotic related inflammation responses are cytokine expression, specifically tissue necrosis factor alpha (TNF α) and interleukin 1 beta (IL-1 β), and matrix metalloproteinase (MMP) activation. Macrophage activation leads to increased secretion of cytokines TNF α and IL-1 β (20), which have a significant impact on the escalation of atherosclerosis. (21-23) Matrix metalloproteinases affect the degradation of extracellular matrix and non-matrix components and are typically only active during growth and remodeling. (24-27) Macrophage foam cells and atherosclerotic lesion development have been linked to the expression of MMPs that are not ordinarily expressed in healthy vessels, therefore it is hypothesized that decreasing activated macrophage cells in and around an atherosclerotic lesion will lower MMP expression, and thus ameliorate the formation of thrombi and aneurysms. (28-33)

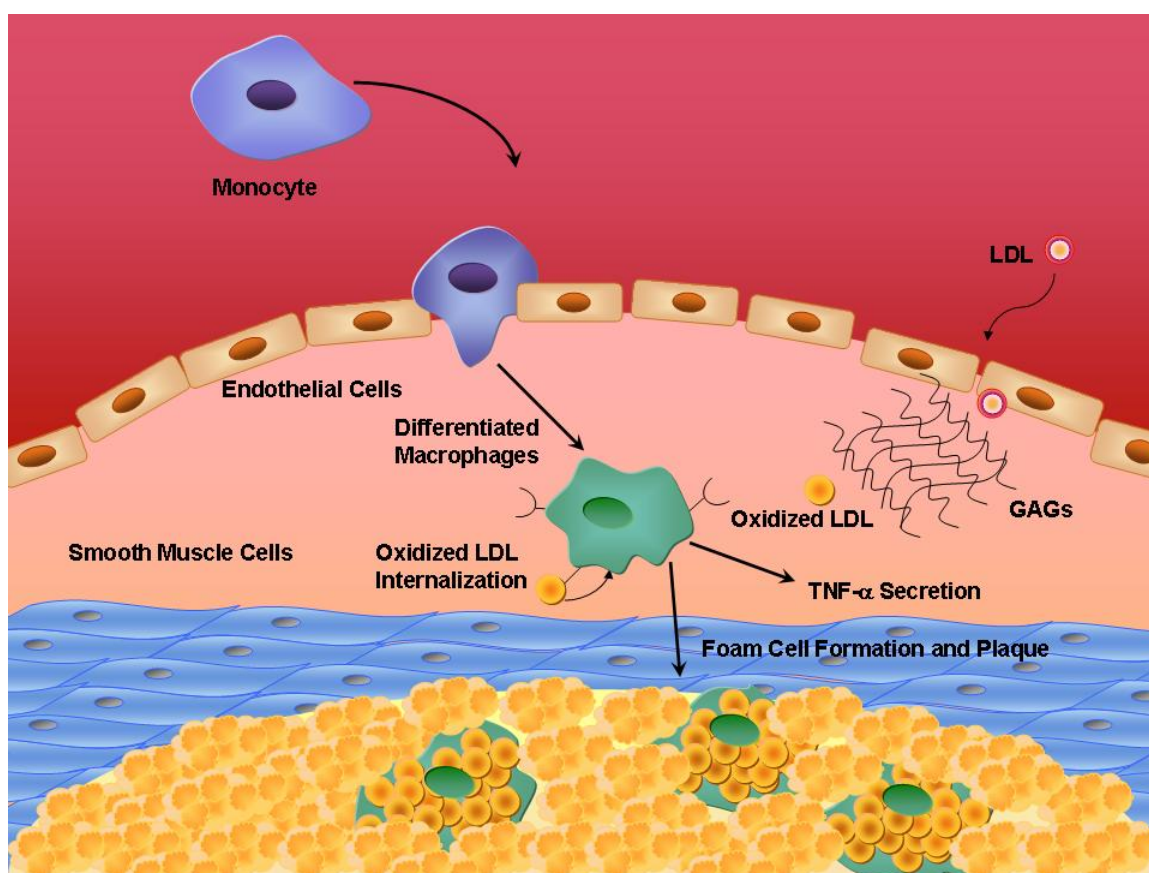


Figure 1.1:

Schematic of the progression of atherosclerosis within the blood vessel wall. Briefly, circulating monocytes migrate into the intimal layer of the artery where they differentiate into macrophage cells. Simultaneously, systemic LDL crosses the vessel wall's endothelial layer and binds to glycosaminoglycans (GAGs). Through progressive modifications, LDL is oxidized and released from the GAGs. Macrophage cells internalize oxidized LDL through scavenger receptors until cells become foamy, establish the growth of plaques and secrete pro-inflammatory cytokines, specifically tissue necrosis factor alpha (TNF α).

1.3 Current Preventative Treatment Options

Current cholesterol management strategies primarily include drugs that aim to lower systemic levels of cholesterol in circulating blood and can be broken down into four classes; bile acid resins, statins, fibrates, and nicotinic acid. Small LDL alterations, ten to twenty percent, are possible with the removal of cholesterol containing bile acids from the intestines, accomplished through the administration of bile acid resins. Nicotinic acids are also able to lower LDL levels as well as triglycerides and increase HDL levels, but their administration must be closely monitored due to common side effects. Statins lower total LDL concentration twenty to sixty percent, more significantly than bile acid resins or nicotinic acids. Through interactions with HMG-CoA reductase, an enzyme that controls the body's rate of cholesterol production, statins inhibit cholesterol production and increase clearance through the liver. An additional benefit of statins is that they decrease triglycerides and increase HDL. The fourth class of cholesterol lowering drugs is fibrates, which lowers triglyceride production and increases HDL levels but does not alter LDL concentration and is therefore not commonly used for patients with heart disease. Despite the clinical success of these classes of drugs, all of these pharmacologic treatments can lead to adverse side effects, ranging from abnormal liver tests to myopathy, a muscle wasting disease. (34) For example, in 2001 a statin called cerivastatin was withdrawn from the market due to unusually high number of patients with rhabdomyolysis, a disease in

which skeletal muscles are rapidly broken down and potentially resulting in kidney failure. (34)

1.4 Surgical Treatment Options

When preventative pharmacologic therapies are not adequate surgery is the only major treatment option, which includes coronary artery bypass graft (CABG) or catheterization. CABG is a surgery in which a healthy vessel is removed from another part of the patient's body, or a synthetic alternative is used, and it is utilized to deliver a sufficient blood supply to the area of the heart that is under-oxygenated due to narrowing or complete blockage of the original coronary artery. (35) CABG is reported to lead to an increase in patient survival rate (36) and quality of life (37, 38) but there is also a risk of post-surgery reoccurrence and enhanced mortality rate. (39-46) Several risk factors, including high LDL levels, lead to increased atherosclerosis in vein grafts after CABG is performed, hence proactive lipid lowering drugs are an important form of secondary prevention. (47, 48)

Placement of a bypass graft involves an invasive surgery and long recovery times, in contrast to the generally non-invasive catheterization procedure in which the patient is not anesthetized and quickly recovers from the one small thigh incision. In a catheterization procedure there are two options, percutaneous transluminal coronary angioplasty or the vascular placement of a stent. In both of these options, a surgeon makes an incision in the patient's femoral artery and threads a catheter into the heart

where radio-opaque dye allows vessel visualization and treatment. Balloon angioplasty involves inflating a balloon located on the catheter to open the vessel and push the blockage against the vessel wall, consistently showing increased lumen diameter. (49) Despite the therapeutic success of angioplasty, a third of the patients that receive treatment will develop restenosis, a renarrowing of the vessel after surgery, typically within the first six months. (50, 51) Restenosis in balloon angioplasty patients occurs through different mechanisms, including recoil, arterial vessel remodeling and neointimal hyperplasia. (52, 53) Restenosis associated with coronary angioplasty recoil can be avoided by stent placement, a mechanical barrier against the vessel wall. (54) Stents reduce restenosis in comparison to balloon angioplasty but migration and proliferation of cells, typically smooth muscle cells, causes in-stent restenosis in ten to sixty percent of patients. Outcomes from interventions aimed at lowering circulating cholesterol levels are reported to correlate with a reduction of in-stent restenosis. (55-62)

1.5 Nanoscale Biomaterials for Treatment of Atherosclerosis

Nanoscale biomaterials are an emerging option for cardiovascular treatment, both as systemic “prodrugs” and intravascular biomedical devices. One area where biomaterials have had translational impact is stent coatings; specifically for controlled release of antiproliferation drugs to inhibit restenosis (63), chemoattractant gradients to direct cell migration (64) and nanotextured coatings for selective enhancement of

cell attachment and re-endothelialization and proliferation (65). Nanoparticles are also used for encapsulation and localized delivery of drugs and bioactive molecules (an important facet in drug delivery due to metabolism), excretion and non-related tissue toxicity issues that can arise with systemic drug delivery. (66) By encapsulating drugs in nanospheres (67), erodible self-assembled structures (68) or $\alpha_v\beta_3$ -integrin targeted paramagnetic nanoparticles, concurrently used for drug delivery and imaging, (69) specificity in drug release can be introduced.

Polymeric micelle drug delivery systems have been extensively studied due to their ability to entrap and deliver hydrophobic drugs similar to naturally occurring carriers, such as lipoproteins, which transport triglyceride fats and cholesterol esters in the body. (70) Nanoscale features of micelles enable carriers to circulate in the blood stream and cross the cell barrier to get into the vessel wall. Besides size, biocompatibility and critical micelle concentration are essential characteristics of drug delivery micelle design, collectively impacting cell toxicity, drug internalization and bioavailability. (71-76)

Biocompatibility is particularly important following the implantation of synthetic biomaterials within the blood stream. Thrombus formation, resulting from biomaterials, can lead to altered blood flow patterns, mechanical obstruction of valves, a decrease in gas exchange and arterial occlusion. (77) One of the widely used approaches to promote biocompatibility of materials is through the incorporation of poly(ethylene glycol) (PEG) (77) PEG can be highly hydrated due to H-bonds between water and the oxygen of the ethylene glycol repeat units (78). PEG provides biologically

significant advantage such as protein resistivity (79), lack of toxicity and immunogenicity, nonbiodegradability, low non-specific clearance or high circulation time, and excretion from living organisms (80). Particularly for amphiphilic polymers containing PEG, the hydrophobic blocks of non-PEG containing domains likely form a compact core structure within aqueous environments(81); while the hydrophilic blocks loosely swinging outside to form the shell. This is also responsible for micellar interfacial stabilization and interactions with plasma proteins and cell membranes (82).

Various micelle-enabled hydrophobic drug delivery methods have previously been utilized, including Cremophor EL (a non-surfactant polyoxyethylated castor oil) and Tween 80 (polysorbate 80). (83, 84) Unfortunately, these formulations are associated with serious, dose-limiting toxicities including biological activity, sensory neuropathy and leaching plasticizers from di(2-ethylhexyl)phthalate (standard intravenous tubing). (83, 85-87)

The Moghe-Uhrich laboratories at Rutgers University have proposed the design of amphiphilic macromolecules (AMs) that address four specific considerations: degree of amphiphilicity; biocompatibility and serum stability; biodegradability; and tissue targeting potential. (88)

The amphiphilic micelles are produced in two steps, the synthesis of mucic acid derivative and conjugation of hydrophilic PEG (Figure 1.2). (88) The branched hydrophobic core increases the micelle's ability to self-assemble and causes it to be very stable, with a low critical micelle concentration and *in vivo* disassociation rate. The AMs form 10-20nm diameter micelles that bind to and clear native LDL and mildly

oxidized LDL; additionally, they exhibit binding to cationic macrophage scavenger receptors and competitively inhibit hoxLDL uptake. (88-91) In addition to altering LDL dynamics, the amphiphilic nature of AMs makes them ideal for solubilizing hydrophobic drug molecules in aqueous environments and facilitating cell-targeted delivery. (88, 92)

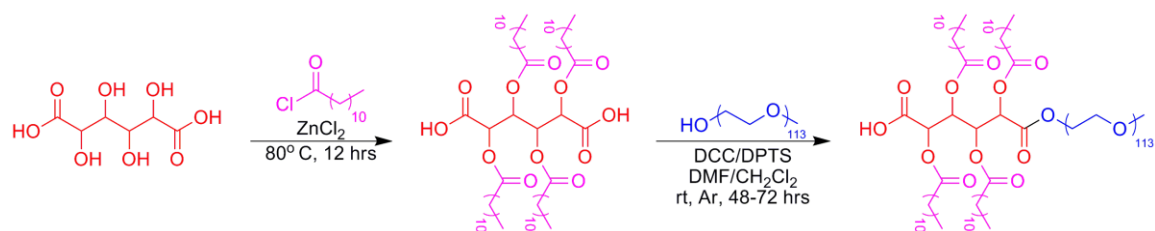


Figure 1.2:

Synthesis of carboxy-terminated AM by acylation of the hydroxyls of mucic acid with lauroyl chloride followed by esterification of one carboxylic acid with hydroxyl-terminated PEG

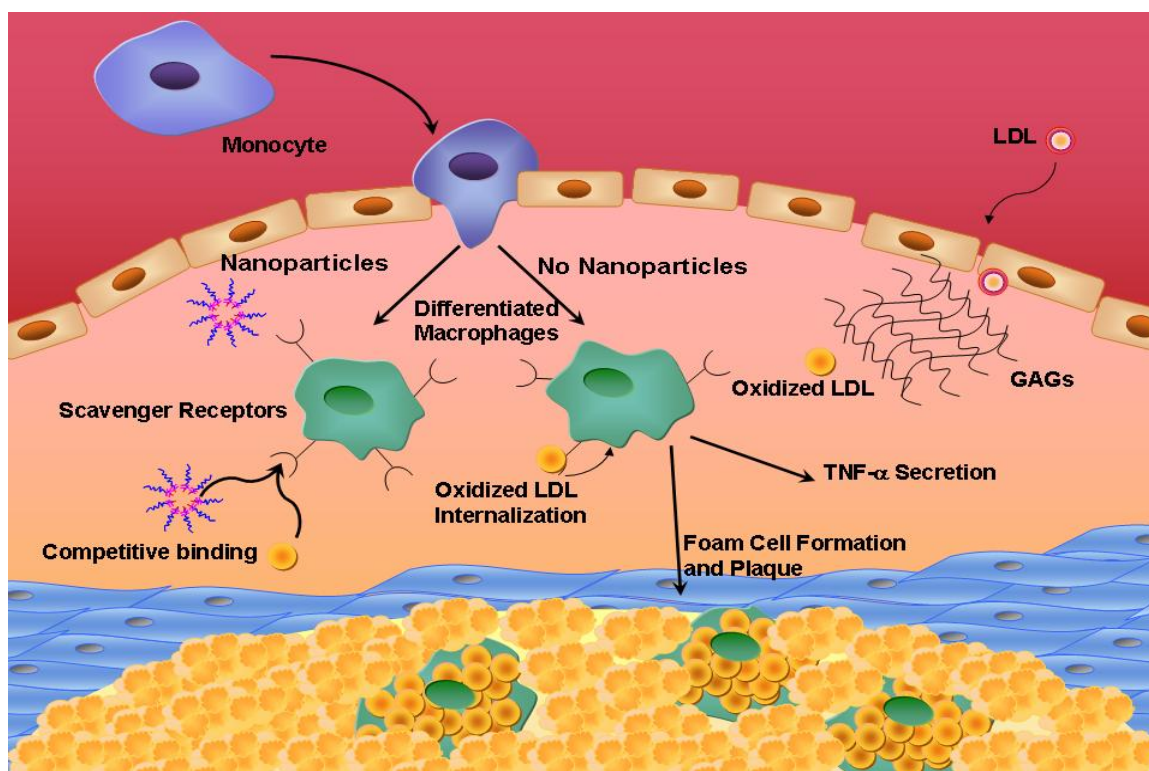


Figure 1.3:

Polymers inhibit hoxLDL uptake by human macrophage cell scavenger receptors through competitive inhibition, potentially halting the progression of cytokine secretion and foam cell and plaque formation.

1.6 Intracellular Cholesterol Metabolism

Cellular cholesterol metabolism is controlled by multiple pathways including enzymes, such as phospholipases, which metabolize phospholipids through acylhydrolases, lysophospholipases or phosphodiesterases, (93-95) and transcription factors(96), including AP-1(97, 98), NF-K B(97), PPAR(99) and LXR(100). Liver-X

Receptor belongs to a family of nuclear membrane proteins that become transcriptionally activated through ligand binding (101). A number of LXR target genes in macrophage cells have been linked to the regulation of reverse cholesterol transport, where excess cholesterol is transported from extra-hepatic tissues, such as arterial macrophage cells, to the liver via HDL particles (101). Treatment of HepG2 cells with small molecule LXR agonists GW3965, T0901317 and SB742881 have been shown to alter cholesterol synthesis, influx and efflux, causing an overall decrease of 36% to 39% cellular cholesterol after 96 hours. (102) *In vivo* findings are consistent with these *in vitro* results, murine models have shown that LXR is an important factor in determining inflammation and atherosclerosis in animals. (103, 104)

CHAPTER 2

Controllable Inhibition of Cellular Uptake of Oxidized Low Density Lipoproteins: Structure-Property Relationships for Nanoscale Amphiphilic Macromolecules

2.1 Abstract

A family of anionic nanoscale amphiphilic macromolecules (AMs) was developed for controlled inhibition of highly oxidized low density lipoprotein (hoxLDL) uptake by macrophages. The basic AM structure is composed of a hydrophobic portion formed from a mucic acid sugar backbone modified at the four hydroxyls with lauroyl groups and conjugated to hydrophilic poly(ethylene glycol) (PEG). The AM structure-activity relationships were probed by synthesizing AMs with six key variables: length of the PEG chain, carboxylic acid location, type of anionic charge, number of anionic charges, rotational motion of the anionic group, and PEG architecture. All AM structures were confirmed by nuclear magnetic resonance spectroscopy and their ability to inhibit hoxLDL uptake in THP-1 human macrophage cells was compared in the absence and presence of serum.

We report that AMs with one, rotationally restricted carboxylic acid within the hydrophobic portion of the polymer was sufficient to yield the most effective AM for inhibiting hoxLDL internalization by THP-1 human macrophage cells under serum-containing conditions. Further, increasing the number of charges and altering the PEG architecture in an effort to increase serum stabilization did not significantly impair the ability of AMs to inhibit hoxLDL internalization, suggesting that selected modifications

to the AMs could potentially promote multifunctional characteristics of these nanoscale macromolecules.

2.2 Introduction

Elevated levels of cellular and plasma cholesterol have serious consequences on the progression of cardiovascular disease, the leading cause of death in America. (105-107) The major carriers of cholesterol in blood plasma are low-density lipoproteins (LDLs), which enter the arterial walls through injured or leaky endothelial lining on the intima.(107, 108) Once LDL enters the intima, it can be oxidized, causing compositional alterations and compromising the ability of native LDL receptors on macrophage cells to recognize the particle. (109) Rapid uptake of highly oxidized LDL (hoxLDL) occurs through scavenger receptors on the macrophage cellular membrane, including scavenger receptor A (SRA), scavenger receptor B (SRB), CD36 and CD68. Scavenger receptors lack a feedback mechanism to control internalization, leading to excess cholesterol accumulation within the cytoplasm and triggering the development of foam cells and fatty streaks, a key characteristic of early atherogenesis. (19, 110-118)

We previously explored AMs for inhibiting hoxLDL uptake through competitive inhibition of scavenger receptors on murine macrophages. (89-91, 119, 120) These AMs are biocompatible polymers, (121) composed of poly(ethylene glycol), mucic acid and four aliphatic acid chains, that form nanoscale micelles with an extremely low critical micelle concentration (10^{-7}M) in aqueous media. (88)

Despite the early promise of the AMs, the structure-activity relations for controlled inhibition of uptake of cholesterol are lacking, particularly under physiological conditions. In this study, we synthesized AMs with systematic variations to identify the critical elements that contribute to the ability of AMs to inhibit hoxLDL

uptake by human THP-1 macrophage cells cultured *in vitro*, under serum-lacking and serum-containing conditions. Six key parameters were varied and the degree of hoxLDL uptake was quantitatively compared: length of the PEG chain, anionic charge location, type of anionic charge, number of anionic charges, rotational motion of the anionic group, and PEG architecture. We hypothesize that the most efficient polymer for hoxLDL inhibition will be: i) amphiphilic, increasing charge density at the scavenger receptors; ii) have the greatest amount of anionic charge possible within the hydrophobic portion, to increase scavenger receptor binding; and iii) have two, short-chain linear PEG chains conjugated to the hydrophobic backbone *via* a branch-point, to better shield the anionic charge and stabilize the nanoassemblies from disruption by serum proteins.

2.3 Materials and Methods

2.3.1 Synthetic Materials

Unless otherwise stated, solvents and reagents were purchased from Fisher Scientific (Pittsburgh, PA) and Sigma-Aldrich (St. Louis, MO) and used as received. PEG 5 kDa was purchased from Polysciences, Inc. (Warrington, PA) and dried by azeotropic distillation from toluene before use. Specialty, functionalized PEGs were purchased from Laysan Bio, Inc (Arab, AL) and used as received.

2.3.2 Polymer Characterization Methods

Polymer characterization was performed by Sarah Sparks in Kathryn Uhlich's laboratory at Rutgers University. Proton nuclear magnetic resonance (^1H -NMR) spectra of the products were obtained using a Varian 400 MHz or 500 MHz spectrophotometer. Samples were dissolved in chloroform- d , with a few drops of dimethyl sulfoxide- d_6 if necessary, with tetramethylsilane as an internal reference. Molecular weights (Mw) and polydispersity indices (PDI) were determined using gel permeation chromatography (GPC) with respect to polyethylene glycol standards (Sigma-Aldrich) on a Waters Stryagel® HR 3 THF column (7.8 x 300 mm). The Waters LC system (Milford, MA) was equipped with a 2414 refractive index detector, a 1515 isocratic HPLC pump, and 717plus autosampler. An IBM ThinkCentre computer with Waters Breeze Version 3.30 software installed was used for collection and processing of data. Samples were prepared at a concentration of 10 mg/mL in tetrahydrofuran, filtered using 0.45 μm pore size nylon or poly(tetrafluoroethylene) syringe filters (Fisher Scientific) and placed in sample vials to be injected into the system. Melting points were determined by DSC on a TA DSC Q200. TA Universal Analysis 2000 software was used for data collection on a Dell Dimension 3000 computer. Samples (3-5 mg) were heated under dry nitrogen gas. Data were collected at heating and cooling rates of 10 $^{\circ}\text{C}/\text{min}$ with a two-cycle minimum.

2.3.3 Polymer Synthesis

1cM

*Polymer synthesis was performed by Sarah Sparks in Kathryn Uhirsch's laboratory at Rutgers University as previously described. Briefly, mucic acid was acylated with lauroyl chloride in the presence of zinc chloride to obtain **1**, which was then esterified with hydroxy-poly (ethylene glycol) (5 kDa) with DCC as the dehydrating reagent and DPTS as the catalyst at room temperature for 48 hours under argon gas. DCU byproduct was removed by vacuum filtration and the filtrate washed with 0.1 N HCl and brine, dried over $MgSO_4$, and concentrated. The desired product was then precipitated from CH_2Cl_2 by addition of 10-fold diethyl ether and the solid collected by centrifugation. Solvent was removed by decanting and the resulting yellow solid was dried under ambient atmosphere (12 hrs) and under high vacuum (12 hrs). (88)*

1cM-2000

*Polymer synthesis was performed by Sarah Sparks in Kathryn Uhirsch's laboratory at Rutgers University as previously described. Briefly, mucic acid was acylated with lauroyl chloride in the presence of zinc chloride to obtain **1**, which was then esterified with hydroxy-poly (ethylene glycol) (2 kDa) with DCC as the dehydrating reagent and DPTS as the catalyst at room temperature for 48 hours under argon gas. DCU byproduct was removed by vacuum filtration and the filtrate washed with 0.1 N HCl and brine, dried over $MgSO_4$, and concentrated. The desired product was then precipitated from CH_2Cl_2 by*

addition of 10-fold diethyl ether and the solid collected by centrifugation. Solvent was removed by decanting and the resulting yellow solid was dried under ambient atmosphere (12 hrs) and under high vacuum (12 hrs). (88)

ocM

*Polymer synthesis was performed by Sarah Sparks in Kathryn Uhlich's laboratory at Rutgers University as previously described. Briefly, **1cM** was esterified with N-hydroxysuccinimide with DCC as the dehydrating reagent in anhydrous CH_2Cl_2 and DMF. The reaction was stirred for 24 hours at room temperature under argon gas before DCU byproduct was removed by vacuum filtration and the filtrate washed with 0.1 N HCl and 50:50 brine/ H_2O , dried over MgSO_4 , and concentrated. The desired product was then precipitated from CH_2Cl_2 by addition of 10-fold diethyl ether and the solid collected by centrifugation. Solvent was removed by decanting and the resulting yellow solid was dried under ambient atmosphere (12 hrs) and under high vacuum (12 hrs). (88)*

2cM

*Polymer synthesis was performed by Sarah Sparks in Kathryn Uhlich's laboratory at Rutgers University as previously described. Briefly, to **ocM** in CH_2Cl_2 , β -glutamic acid in the presence of triethylamine was added and the reaction stirred for 8 hours at room temperature. The reaction mixture was then washed with 0.1 N HCl and brine, dried over MgSO_4 , and concentrated. The desired product was then precipitated from CH_2Cl_2 by addition of 10-fold diethyl ether and the solid collected by centrifugation. Solvent was*

removed by decanting and the resulting yellow solid was dried under ambient atmosphere (12 hrs) and under high vacuum (12 hrs). (119)

1cP

Polymer synthesis was performed by Sarah Sparks in Kathryn Uhlich's laboratory at Rutgers University as previously described. Briefly, **1cM** was esterified with N-hydroxysuccinimide with DCC as the dehydrating reagent in anhydrous CH_2Cl_2 and DMF at room temperature overnight. This product was then coupled with a heterobifunctional PEG, $\text{H}_2\text{N-PEG-COOH}$ ($M_w = 5 \text{ kDa}$), in CH_2Cl_2 and triethylamine at room temperature overnight. The reaction mixture was then washed with 0.1 N HCl and brine, dried over MgSO_4 , and concentrated. The desired product was then precipitated from CH_2Cl_2 by addition of 10-fold diethyl ether and the solid collected by centrifugation. Solvent was removed by decanting and the resulting yellow solid was dried under ambient atmosphere (12 hrs) and under high vacuum (12 hrs). (91)

1cM-2000x2

Polymer synthesis was performed by Sarah Sparks in Kathryn Uhlich's laboratory at Rutgers University as previously described. Briefly, 5-aminoisophthalic acid was N-boc protected with di-tert-butyl dicarbonate (1eqv) in 1,4-dioxane by dissolving the 5-aminoisophthalic acid in 1N NaOH, cooling to 0 °C, and a solution of di-tert-butyl dicarbonate in 1,4-dioxane was added slowly over 1 hr. The solution was then allowed to warm to room temperature over 3 hrs, at which it stirred overnight. 2 was precipitated by

acidifying the solution to pH 5 with 1N HCl and subsequently removed by filtering. **2** was subsequently esterified with mono-hydroxy-poly (ethylene glycol) ($M_w = 2$ kDa) in the presence of DCC and DPTS in anhydrous CH_2Cl_2 and DMF at room temperature for 48 hours under argon gas. Following work-up and precipitation into diethyl ether, **3** was purified by flash chromatography (mobile phase Sephadex G, stationary phase H_2O). The N-boc group was then cleaved using trifluoroacetic acid at 0 °C for two hours. **1** was then added to **3** via amide coupling, using DCC as the dehydrating reagent and DPTS as the catalyst, in anhydrous CH_2Cl_2 and DMF for 24 hours. The DCU byproduct was then removed by vacuum filtration and the filtrate washed with 0.1 N HCl and 50:50 brine/ H_2O , dried over $MgSO_4$, and concentrated. The desired product was then precipitated from CH_2Cl_2 by addition of 10-fold diethyl ether and the solid collected by centrifugation. Solvent was removed by decanting and the resulting yellow solid was dried under ambient atmosphere (12 hrs) and under high vacuum (12 hrs). (122)

2cbM

Polymer synthesis was performed by Sarah Sparks in Kathryn Uhlich's laboratory at Rutgers University. The carboxylic acid of 1cM (0.56 g, 0.094 mmol) was activated with $SOCl_2$ (50 mL) at 90 °C overnight under argon gas. Excess $SOCl_2$ was removed via rotary evaporation and the yellow oil subsequently dissolved in anhydrous THF (15 mL) and anhydrous pyridine (1 mL). 5-Aminoisophthalic acid (0.14 g, 0.75 mmol) in anhydrous THF (16 mL) and anhydrous pyridine (2 mL) was then added to the reaction flask and allowed to react for 48 hours at room temperature under argon. THF and pyridine were removed

via rotary evaporation and the resulting oil dissolved in CH_2Cl_2 , washed with 1N HCl and brine, dried over MgSO_4 , and concentrated. The desired product was then precipitated from CH_2Cl_2 by addition of 10-fold diethyl ether and the solid collected by centrifugation. Solvent was removed by decanting and the resulting yellow solid was dried under ambient atmosphere (12 hrs) and under high vacuum (12 hrs). Yield: 0.52 g, 91 %. $^1\text{H-NMR}$ (CDCl_3): δ 8.61 (m, 1H, ArH), 8.17 (m, 2H, ArH), 5.70 (m, 2H, CH), 5.20 (m, 2H, CH), 4.24 (m, 2H, CH_2), 3.60 (m, ~ 0.45 kH, CH_2O), 3.38 (s, 3H, CH_3), 2.44 (m, 4H, CH_2), 2.29 (m, 4H, CH_2), 1.60 (m, 8H, CH_2), 1.26 (m, 6H, CH_2), 0.88 (t, 12H, CH_3). $T_m = 56^\circ\text{C}$ GPC: M_w : 6.3 kDa; PDI: 1.09.

15M

Polymer synthesis was performed by Sarah Sparks in Kathryn Uhlich's laboratory at Rutgers University. 2-Aminoethyl hydrogen sulfate (7.0 mg, 0.050 mmol) was dissolved in DMSO (2 mL) by warming over medium heat on a stir plate for 15-30 min. After cooling to room temperature, 0.5 M NaOH (101 μL) was added and the solution stirred for 30 min. In a separate flask, ocM (0.20 g, 0.033 mmol) was dissolved in CH_2Cl_2 (6.0 mL) and subsequently added to the solution of 2-aminoethyl hydrogen sulfate drop wise and the reaction stirred overnight (12 hrs). The CH_2Cl_2 was then removed via rotary evaporation then the DMSO removed via lyophilization. The resulting solid was dissolved in CH_2Cl_2 and the solution filtered to remove excess 2-aminoethyl hydrogen sulfate and the N-hydroxysuccinimide by-product. The desired product was precipitated from CH_2Cl_2 by addition of 10-fold diethyl ether and the solid collected by centrifugation. Solvent was

removed by decanting and the resulting yellow solid was dried under ambient atmosphere (12 hrs) and under high vacuum (12 hrs). Yield: 0.16 g, 78 %. $^1\text{H-NMR}$ (CDCl_3): δ 5.83 (m, 2H, CH), 5.48 (m, 2H, CH), 3.67 (m, ~ 0.45 kH, CH_2O), 3.38 (s, 3H, CH_3), 2.32 (m, 8H, CH_2), 1.60 (m, 8H, CH_2), 1.22 (m, 64H, CH_2), 0.88 (t, 12H, CH_3). $T_m = 55$ °C. GPC: M_w : 6.4 kDa; PDI: 1.08.

oCM-2000x2

Polymer synthesis was performed by Bahar Demirdirek in Kathryn Uhlich's laboratory at Rutgers University. 1cM-2000x2 (0.18 g, 0.035 mmol) was esterified with *N*-hydroxysuccinimide (0.040 g, 0.34 mmol) with DCC (1.0 mmol) as the dehydrating reagent in anhydrous CH_2Cl_2 (20 mL) and anhydrous DMF (10 mL). The reaction was stirred for 12 hrs at room temperature under argon gas before the DCU byproduct was removed by vacuum filtration. The filtrate was then washed with 0.1 N HCl and brine, dried over MgSO_4 , and concentrated. The desired product was then precipitated from CH_2Cl_2 by addition of 10-fold diethyl ether and the solid collected by centrifugation. Solvent was removed by decanting and the resulting yellow solid was dried under ambient atmosphere (12 hrs) and under high vacuum (12 hrs). Yield: 0.11 g, 67 %. $^1\text{H-NMR}$ (CDCl_3): δ 8.42 (s, 1H, ArH), 8.38 (s, 2H, ArH), 5.75 (d, 2H, CH), 5.51 (m, 1H, CH), 5.14 (d, 1H, CH), 4.43 (t, 4H, CH_2), 3.68 (m, ~ 0.36 kH, CH_2O), 2.81 (t, 4H, CH_2), 2.37 (m, 4H, CH_2), 2.25 (m, 4H, CH_2), 1.59 (m, 8H, CH_2), 1.24 (m, 64H, CH_2), 0.84 (t, 12H, CH_3). $T_m = 45$ °C. GPC: M_w : 4.9 kDa; PDI = 1.07.

2cbM-2000x2

Polymer synthesis was performed by Bahar Demirdirek in Kathryn Uhlich's laboratory at Rutgers University. The carboxylic acid of 1cM-2000x2 (0.18 g, 0.035 mmol) was activated with SOCl_2 (20 mL) at 70 °C for four hours under argon gas. Excess SOCl_2 was removed via rotary evaporation and product dried under high vacuum overnight. The product was then dissolved in CH_2Cl_2 (5 mL) and was added to a solution of 5-aminoisophthalic acid (0.06 g, 0.35 mmol) in anhydrous THF (10 mL) and anhydrous pyridine (2 mL) and stirred for 6 hours at room temperature. The THF and pyridine were then removed via rotary evaporation and the resulting oil dissolved in CH_2Cl_2 , washed with 0.1N HCl and brine, dried over MgSO_4 , and concentrated. The desired product was then precipitated from CH_2Cl_2 by addition of 10-fold diethyl ether and the solid collected by centrifugation. Solvent was removed by decanting and the resulting yellow solid was dried under ambient atmosphere (12 hrs) and under high vacuum (12 hrs). Yield: 0.12 g, 67 %.

$^1\text{H-NMR}$ (CDCl_3): δ 8.42 (s, 2H, ArH), 8.38 (s, 4H, ArH), 5.75 (d, 2H, CH), 5.51 (m, 1H, CH), 5.14 (d, 1H, CH), 4.43 (t, 4H, CH_2), 3.68 (m, \sim 0.36 kH, CH_2O), 2.37 (m, 4H, CH_2), 2.25 (m, 4H, CH_2), 1.59 (m, 8H, CH_2), 1.24 (m, 64H, CH_2), 0.84 (t, 12H, CH_3). $T_m = 50$ °C. GPC: M_w : 4.4 kDa; PDI = 1.05.

2.3.4 Cell Culture

Human THP-1 monocytes (ATCC), were grown in suspension, at a concentration of 100,000 cells/cm² with RPMI medium containing 0.4 mM Ca^{2+} and Mg^{2+} (ATCC) and supplemented with 10 % fetal bovine serum (FBS), in an incubator with 5% CO_2 at 37 °C

and split every four days through centrifugation. The cells were seeded at a concentration of 100,000 cells/cm² and differentiated from monocytes into adherent macrophage cells by the addition of 16 nM phorbol myristate acetate. (123) Once differentiated, the macrophage cells were not propagated and were used within one week of differentiation.

2.3.5 *LDL Oxidation to hoxLDL*

Highly oxidized LDL (hoxLDL) was prepared by oxidation of LDL within five days of each experiment. BODIPY-labeled human plasma derived LDL (Molecular Probes, OR) was oxidized by incubation with 10 μ M CuSO₄ (Sigma) for 18 hrs at 37 °C with 5% CO₂ before oxidation was stopped with the addition of 0.01% w/v EDTA (Sigma). (13, 14) Characterization of hoxLDL has been previously reported. (91)

2.3.6 *hoxLDL Internalization*

Internalization of hoxLDL by macrophage cells was assayed, either with or without 5% FBS, by incubating fluorescently labeled hoxLDL (10 μ g/mL) and the various polymer conditions, at 10⁻⁶ M, with cells for 24 or 48 hours at 37 °C and 5 % CO₂. Test conditions also included two controls: RPMI medium and polymers alone to ensure that no cell auto-fluorescence was observed. The cells were then washed twice with PBS and imaged for cell-associated fluorescence. Images were analyzed using Image Pro Plus 5.1 software (Media Cybernetics, San Diego, CA) and fluorescence was normalized to cell number before being compared to the sample with only hoxLDL, the

negative control run in every experiment. An SRA antibody (10 µg/mL; clone 351620; R&D Systems, Minneapolis, MN) was used as a positive control for the assay for 24 hours in serum free conditions.

2.3.7 Statistical Analysis

Error bars on graphs indicate standard error of the mean based upon biological triplicate samples in each experiment and three separate experiments for each condition. Single factor ANOVA with Tukey's post-hoc analysis, performed on SPSS software, was used for statistical analysis. Significance is claimed for differences of $p < 0.05$, full table of statistical significance can be found in supplementary materials.

2.4 Results and Discussion

2.4.1 Synthesis and Characterization of AMs

*Polymer synthesis and characterization was performed by Sarah Sparks in Kathryn Uhlich's laboratory at Rutgers University. A range of AMs were designed (see **Table 1**) based upon results from previous work (89-91, 119, 120, 122) and synthesized to determine the most effective inhibitor of hoxLDL uptake. Several AMs were previously synthesized for a variety of applications. (88-91, 119-122, 124-127) New AMs were synthesized from these previously published compounds as summarized in **Scheme 1**.*

*The parent compounds, **1cM** and **1cM-2000x2**, served as building blocks for subsequent modifications. Specifically, the carboxylic acid on the mucic acid backbone of*

1cM and **1cM-2000x2** was activated with *N*-hydroxysuccinimide or thionyl chloride to functionalize the polymers with a small linker molecule containing the desired functionality, such as a sulfate to yield **1sM** or di-carboxylic acid to yield **2cbM** and **2cbM-2000x2**. Polymer structure was verified by ^1H NMR and molecular weight determined by GPC relative to PEG standards. Due to the abundance of PEG in the polymers (~83 % of protons), it was often difficult to detect the presence of new protons in the ^1H NMR, particularly from 0.8 to 2.4 ppm where the methylene protons of the hydrophobic arms make up the majority of that region. Thus, spectra were monitored for the disappearance of the protons of the activating group (*N*-hydroxysuccinimide), 2.8 ppm, or the appearance of aromatic protons (**2cbM** and **2cbM-2000x2**), ~ 8.4 ppm.

In total, ten AMs were tested for their ability to inhibit hoxLDL uptake with and without serum. The characteristics tested were amphiphilicity, branching of the hydrophobic region, length of the PEG chain, anionic charge location, type of anionic charge, number of anionic groups, rotational motion of the charged group, and PEG architecture. Structures of all polymers, schematics representing the placement of anionic charge, and information regarding specific variable parameters are shown in **Table 1**. It was hypothesized that by altering each of these key parameters, the optimal AM structure for inhibiting hoxLDL uptake would be determined.

2.4.2 AM Inhibition of hoxLDL Uptake

The ability of the AMs to inhibit hoxLDL uptake was tested without serum, to remove the possible interactions between serum proteins and AMs, for 24 hours and

with serum for 24 and 48 hours, to allow for increased cell viability at longer time points. The combined results for hoxLDL uptake normalized to respective cell number across all polymer configurations synthesized are shown in **Figure 1**. Additionally, fluorescent images of BODIPY-labeled hoxLDL uptake for the two most efficient AMs (**1cM** and **2cbM-2000x2**) compared with hoxLDL uptake alone are shown in **Figure 7 (bottom)**. It should be noted that the highly efficient AMs perform comparably to positive control (SRA antibody blockage), with hoxLDL uptake inhibited by about 20% after 24 hours in serum free conditions. It can also be noted that the early serum free data appears to correlate well with the 48 h data in serum conditions. These trends suggest that it takes longer (more than 24 h) to reverse the serum protein-mediated competitive blockage of polymer-receptor binding via serum proteins. Thus, behaviors of polymer binding to macrophages at early times in serum free conditions, which may be primarily scavenger receptor mediated, manifest similarly to the behaviors seen at longer times in serum conditions. The multiple variables that alter hoxLDL internalization are systematically evaluated in following sections.

We note that the inhibitory results found were not due to polymer cytotoxicity as judged by cell morphology and cell counts for each polymer. We have previously reported using IC21 murine macrophage cultures that these polymers are highly biocompatible in vitro, even at two orders of magnitude higher concentrations than those used in the current study [17]. Recent reports show that these polymers are non-cytotoxic in human umbilical endothelial cells (HUVEC), umbilical arterial smooth muscle cells (UASM), and normal dermal human fibroblasts (NDHF). (121)

2.4.3 Amphiphilicity

To examine the role of the amphiphilicity, the efficiency of control polymers, **PEG** and **PEG-COOH**, to inhibit hoxLDL internalization was tested. **PEG** is a common hydrophilic polymer chosen for its biocompatibility and ability to evade excretion from the bloodstream by the reticuloendothelial system (RES). (128-130) The PEGs tested here were chosen because they have the same average molecular weight as the PEG of **1cM**. **PEG-COOH** was chosen due to the presence of the anionic charge, which has been found to be a key parameter for AM inhibition of hoxLDL uptake. (89-91, 119, 120) Additionally, in modeling studies, Plourde et. al. observed the binding energy of a **PEG-COOH** model when docked with an SR-A collagen-like domain homology model was favorable, but with two-times more energy than **1cM**. (120) Based on these modeling results, **PEG-COOH** was anticipated to inhibit hoxLDL better than **ocM**, but to a lower extent than **1cM**, while **PEG** was anticipated to behave like **ocM** or have no effect at all.

As shown in **Figure 2**, the amphiphilic polymers, **ocM** and **1cM**, consistently inhibited hoxLDL internalization to a greater extent than both anionically terminated and unfunctionalized hydrophilic **PEGs** under all conditions. Notably, **1cM** was the only polymer that showed significant inhibition of uptake at all conditions, whereas **ocM** showed modest levels of effect, suggesting that the combination of amphiphilicity and anionic charge presentation may be operative in early competitive studies. Additionally, as **PEG-COOH** had little effect with or without serum, this suggests that

the anionic group on the hydrophobic portion of the polymer may be more effective, which is discussed later.

2.4.4 *Branching of the Hydrophobic Region*

To examine the effect of the branched hydrophobic region of AMs, the well-known amphiphiles **Pluronic P85** and **Cremophor EL** were tested for their ability to effect internalization of hoxLDL. **Pluronic P85** and **Cremophor EL** were chosen based on their structural similarity to AMs with respect to their hydrophilic PEG regions. Additionally, like AMs, they are amphiphilic, biocompatible and widely studied for pharmaceutical applications. (86, 131-133)

As shown in **Figure 2**, compared with **Pluronic P85** and **Cremophor EL**, the AMs, specifically **1cM** and **ocM** shown here, competed far more effectively with hoxLDL uptake whereas **Pluronic P85** and **Cremophor EL** had little effect on hoxLDL uptake. These results highlight the importance of the branched architecture of the hydrophobic component of the AMs, which allows them to significantly reduce hoxLDL uptake.

2.4.5 *Length of the PEG Chain*

The ability of PEG to evade excretion by the RES system is generally attributed to PEG's ability to shield the system from disruption by serum proteins. (128-130) Based upon literature, a longer PEG chain length was anticipated to yield increased stability in serum caused by additional PEG density resulting in more chain entanglements, providing enhanced micelle stability and protection of the critical

anionic charge. (128-130) This expectation was confirmed in testing AMs with hydrophilic PEG molecular weights of 2 kDa (**1cM-2000**) and 5 kDa (**1cM**). As shown in **Figure 3**, at the 24 hour time point with and without serum, **1cM** and **1cM-2000** have comparable levels of hoxLDL inhibition. However, after 48 hours in the presence of serum, the longer PEG chain length was most effective at hoxLDL inhibition. This result confirms the hypothesis that increased PEG length results in increased chain entanglements and better micelle stability and protection of the anionic charge from serum protein disruption.

2.4.6 Carboxylic Acid Location

As previously stated, AM inhibition of hoxLDL uptake by macrophage cells occurs by competitive binding between AMs and hoxLDL for positively charged scavenger receptors. (90, 120) Thus, it is necessary for the anionic group of AMs to be readily available and easily bound in the receptor pocket. Therefore, it was initially anticipated that the anionic group on the hydrophilic, or external, portion of the micelle would be more readily available for binding to scavenger receptors and increased binding would lead to better inhibition of hoxLDL uptake. However, modeling studies and *in vitro* testing in the absence of serum demonstrated that the anionic charge in the hydrophobic region of the polymer was more effective at inhibiting hoxLDL uptake than having the anionic charge within the hydrophilic region. (90, 119, 120) These results were confirmed herein and, expanding on previous work, in the presence of serum both at 24 and 48 hours **1cM** performed significantly better than **1cP**, as shown

in **Figure 4**. This effect is likely due to the interaction of serum proteins with the carboxylic group, which is not shielded by PEG when it is positioned on the hydrophilic portion of the micelle. For serum and non-serum containing conditions it is postulated that the greater charge density that results from having the anionic charge within the hydrophobic interior when micellization occurs leads to greater hoxLDL inhibition. In addition, the hydrophobic core is conformationally rigid, such that the carboxylic acid has less freedom of rotation and a better ability to lock into the active site on scavenger receptors. (134)

2.4.7 *Type of Anionic Charge*

Like carboxylic acids, sulfates have also been shown to bind to scavenger receptors and thus inhibit hoxLDL uptake.(135) To investigate this possibility with the AM structure, a sulfate moiety (**1sM**) was incorporated into the hydrophobic portion of the polymer. In the absence of serum, both **1cM** and **1sM** inhibited hoxLDL uptake more than the non-acidic system (**ocM**), but **1cM** did so to a far greater extent than **1sM**, as shown in **Figure 5**. However, in serum-containing conditions, at 24 and 48 hours, **1sM** inhibited hoxLDL uptake on a similar level to **ocM**, significantly less than **1cM**. This result may be due to the decreased steric hindrance surrounding the sulfate, making it more readily available for interactions such as hydrogen bonding with other residues of the scavenger receptor. Additionally, the methylene spacer increases the rotational motion available to the **1sM**, which may result in inadequate binding to the

active receptor site. The role of decreased steric hindrance surrounding the anionic group and increased rotational motion will be discussed in later sections.

2.4.8 *Number of Anionic Charges*

The number of anionic charges was investigated by comparing **1cM**, **ocM**, and **2cbM**. It was hypothesized that increasing the number of charge groups would result in greater charge density which would result in more significant attraction of the AMs to the positively charged binding pocket on scavenger receptors and therefore greater hoxLDL uptake inhibition. Additionally, it was anticipated that the addition of a spacer molecule would reduce the steric hindrance surrounding the carboxylic acid and allow better access to the binding site, which would decrease hoxLDL uptake. However, as shown in **Figure 6**, the addition of an additional carboxylic acid with an aromatic spacer, **2cbM**, shows hoxLDL uptake inhibition comparable to that of **1cM** for all time points.

We postulate that this result is due to the ability of only one carboxylic acid to bind to scavenger receptors at a time. Thus, the addition of more carboxylic acids does not provide any additional benefit. In fact, in modeling studies by Plourde et al. additional carboxylic acids actually lowered the overall AM binding affinity to a scavenger receptor model due to hydrogen bonding of the carboxylic acids with residues in the binding pocket that inhibited binding of the AM to the active site. (120) This result suggests that the carboxylic acids are too readily available and accessible for the first interaction they encounter, which is hydrogen bonding rather than binding in

the active site. Further, this data indicates that despite the steric hindrance surrounding the carboxylic acid of **1cM**, the carboxylic acid is available for binding and that adding a spacer molecule to increase availability may potentially hinder binding.

2.4.9 *Rotational Motion of the Anionic Group*

To analyze the effect of the rotational motion of the carboxylic acid charge, the aromatic dicarboxylic acid-containing **2cbM** was compared with the aliphatic dicarboxylic acid-containing **2cM**, which would allow the carboxylic acids more freedom for rotation and movement. We anticipated that changing the rotational motion would have a significant impact on scavenger receptor ability to bind the carboxylic acid. As **2cM** has aliphatic carboxylic acids, the rotational motion is less restricted than the aromatic carboxylic acids of **2cbM**. As shown in **Figure 6**, the aromatic carboxylic acids on **2bcM** result in significantly greater hoxLDL uptake inhibition than **2cM** for all time points with and without serum. Also, **2cM** behaves like **1cP** with respect to the extended time point in serum, both of which did not result in lower percent hoxLDL per cell than the 24 hour time point in serum. Although the carboxylic acids are in different regions of the polymer, in both **1cP** and **2cM** the carboxylic acids have significantly more rotational motion as aliphatic components. These results indicate that restriction of rotational motion of the anionic group is essential for the carboxylic acid to effectively bind to the active site on scavenger receptors. Additionally, this result also suggests that the steric hindrance surrounding the carboxylic acid of **1cM** restrict the

rotational motion of the carboxylic acid such that the carboxylic acid is better capable of binding to the active site.

2.4.10 PEG Architecture: Shorter Chain PEGs from a Branch Point

Finally, it was hypothesized that utilizing a structural branching point to which two, short-chained PEGs were attached would provide increased stabilization against serum proteins in the blood stream. (122, 136) To maintain overall PEG content, each PEG arm was synthesized to be 2 kDa, compared to the linear AMs with PEG 5 kDa. AMs with zero, one, and two carboxylic acids in the hydrophobic core were synthesized with this architectural branching point and tested for their ability to inhibit hoxLDL uptake. As shown in **Figure 7**, all AMs with the PEG branching point inhibited hoxLDL more significantly than their linear counterparts without serum. In the absence of serum, **2cbM-2000x2** results in the lowest percent of hoxLDL per cell overall, edging out **1cM** which typically outperforms all other polymers. In serum-containing conditions for both 24 and 48 hours, the AMs with a PEG branching point inhibited hoxLDL at similar levels to their linear counterparts except for the **2cbM-2000x2** and **2cbM** polymers. At 48 hours, the **2cbM-2000x2** significantly inhibited hoxLDL internalization more than **2cbM**. However, while **2cbM-2000x2** outperforms its linear counterpart, inhibition of hoxLDL uptake is statistically the same as **1cM**.

Generally, utilizing two, short-chain PEGs emanating from a branch-point resulted in more efficient hoxLDL inhibition compared to their linear counterparts under serum-free conditions. However, providing a PEG branching point did not

significantly alter the polymer's hoxLDL inhibitory capabilities compared with the linear polymers in serum-containing conditions. While a PEG branching point likely increases shielding of the micelle hydrophobic core, it is proposed that the linear PEG 5 kDa results in significant chain entanglements, as seen with the **1cM-2000** and **1cM** polymers, such that utilizing a branching point with lower molecular weight PEGs did not significantly increase the barrier against serum proteins, and therefore did not significantly alter the hoxLDL inhibition.

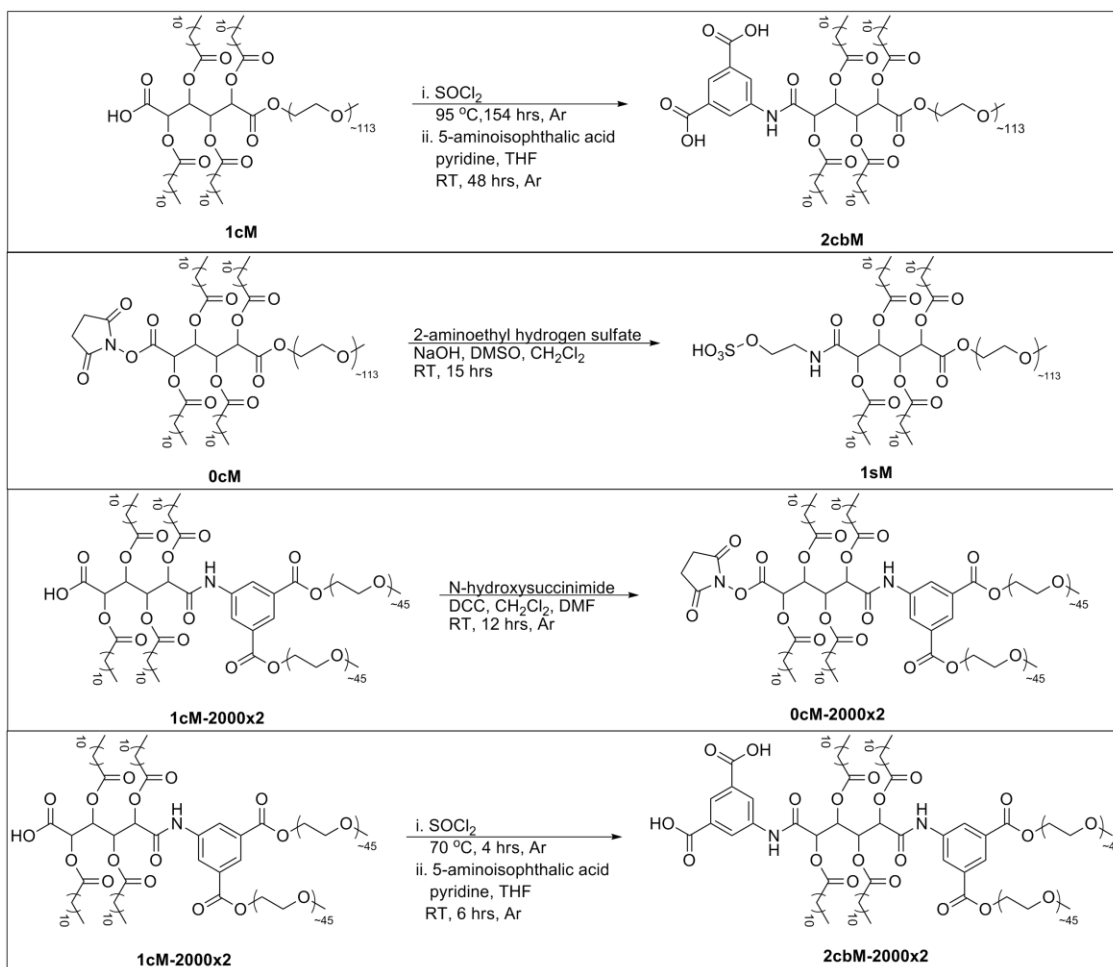
2.5 Conclusions

Overall, we report that AMs exhibit a rich structure-function relationship range for inhibition of hoxLDL uptake in macrophages. Within the AM architecture, longer PEG chains were more efficient at protecting AMs in serum-containing conditions. One rotationally-restricted carboxylic acid within the hydrophobic core was sufficient for producing the most effective hoxLDL inhibiting AM. By increasing charge and changing the PEG architecture to two, short-chain, linear PEGs emanating from a branch point, no significant improvements were found with respect to decreasing hoxLDL uptake. These findings could have implications for the design of polymers for improved competitive inhibition of intimal cholesterol uptake under physiological as well as pathologic conditions, assisting or replacing current systemic approaches that may elicit unwanted side effects. (137, 138)

In summary, the tunability of the parent AMs enables structure optimization to fit specific applications. In this work, the goal was to inhibit hoxLDL uptake for the

treatment of cardiovascular disease. To optimize the AM properties, several structural characteristics were analyzed: length of the PEG chain, carboxylic acid location, type of anionic charge, number of anionic charges, rotational motion of the anionic group, and PEG architecture. Each AM was tested without serum and in the presence of serum for 24 and 48 hours to determine its ability to inhibit hoxLDL uptake in THP-1 human macrophage cells. The parent AM **1cM**, with its rigid, hydrophobic carboxylic acid and linear PEG chain of 5 kDa was the most efficient at inhibiting hoxLDL internalization by THP-1 human macrophage cells in the presence of serum. While altering the PEG architecture, **1cM-2000x2** and **2cbM-2000x2**, produced AMs equally as efficient in their inhibition of hoxLDL uptake, **1cM** is far superior when considering cost and production time. Future work will delve deeper into the mechanism of action that causes the hoxLDL inhibition and the ability of this AM for use as a treatment for atherosclerosis.

2.6 Figures, Schemes, and Tables



Scheme 2.1:

Synthetic scheme for newly synthesized polymers 2cbM, 1sM, 0cM-2000x2, and 2cbM-2000x2

Polymer Name	Final Structure	Schematic	PEG Length	Charge Location	Charge Number	Type of Charge	PEG Architecture
1cM			Long	Hydrophobic	1	Carboxylic Acid	1 Linear
1cM-2000			Short	Hydrophobic	1	Carboxylic Acid	1 Linear
ocM			Long	None	0	None	1 Linear
1cP			Long	Hydrophilic	1	Carboxylic Acid	1 Linear
1sM			Long	Hydrophobic	1	Sulfate	1 Linear
2cM			Long	Hydrophobic	2	Carboxylic Acid	1 Linear
2cbM			Long	Hydrophobic	2	Carboxylic Acid	1 Linear
1cM-2000x2			Short x2	Hydrophobic	1	Carboxylic Acid	2 Linear from a branch point
ocM-2000x2			Short x2	None	0	None	2 Linear from a branch point

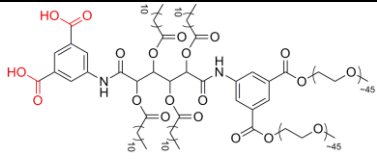
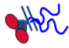
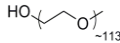

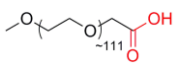

2cbM- 2000x2			Short x2	Hydrophobic	2	Carboxylic Acid	2 Linear from a branch point
PEG		 Non- amphiphilic	Long	None	0	None	1 Linear
PEG- COOH		 Non- amphiphilic	Long	Hydrophilic	1	Carboxylic Acid	1 Linear

Table 2.1:

Chemical structures, schematics representing the placement of anionic charge, and information regarding PEG length, charge location, number of charges, type of anionic charge, and PEG architecture for all AMs.

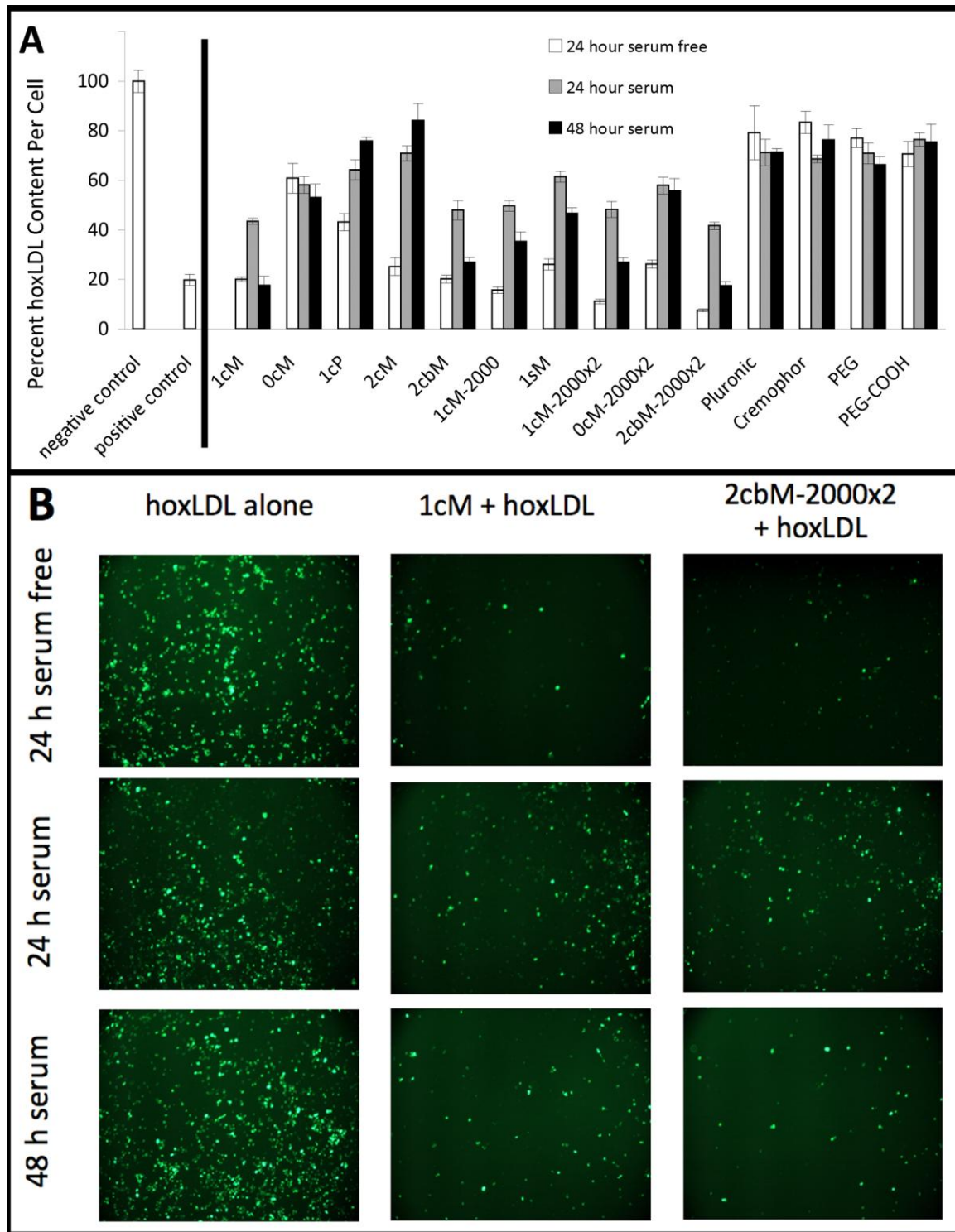


Figure 2.1:

Internalization of hoxLDL by THP-1 macrophage cells after incubation with 10^{-6} M AMs for 24 or 48 hours, in the presence or absence of 5% FBS; (Top)

Comparison of all polymers tested, (Bottom) Fluorescent images of BODIPY-labeled hoxLDL uptake for hoxLDL alone (negative control), hoxLDL with **1cM**, and hoxLDL with **2cbM-2000x2** (the two most efficient polymers at inhibiting hoxLDL uptake).

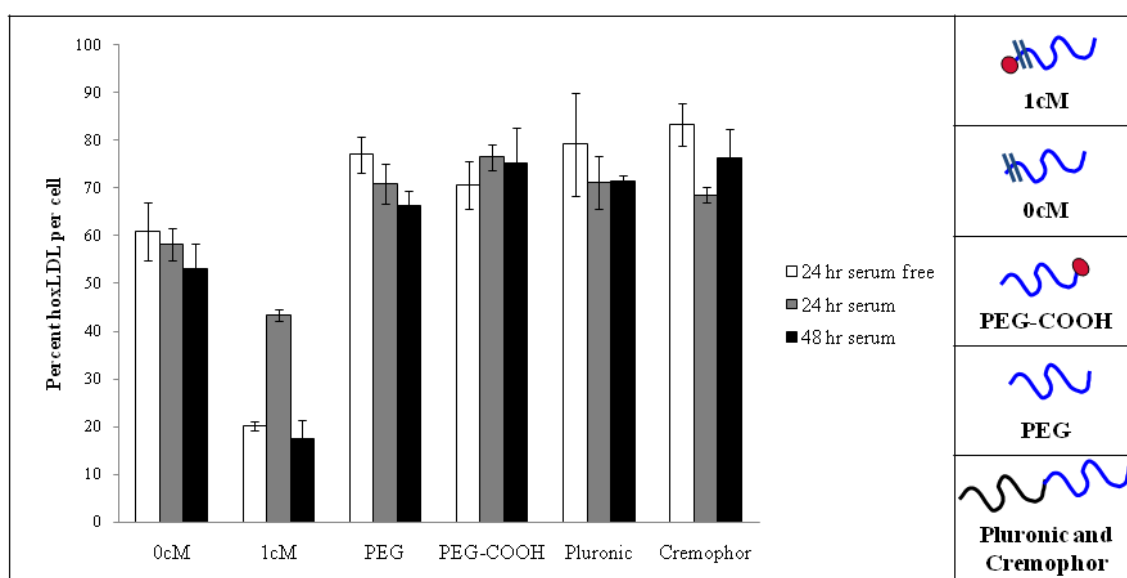


Figure 2.2:

Role of amphiphilicity and branching of the hydrophobic region on degree of inhibition of hoxLDL uptake in THP-1 macrophages. Levels of hoxLDL were measured and quantified in comparison to corresponding hoxLDL treated cells that were not treated with any polymers.

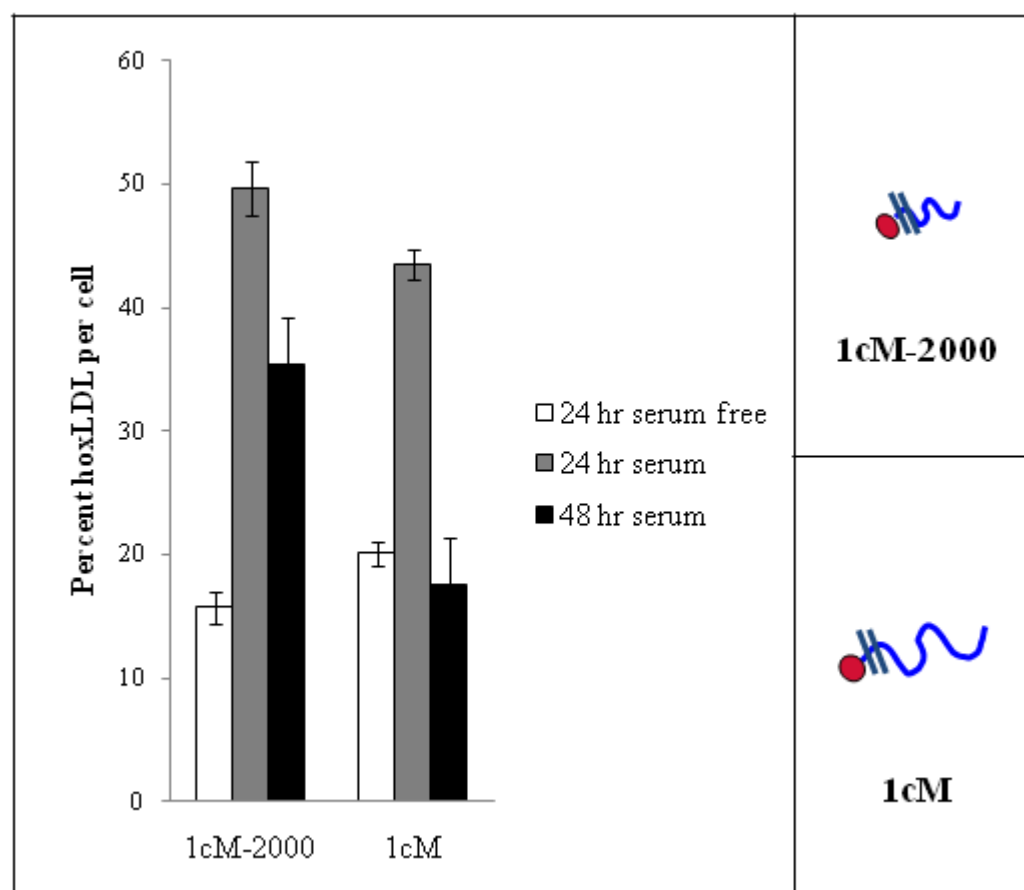


Figure 2.3:

Role of PEG chain length on degree of inhibition of hoxLDL uptake in THP-1 macrophages.

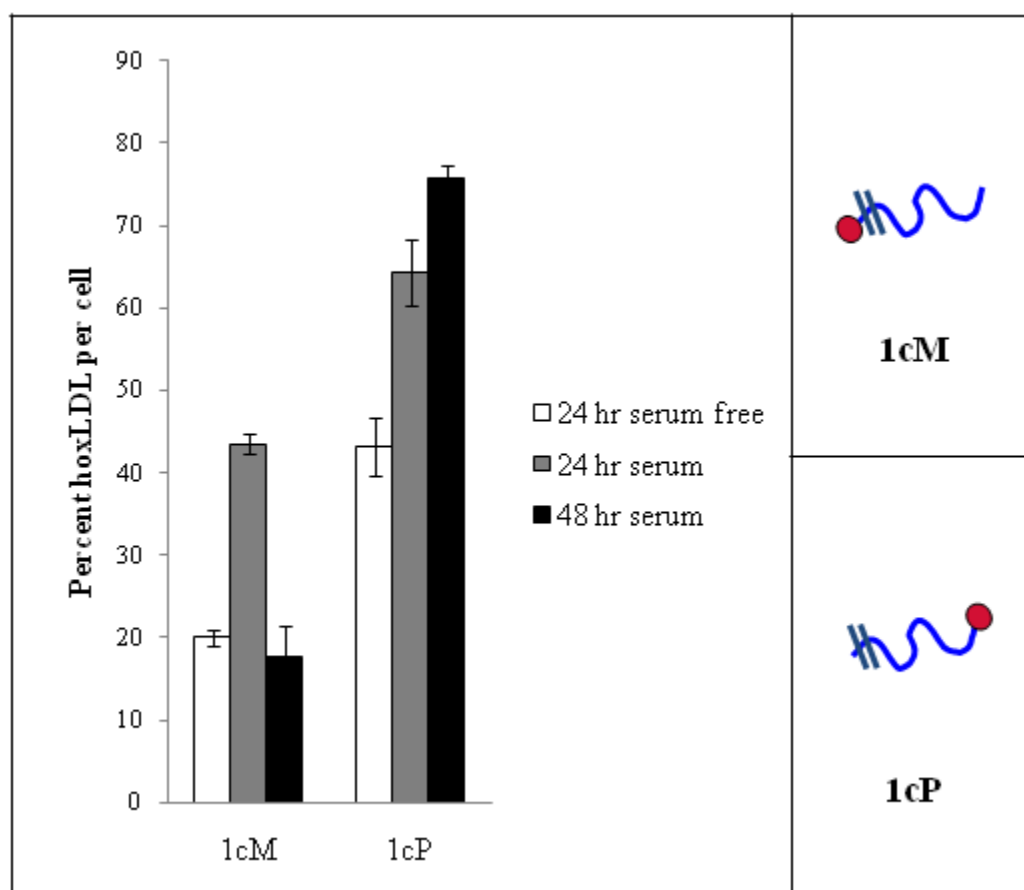


Figure 2.4:

Role of carboxylic acid location on degree of inhibition of hoxLDL uptake in THP-1 macrophages.

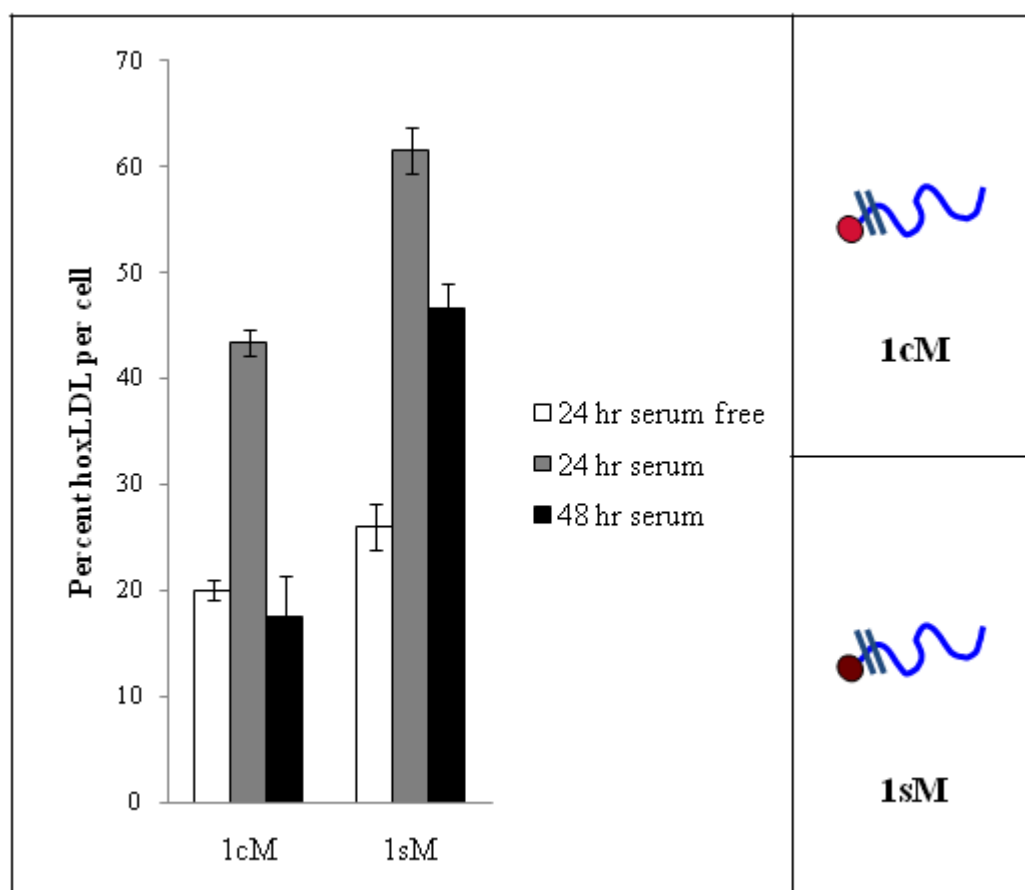


Figure 2.5:

Role of the type of anionic group on degree of inhibition of hoxLDL uptake in THP-1 macrophages.

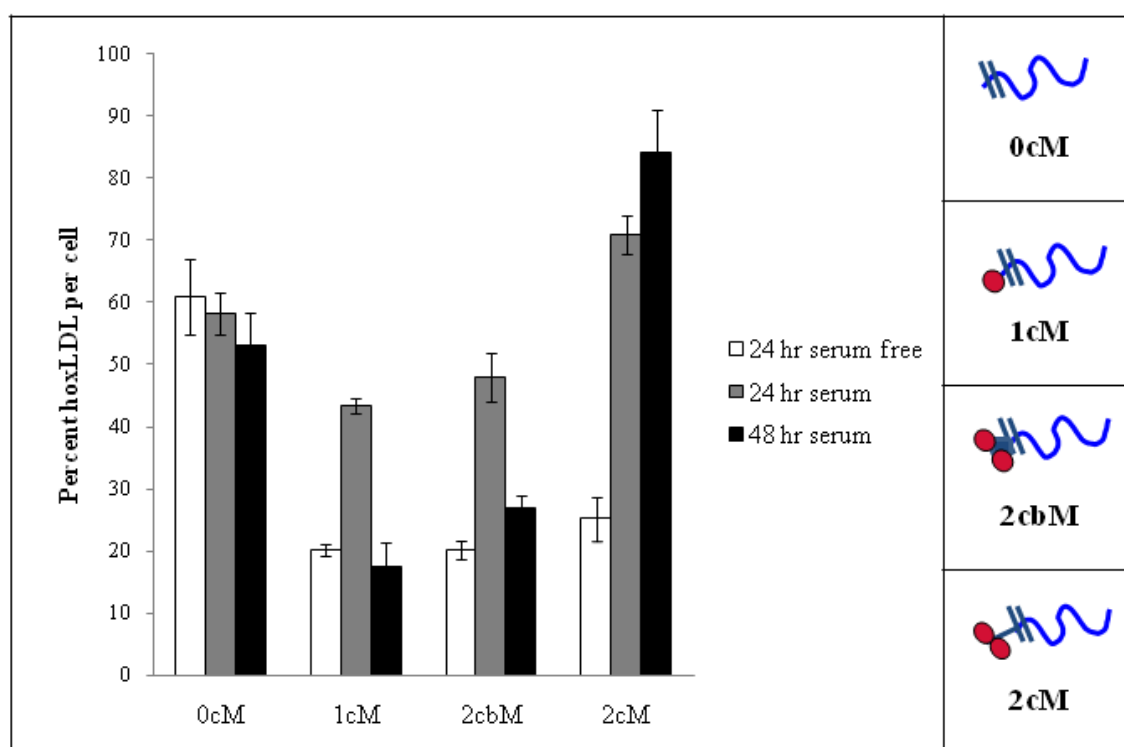


Figure 2.6:

Role of number of anionic charges and rotational motion on degree of inhibition of hoxLDL uptake in THP-1 macrophages.

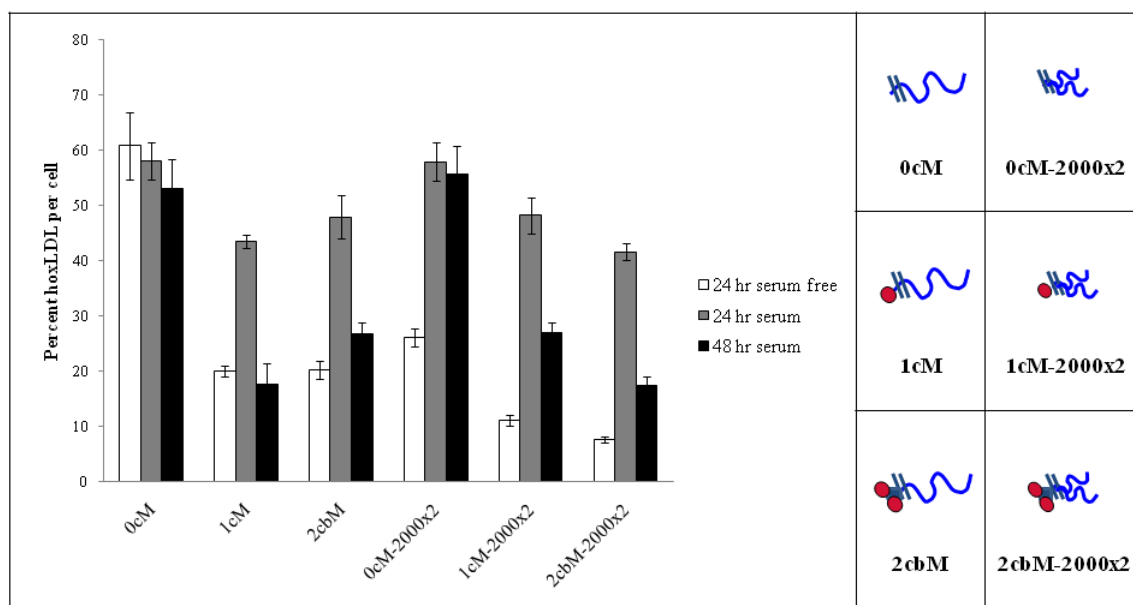


Figure 2.7:

Role of PEG architecture on degree of inhibition of hoxLDL uptake in THP-1 macrophages.

2.7 Supplemental Material

A

Figure 2	1cM	0cM	PEG	PEG-COOH	Pluronic	Cremophor
hoxLDL	YES	YES	NO	NO	NO	NO
1cM		YES	YES	YES	YES	YES
0cM			NO	NO	NO	NO
PEG				NO	NO	NO
PEG-COOH					NO	NO
Pluronic						NO

Figure 3	1cM	1cM-2000
hoxLDL	YES	YES
1cM		NO

Figure 4	1cM	1cP
hoxLDL	YES	YES
1cM		YES

Figure 5	1cM	1sM
hoxLDL	YES	YES
1cM		YES

Figure 6	1cM	0cM	2cbM	2cM
hoxLDL	YES	YES	YES	YES
1cM		YES	NO	NO
0cM			YES	YES
2cbM				NO

Figure 7	1cM	0cM	2cbM	1cM-2000x2	0cM-2000x2	2cbM-2000x2
hoxLDL	YES	NO	YES	YES	YES	YES
1cM		YES	NO	YES	YES	YES
0cM			YES	YES	YES	YES
2cbM				YES	YES	YES
1cM-2000x2					YES	NO
0cM-2000x2						YES

B

Figure 2	1cM	0cM	PEG	PEG-COOH	Pluronic	Cremophor
hoxLDL	YES	YES	NO	NO	NO	NO
1cM		YES	YES	YES	YES	YES
0cM			NO	NO	NO	NO
PEG				NO	NO	NO
PEG-COOH					NO	NO
Pluronic						NO

Figure 3	1cM	1cM-2000
hoxLDL	YES	YES
1cM		NO

Figure 4	1cM	1cP
hoxLDL	YES	YES
1cM		YES

Figure 5	1cM	1sM
hoxLDL	YES	YES
1cM		YES

Figure 6	1cM	0cM	2cbM	2cM
hoxLDL	YES	YES	YES	YES
1cM		YES	NO	YES
0cM			NO	YES
2cbM				YES

Figure 7	1cM	0cM	2cbM	1cM-2000x2	0cM-2000x2	2cbM-2000x2
hoxLDL	YES	YES	YES	YES	YES	YES
1cM		YES	NO	NO	YES	NO
0cM			NO	NO	NO	YES
2cbM				NO	NO	NO
1cM-2000x2					NO	NO
0cM-2000x2						YES

C

Figure 2	1cM	0cM	PEG	PEG-COOH	Pluronic	Cremophor
hoxLDL	YES	YES	YES	NO	YES	NO
1cM		YES	YES	YES	YES	YES
0cM			NO	NO	YES	NO
PEG				NO	NO	NO
PEG-COOH					NO	NO
Pluronic						NO

Figure 3	1cM	1cM-2000
hoxLDL	YES	YES
1cM		YES

Figure 4	1cM	1cP
hoxLDL	YES	YES
1cM		YES

Figure 5	1cM	1sM
hoxLDL	YES	YES
1cM		YES

Figure 6	1cM	0cM	2cbM	2cM
hoxLDL	YES	YES	YES	NO
1cM		YES	NO	YES
0cM			YES	NO
2cbM				YES

Figure 7	1cM	0cM	2cbM	1cM-2000x2	0cM-2000x2	2cbM-2000x2
hoxLDL	YES	YES	YES	YES	YES	YES
1cM		YES	NO	NO	YES	NO
0cM			YES	YES	NO	YES
2cbM				NO	YES	NO
1cM-2000x2					YES	NO
0cM-2000x2						YES

Table 2.2:

Single factor ANOVA with Tukey's post-hoc analysis, performed on SPSS software, was used for statistical analysis. Significance is claimed for differences of $p < 0.05$. Tables show statistical comparison for each condition with 'Yes' representing statistical significance ($p < 0.05$) and 'No' representing no statistical significance ($p \geq 0.05$). A) 24 hour serum free conditions B) 24 hour serum containing conditions and C) 48 hour serum containing conditions.

Chapter 3

Anti-Atherogenic Polymers for Coordinated Rescue of Cholesterol Dynamics in Activated Macrophages

3.1 Abstract

The internalization of oxidized low density lipoprotein (oxLDL) by vascular wall bound macrophage cells is a major precursor to the escalation of atherosclerosis. We report on findings of a two-pronged strategy featuring polymeric drug vehicles for preferential binding to inflamed macrophages and delivery of a drug cargo triggering cholesterol efflux. A self-assembled, amphiphilic polymer based on polyethylene glycol corona and a hydrophobic mucic acid backbone was designed with terminal, anionic carboxylate groups to exhibit preferential binding to cationic scavenger receptors on “activated” human macrophages. These polymers, used alone, competitively lowered oxLDL uptake in cultured THP-1 macrophages by 40%. The amphiphilic nature of the polymers was further exploited to encapsulate 10^{-7} M hydrophobic agonist against nuclear Liver-X receptor α (LXR). In combination with the encapsulated LXR-agonist, the polymer vehicles were found to reduce oxLDL accumulation by 88% *in vitro*. The drug administered at 10^{-7} M, 10^{-6} M and 10^{-5} M unaccompanied by the polymer caused no significant decline in oxLDL accumulation. We then tested the *in vivo* efficacy of the polymers to counteract the effects of localized adventitial release of oxLDL around injured carotid arteries within Sprague Dawley rats fed high fat diet. The combination of injury and oxLDL treatment enhanced cholesterol accumulation and macrophage

recruitment. The polymer vehicles lowered the intimal levels of accumulated cholesterol (50% for polymers alone; 70% for drug-encapsulated polymers) and also inhibited macrophage retention (92% for polymers; 96% for drug-encapsulated polymers) relative to non-treated controls. Our study indicates the promise of coordinated use of polymer vehicles for targeting of inflammatory cells and atherogenesis, which may be relevant to targeted management of atherosclerosis.

3.2 Introduction

Atherosclerosis, triggered by macrophage, smooth muscle and endothelial cell interactions with low density lipoproteins (LDL) within the vascular wall, is the major cause of cardiovascular disease and the leading cause of death in developed countries. (1) Elevated LDL plasma levels lead to the accumulation of LDL within the arterial wall, where LDL is oxidized and modified, thus activating endothelial cells, which, in turn recruit circulating monocytes that differentiate into macrophages. This cycle is believed to trigger foam cell formation and the advancement of atherosclerosis as macrophages endocytose oxidized LDL (oxLDL) through unregulated scavenger receptors. (107-109, 139, 140)

The localized build-up of cholesterol within the vascular intima presents a major challenge to current therapeutic strategies. Major pharmacologic modalities aim to lower systemic levels of cholesterol through liver-based synthetic pathways. Although widely practiced, these therapies cannot be directed to rescue atherogenic "hot spots" and frequently cause adverse side effects (from gastrointestinal complaints to liver enzyme elevation and myopathy). (34, 138) A number of molecular approaches have been proposed for directed inhibition of atherogenesis, including scavenger receptor knockdown (141, 142) and cholesterol acyl-transferase (ACAT)-1 and ACAT-2 suppression(143). A marked decrease in the progression of advanced necrotic lesions has been noted in ApoE^{-/-} mice through the targeted deletion of scavenger receptors

SR-A and CD36, which are upregulated in inflamed macrophages (144), indicating that scavenger receptors play a role in disease progression. Atherosclerotic progression may further be controlled through management of atherosclerotic lesion macrophage infiltration, (145) which Yamakawa et al. has recently restricted via the administration of dehydroepiandrosterone (DHEA), independent of systemic cholesterol levels. (146)

In this study, we utilized the multifunctional nature of nanoscale amphiphilic polymers composed of mucic acid sugar backbone, aliphatic side-chains, and poly(ethylene glycol) (PEG); to target inflammatory cells and rescue their atherogenic phenotype. The amphiphilic polymers self-assemble to form nanoscale micelles with the ability to bind to macrophage scavenger receptors with high affinity. At concentrations above the critical micelle concentration (CMC) of 10^{-7} M, these polymers competitively inhibit cellular internalization of oxLDL. Further, the hydrophobic core of the polymers supports good loading efficiency and sustained release of biologically active hydrophobic drug molecules, enabling the use of polymeric vehicles for drug encapsulation and intracellular delivery. (127)

The current study explores the potential of amphiphilic polymers to reverse atherogenesis through two complementary ways: by reducing cholesterol uptake through binding and blockage of scavenger receptors; and by solubilizing and intracellularly delivering a hydrophobic agonist molecule, which depletes accumulated cholesterol by activating efflux channels. The success of this approach is demonstrated using model agonist GW3965, a synthetic small molecular weight agonist to nuclear membrane receptor liver-X receptor α (LXR), (101) which has been shown to alter

cholesterol synthesis, influx and efflux causing an overall decrease of 36% to 39% cellular cholesterol after 96 hours as well as regulating inflammation and atherosclerosis in animal models. (102-104)

We report that the combination of polymer-mediated scavenger receptor binding and intracellular delivery of the liver-X receptor agonist (LXRA) for lipoprotein metabolism was particularly effective at almost 90% inhibition of cholesterol accumulation *in vitro*. We also demonstrate the efficacy of dual-pronged targeting via drug-loaded polymer vehicles to ameliorate both recruitment of inflammatory macrophages and cholesterol accumulation *in vivo*. This work reveals the potential of polymers to target and rescue inflamed macrophage cells from the atherosclerotic phenotype.

3.3 Materials and Methods

3.3.1 Cell Culture

Human THP-1 monocytes (ATCC) were grown in suspension with RPMI-1640 medium containing 0.4 mM Ca^{2+} and Mg^{2+} , (ATCC) and supplemented with 10 % FBS, in an incubator with 5 % CO_2 at 37 °C and split every four days through centrifugation. The cells were seeded at a concentration of 100,000 cells/cm² and differentiated into macrophage cells by 14 hours incubation in 16nM phorbol myristate acetate. After the 14 hour differentiation period the cells were incubated for an additional 58 hours in RPMI-1640 medium and then tested within three days. Human Aortic Smooth Muscle

Cells (HASMC) were maintained at 37 °C with 5% CO₂ cultured in F-12K medium (ATCC) supplemented with 0.05 mg/mL ascorbic acid, 0.01 mg/mL insulin, 0.01 mg/mL transferrin, 10 ng/mL sodium selenite, 0.03 mg/mL Endothelial Cell Growth Supplement (ECGS), 10% FBS, and 10 mM TES. Human Coronary Artery Endothelial Cells (HCAEC) (Lonza) were maintained at 37 °C with 5% CO₂ in endothelial cell basal medium-2 (EBM-2) supplemented with EGM-2-MV singlequots (Lonza).

3.3.2 LDL Oxidation

OxLDL was prepared within five days of each experiment. BODIPY-labeled and unlabeled human plasma derived LDL (Molecular Probes, OR) was oxidized by 18 hours of incubation with 10 µM CuSO₄ (Sigma) at 37 °C with 5 % CO₂ (14, 147) After 18 hours the oxidation was stopped with 0.01 % w/v EDTA and the degree of oxidation characterized using standard biochemical assays. (89)

3.3.3 Polymer Synthesis

AAP

Polymer synthesis was performed by Sarah Sparks in Kathryn Uhlich's laboratory at Rutgers University as previously described. Briefly, mucic acid was acylated with lauroyl chloride in the presence of zinc chloride, which was then esterified with hydroxy-poly (ethylene glycol) (5 kDa) with DCC as the dehydrating reagent and DPTS as the catalyst at room temperature for 48 hours under argon gas. DCU byproduct was removed by vacuum filtration and the filtrate washed with 0.1 N HCl and brine, dried over MgSO₄,

and concentrated. The desired product was then precipitated from CH₂Cl₂ by addition of 10-fold diethyl ether and the solid collected by centrifugation. Solvent was removed by decanting and the resulting yellow solid was dried under ambient atmosphere (12 hrs) and under high vacuum (12 hrs). (88)

NAP

*Polymer synthesis was performed by Sarah Sparks in Kathryn Uhlich's laboratory at Rutgers University as previously described. **AAP** was esterified with N-hydroxysuccinimide with DCC as the dehydrating reagent in anhydrous CH₂Cl₂ and DMF. The reaction was stirred for 24 hours at room temperature under argon gas before DCU byproduct was removed by vacuum filtration and the filtrate washed with 0.1 N HCl and 50:50 brine/H₂O, dried over MgSO₄, and concentrated. The desired product was then precipitated from CH₂Cl₂ by addition of 10-fold diethyl ether and the solid collected by centrifugation. Solvent was removed by decanting and the resulting yellow solid was dried under ambient atmosphere (12 hrs) and under high vacuum (12 hrs). (125)*

3.3.4 Polymer Attachment

HCAEC, HA-SMC and differentiated THP-1 cells were incubated with **AAP** at 10⁻⁶ M for 24 hr in 5% serum RPMI-1640 at 37 °C in both basal and inflamed states with and without 10 µg/mL SR-A antibody blocking (R&D Systems). Cells were washed, fixed with 4% paraformaldehyde and imaged on a Nikon Eclipse TE2000-S fluorescent microscope to determine fluorescently tagged polymer attachment. The images were

analyzed with Image Pro Plus 5.1 software (Media Cybernetics, San Diego, CA) and fluorescence data normalized to cell count.

Differentiated THP-1 macrophage cells were incubated with **AAP** and **NAP** at 10^{-6} M for 24 hr in 5% serum RPMI-1640 at 37°C in both basal and inflamed states with and without SR-A antibody blocking (R&D Systems). Cells were washed, fixed with 3.7% formaldehyde and imaged to determine fluorescently tagged polymer attachment. The images were analyzed with Image Pro Plus 5.1 software (Media Cybernetics, San Diego, CA) and fluorescence data normalized with cell number.

3.3.5 Encapsulation of LXR Agonist

*Drug encapsulation and concentration verification was originally performed by Jinzhong Wang in Kathryn Uhrich's laboratory at Rutgers University. The LXR agonist, GW3965, was encapsulated within **AAP** using oil/water emulsion. Specifically, GW3965 in CH_2Cl_2 was added drop wise to a magnetically stirring solution of **AAP** in water at a concentration of 1×10^{-4} M **AAP** and 1×10^{-5} M GW3965. The solution was stirred continuously for 24 hours in a closed vessel. The vessel was then opened and the solution exposed to ambient atmosphere for 16 hours to facilitate evaporation of the CH_2Cl_2 . The resulting solution was filtered with a 0.20 μm syringe filter (Fisher Scientific) and diluted to the desired concentration.*

Encapsulated GW3965 concentration was determined by UV absorption on a Beckman DU®520 General Purpose UV/Vis Spectrophotometer at 270 nm. Once encapsulated, the GW absorption peak disappeared due to micelle shielding. The micelles

were then disrupted by addition of 50% DMSO and GW3965 concentration quantified by absorption at 270 nm in comparison to a calibration curve.

3.3.6 Cellular Internalization of LXR Agonist

Differentiated THP-1 macrophages were incubated with **AAP** at 10^{-6} M and/or 10^{-7} M LXRA for 5 hr in serum-free RPMI at 37 °C. Cells were washed and fixed and examined under multiphoton microscopy to detect internalized LXR agonist (LXRA) on a Leica TCS SP2 system (Leica Microsystems, Inc., Exton, PA). The cells were illuminated using a titanium: sapphire femtosecond laser with a tunable wavelength set at 780 nm excitation (Mai Tai, repetition rate 80 Mhz, 100 fs pulse duration, 800 mW) and 470-500 nm emission.

3.3.7 Biological Activity of LXRA Delivery: Gene Expression Studies

The mRNA levels of key downstream genes targeted by the LXR agonist, LXRA, were quantified using QRT²-PCR based gene expression analysis. The RNA of the samples was extracted with the RNeasy Mini kit from Qiagen. Briefly, cells were lysed with β -mercaptoethanol and QiaShredder before extraction of and purification of the samples. Reverse transcription was performed with a High Capacity cDNA Reverse Transcription Kit from Applied Biosystems. DNA expansion of lipid transport and inflammatory genes was performed with Quantitative RT²-PCR conducted on a Roche plate reader 480 with a custom PCR array from SA Biosciences and β -actin as a housekeeping gene (SA Biosciences, Frederick, MD).

3.3.8 LDL Influx

The internalization of oxLDL by macrophage cells was assayed by incubating BODIPY labeled oxLDL (10 $\mu\text{g/mL}$) with cells for 24 hours at 37 °C and 5% CO_2 . Conditions included a control of RMPI-1640 medium, **AAP** alone (10^{-6} M), non-encapsulated LXRA (10^{-7} M) admixed with **AAP** (10^{-6} M), and encapsulated **AAP**[LXRA] (10^{-6} M/ 10^{-7} M). The cells were then washed twice with 1xPBS and imaged on a Nikon Eclipse TE2000-S fluorescent microscope to determine fluorescently tagged oxLDL attachment. The images were analyzed with Image Pro Plus 5.1 software (Media Cybernetics, San Diego, CA) and fluorescence was normalized to cell count and medium alone condition.

3.3.9 Rescue of Cholesterol Pre-loaded Cells

The **AAP**[LXRA] rescue of macrophage cells was quantified following pre-incubation of cells with excess oxLDL. Macrophage cells were incubated with BODIPY-labeled oxLDL (10 $\mu\text{g/mL}$) and 5 % FBS serum for 2 hours at 37 °C and 5 % CO_2 . Excess oxLDL solution was then removed from all conditions and the test conditions, in the presence of 5% FBS, were added and incubated for 24, 48, 72, 96 and 120 hours at 37 °C and 5 % CO_2 . A control condition included RMPI-1640 medium with no additional oxLDL added. The remaining conditions each contained additional oxLDL (10 $\mu\text{g/mL}$); **AAP** (10^{-6} M), LXRA (10^{-7} M), non-encapsulated LXRA (10^{-7} M) admixed with **AAP** (10^{-6} M), and encapsulated **AAP**[LXRA] (10^{-6} M/ 10^{-7} M). At the desired time point the cells

were fixed with 3.7 % formaldehyde and washed twice with 1xPBS and imaged on a Nikon Eclipse TE2000-S fluorescent microscope to determine fluorescently tagged oxLDL attachment. The images were analyzed with Image Pro Plus 5.1 software (Media Cybernetics, San Diego, CA) and fluorescence data normalized with cell number and compared to the control samples.

3.3.10 In vivo Studies of Efficacy of LXRA and AAP

Four groups of male Sprague Dawley rats at twelve weeks of age were used in this study: **AAP** at 10^{-3} M, LXRA at 10^{-4} M, **AAP**[LXRA] at 10^{-4} M LXRA and 10^{-3} M **AAP**, and a control condition with no LXRA or **AAP**. All groups were fed a high fat diet (20 % fat Purina chow) for two weeks prior to surgery where they had their right carotid artery injured through the crush method. (148) Briefly, an arterial clip was placed 1 cm below the bifurcation point. A serrated hemostat was then tightly closed on the carotid artery, held for 5 seconds, opened and repositioned so that the entire area between the arterial clip and bifurcation point was injured. After the injury was complete the arterial clamp was removed and a biodegradable arterial wrap made of collagen type I was applied adventitially around the blood vessel and the wound closed. After 96 hours the animals were sacrificed by formalin perfusion and the injured right artery and non-injured left artery were analyzed for macrophage recruitment and cholesterol accumulation. Oil Red O staining for cholesterol content and CD68 antibody staining for macrophage recruitment were quantified with Image Pro Plus 5.1 software (Media Cybernetics, San Diego, CA) and data normalized with tissue area.

3.3.11 Statistical Analysis

Error bars on graphs indicate standard error of the mean based upon biological triplicate samples in each *in vitro* experiment with three separate experiments for each condition; *in vivo* experiments included two animals per condition with three tissue sections examined per animal. Single factor ANOVA, performed Excel's data package software, was used for statistical analysis. Significance is claimed for differences of $p < 0.05$.

3.4 Results

3.4.1 Polymers Bind Preferentially to Activated Macrophage Cells

Polymers were designed based on a mucic acid backbone, aliphatic side-chains, and poly(ethylene glycol) (PEG) tails which self-assembled to form nanoscale micelles above the CMC (10^{-7} M). Two variants of polymer chemistries were examined; an anionic amphiphilic polymer (**AAP**) included a carboxylate on the mucic acid and the neutral amphiphilic polymer (**NAP**) was used as the uncharged control (**Figure 1a**). Incubation of polymers with THP-1 human macrophage cells showed preferential binding of **AAP** to both basal and TNF- α pretreated macrophage cells while minimal internalization of **NAP** was seen over all conditions (**Figure 1b**). Significantly greater polymer association was found in TNF- α activated macrophage cells, which have been shown to exhibit increased expression of SR-A.(20) When macrophage cells were pre-

treated with an SR-A antibody, polymer attachment fell to non-specific levels (**Figure 1c**), equivalent to those seen with the neutral polymer, **NAP** (**Figure 1b**). Moreover, when TNF- α treated THP-1 cells were exposed to SR-A blocking antibodies, the levels of **AAP** uptake were reduced to non-specific binding levels. TNF- α treatment and SR-A antibody blocking did not alter polymer attachment to HCAECs or SMCs (**Figure 1d**), confirming that preferential **AAP** binding to macrophages can be attributed to SR-A interactions and non-specific binding is consistently minimal among all cell types.

3.4.2 Drug Agonist Encapsulation by Polymer Carriers

*Drug encapsulation concentration was analyzed by Jinzhong Wang in Kathryn Uhrich's laboratory at Rutgers University. Encapsulation within the anionic nanopolymers (**AAP**) of GW3965, a LXR-Agonist (LXRA), was verified by UV analysis before and after micelle disruption, confirming nearly 100% encapsulation when presented in a LXRA:**AAP** weight ratio of 1:100 (see Supplemental Information). Encapsulation of LXRA did not significantly affect the micellar size, as determined by DLS measurements.*

3.4.3 Polymer Vehicles Enhance Cellular Uptake of Drug Agonist via SR-A

AAP micelles were used to encapsulate GW3965, a liver-X receptor agonist (LXRA). LXRA, with and without polymer vehicles, was incubated with THP-1 macrophages in order to elucidate the ability of the cells to bind and internalize the drug agonist (**Figure 2a**). Internalization of LXRA at 10^{-7} M in the absence of polymer vehicles was six-fold less than delivery via encapsulation in **AAP** (**AAP**[LXRA]). The

uptake of non-encapsulated LXRA by cells remained low and was unaffected by SR-A blocking or TNF- α pretreatment, while encapsulated LXRA delivery increased after TNF- α treatment and was significantly inhibited by the administration of SR-A antibody. This finding was similar to the uptake seen for **AAP** alone (**Figure 1d**) and confirmed that LXRA delivery is enhanced through encapsulated polymer shuttling via the scavenger receptor SR-A.

3.4.4 *Expression of Key Atherosclerotic Genes is Altered by LXRA Delivery*

LXRA, at various concentrations, was incubated with THP-1 cells over 24 hr in order to understand the ability of polymer delivery of drug to upregulate ABCA1, as a model gene (**Figure 2b**). The concentration of 10^{-7} M when encapsulated within **AAP** caused a nearly 14-fold upregulation in expression compared to 7-fold increase without polymer vehicles. Further, when LXRA alone was incubated with the cells at higher concentrations (10^{-5} and 10^{-6} M), the upregulation seen with **AAP** delivery could still not be matched.

LXRA, with and without polymer delivery, was incubated with cells over 24 hr in order to understand the variation in THP-1 macrophage gene expression of six anti-atherosclerotic, inflammatory and cholesterol-associated genes (ABCA1, APOA1, APOE, NR1H3, PPARG and RXRA) (**Figure 2c**). Incubation of **AAP** or LXRA alone did not cause a significant change in gene expression for basal or TNF- α treated THP-1 macrophages. The addition of encapsulated **AAP**[LXRA] to macrophage cells resulted in a five-fold or more upregulation of five genes ABCA1, APOA1, APOE, NR1H3 and

PPARG. The sixth anti-atherosclerotic gene tested, RXRA, showed a smaller, but still significant, 2.95-fold upregulation. The administration of **AAP**[LXRA] also caused a 6.25-fold upregulation in SR-A expression (MSR1).

3.4.5 Oxidized LDL Accumulation in Activated Macrophages is Prevented by LXRA Delivery

LXRA, with and without polymer vehicles, was incubated with TNF- α treated THP-1 macrophages in order to elucidate the ability of the **AAP**-LXRA combination to prevent the binding and internalization of oxLDL (**Figure 3a**). The addition of **AAP** to human macrophage cells in the presence of oxLDL caused a 73% decrease in cholesterol uptake after 24 hours in comparison to control condition of no polymer or drug intervention. Introduction of LXRA to cells did not significantly decrease cholesterol content unless **AAP** was admixed with the ligand, resulting in a 4% and 55% decrease respectively. When LXRA was encapsulated within **AAP** (**AAP**[LXRA]) and incubated with macrophages there was an 88% decrease in oxLDL after 24 hours.

3.4.6 Total Cholesterol Content in OxLDL Pre-loaded Macrophages is Reduced through LXRA Delivery

A study was conducted to quantify the efficacy of **AAP** and LXRA treatment on cholesterol depletion within macrophages preloaded with oxLDL in order to assess the ability of the polymer/drug to rescue cells from cholesterol loading (**Figure 3b**). When the macrophages were pre-loaded with oxLDL, the addition of 10^{-7} M LXRA alone did

not significantly alter oxLDL content of cells any time period (24, 48, 72, 96 and 120 hours). The polymer, **AAP**, and **AAP** with non-encapsulated LXRA each showed a trivial decrease in overall oxLDL content at all time points. In contrast, after 120 hr, the LXRA encapsulated polymer, **AAP**[LXRA], reduced the cholesterol content of the cells (45%) to lower levels than seen in control condition, where no additional oxLDL was added after the pre-incubation period (60%).

3.4.7 Total Cholesterol Content in Injured Rat Carotid Artery Model is Reduced through LXRA Delivery

In order to model atherosclerotic lesions *in vivo* and investigate the efficacy of the polymer-drug combination, male Sprague Dawley rats were raised on a high fat diet before a crush injury to the right carotid was performed and a polymer-loaded collagen wrap was inserted (**Figure 4a**). After 96 hours the animals were sacrificed and the injured right artery and non-injured left artery were analyzed for cholesterol accumulation (**Figures 4b and d**). Animals treated with polymers exhibited a 50% decrease in cholesterol accumulation relative to non-treated controls (PBS) in injured rat carotid arteries. However, cholesterol accumulation was drastically decreased in animals treated with encapsulated **AAP**[LXRA] (70% decrease relative to non-treated controls). Notably, treatment with **AAP**[LXRA] reduced cholesterol content to the same level as non-injured arterial sections.

3.4.8 Macrophage Recruitment in Injured Rat Carotid Artery Model is Reduced through LXRA Delivery

Using the atherosclerotic lesion *in vivo* model mentioned above, the animals were sacrificed after 96 hr and the injured right artery and non-injured left artery were analyzed for vessel area and macrophage recruitment (**Figures 4c and e**). Animals treated with **AAP** and **AAP[LXRA]** displayed significantly fewer recruited macrophages in injured arteries (92% and 96% decrease respectively, relative to PBS controls. Notably, treatment with **AAP[LXRA]** reduced cholesterol content to the same level as non-injured arterial sections. (**Figure 4c**) In contrast, LXRA introduced in the absence of polymer vehicles led to no reduction in macrophage recruitment.

3.5 Discussion

Effective therapeutic approaches for cardiovascular disease are limited by pharmacologic approaches that can coordinately manage atherogenesis and inflammation. (1, 107, 145) Major factors underlying the chronic progression of atherosclerotic plaques are the activation and recruitment of macrophages to the vascular injury site, followed by uncontrolled scavenger receptor-mediated internalization of oxLDL. (109, 114, 145, 149) Many disease interventions have been proposed including scavenger receptor inhibitors or knockdowns, acyl-CoA cholesteryl acyl transferase (ACAT) inhibitors and knockdown, and inhibition of macrophage recruitment. (141-143, 146) In this work, a novel, dual-pronged approach to attenuate

cholesterol accumulation was proposed, combining anti-atherogenic agonist delivery to inflamed cells in concert with scavenger receptor-mediated blockage of cholesterol accumulation.

In vitro studies have previously shown that carboxylate-terminated amphiphilic polymers derived from mucic acid and PEG, can self-assemble into micelles, which bind to macrophage scavenger receptors SR-A and CD36. (150) These receptors are present in high concentrations at sites of atherosclerotic lesions. (151, 152) The anionic terminated polymer chains are hypothesized to mediate electrostatic binding to the positive pocket of residues on the SR-A scavenger receptor. (153) We now show that the carboxylate-terminated polymers preferentially bind to scavenger receptor expressing human THP-1 macrophage cells over two other vascular cell types. The increased expression of scavenger receptors in TNF- α activated macrophages further promotes **AAP** attachment; hence the charged polymers may serve as effective candidates for inflamed macrophage targeting *in vivo*.

Previous studies have employed LXR- α and/or LXR- β deficient cells or mice to examine the role of LXR in cardiovascular disease. (106) Since the liver X-receptor agonist GW3965 had been shown to be effective in activating LXR, (104, 154, 155) we examined the ability of the polymers to encapsulate and deliver the hydrophobic agonist to activated cells with some degree of specificity. Our success with the utilization of low concentrations of agonist via polymer encapsulation suggests that increased efficacy can be achieved via polymer vehicle based delivery. Our studies employing direct 2-photon imaging of cell-internalized LXRA confirmed that

carboxylate-terminated polymers are internalized within the cytosol; this polymer internalization allows for drug delivery to the nucleus, where ligand binding is essential for enhanced LXR-signaling, as evidenced by the upregulation of key gene targets.

Our results show a 9-fold increase in LXR α and a 15-fold increase in ABCA after delivery of 10^{-7} M GW3965, while a study by Albers et al. showed that treatment with GW3965 at a 10^{-6} M caused more modest upregulation of LXR α (3-fold) and ABCA₁ (6-fold). (156) While the modes of delivery are different between the two studies, we are able to show significantly greater gene upregulation through **AAP** encapsulation and delivery and it is noteworthy that the variations illustrated in our study result from a lower concentration of the agonist. Polymer encapsulation greatly enhanced LXRA delivery, via scavenger receptor binding, compared to the non-encapsulated conditions, resulting in significant alteration in six key atherosclerosis associated genes. Typically, elevated SR-A expression would promote atherosclerosis progression through increased oxLDL accumulation. (139) However, due to selective binding of polymer-encapsulated LXRA to macrophage SR-A, upregulation allows for enhanced polymer and ligand delivery to inflamed or diseased cells. We have confirmed that the up-regulation of LXR related genes was also accompanied by enhanced anti-atherogenesis related signaling and by rescue of cells pre-loaded with oxLDL and under continuing exposure to oxLDL. These trends illustrate the potential ability of the polymer complexes to inhibit atherosclerosis at the gene signaling level as well as via receptor blockage, which opens possibilities for depleting as well as retarding the accumulation of cholesterol.

The *in vivo* model probed the accumulation of cholesterol following localized vascular injury to the carotid artery. Both the anionic polymer and the polymer-encapsulated LXR agonist caused significant inhibition of cholesterol accumulation in comparison to the drug and non-treated samples. A notable finding was that the addition of both polymer alone and polymer-encapsulated LXRA significantly inhibited (92% and 96% respectively) the presence of macrophage cells near the site of injury, which has been reported to be an important atherosclerosis marker independent of cholesterol content. (145, 146) Macrophage recruitment is regulated by factors such as TNF- α and interleukin 1 beta (IL-1 β). (107, 145, 157) The *in vivo* studies generated bleeding and thrombus formation at the injury site however a marked reduction in macrophage recruitment was observed with **AAP** and **AAP[LXRA]** conditions, suggesting that the polymer vehicles had an inhibitory effect on the activation of recruited macrophages and possibly the further recruitment of monocytes. Our *in vitro* studies show that direct polymer exposure to cultured macrophages markedly attenuate TNF-alpha secretion and MMP-9 secretion (Iverson et al., in preparation). The changes observed for *in vivo* macrophage recruitment/retention raise the possibility of not only targeting activated macrophages but modulating their inflammatory phenotype in concert with regulation of atherogenesis.

In summary, these findings show that liver-X receptor agonists encapsulated within anionic amphiphilic polymers significantly lowered oxLDL accumulation compared to non-encapsulated conditions *in vitro* and also significantly diminished cholesterol content *in vivo*. The implications of our study are much broader than

atherosclerosis; due to the polymers' hydrophobic micelle core, hydrophobic drug encapsulation can lead to directed drug delivery for enhanced treatment of various inflammatory diseases.

3.6 Figures

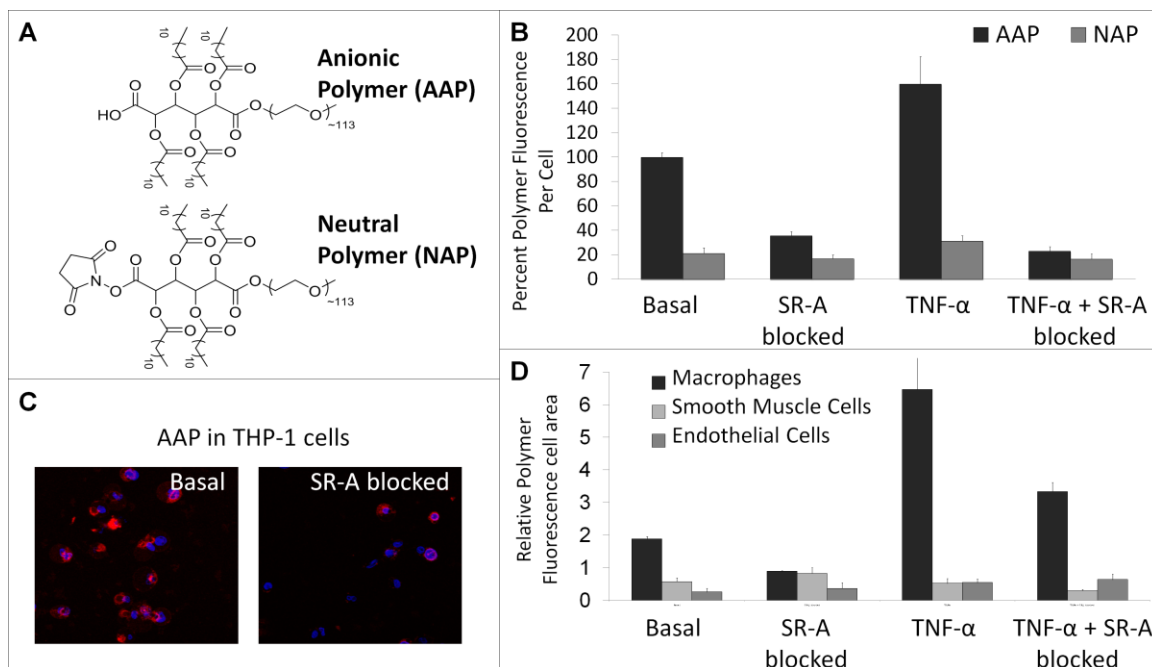


Figure 3.1

Anionic amphiphilic polymers exhibited a high degree of cell specific internalization in activated macrophages due to scavenger receptor-A (SR-A) interactions. A) Chemical structure of unimeric amphiphilic chains of anionic, **AAP**, and neutral, **NAP**, polymers. B) Internalization of texas red-labeled **AAP** and **NAP** polymers within THP-1 macrophages was quantified in the presence and absence of TNF- α pretreatment. Blockage by anti-SR-A antibody confirms a prominent role for scavenger receptor-mediated binding to **AAP** following TNF- α activation. C) Binding of **AAP** (labeled with Texas Red) in THP-1 cells (Hoechst nuclei) with and without SR-A blocking antibodies present was captured using a 63X objective with a Leica TCS SP2 system (Leica Microsystems Inc.). D) Internalization of texas red-labeled **AAP** polymer in THP-

1s, HCAECs, and SMCs: **AAP** exhibits preferential binding and internalization in TNF- α pretreated human macrophages compared to basal and treated endothelial and smooth muscle cells.

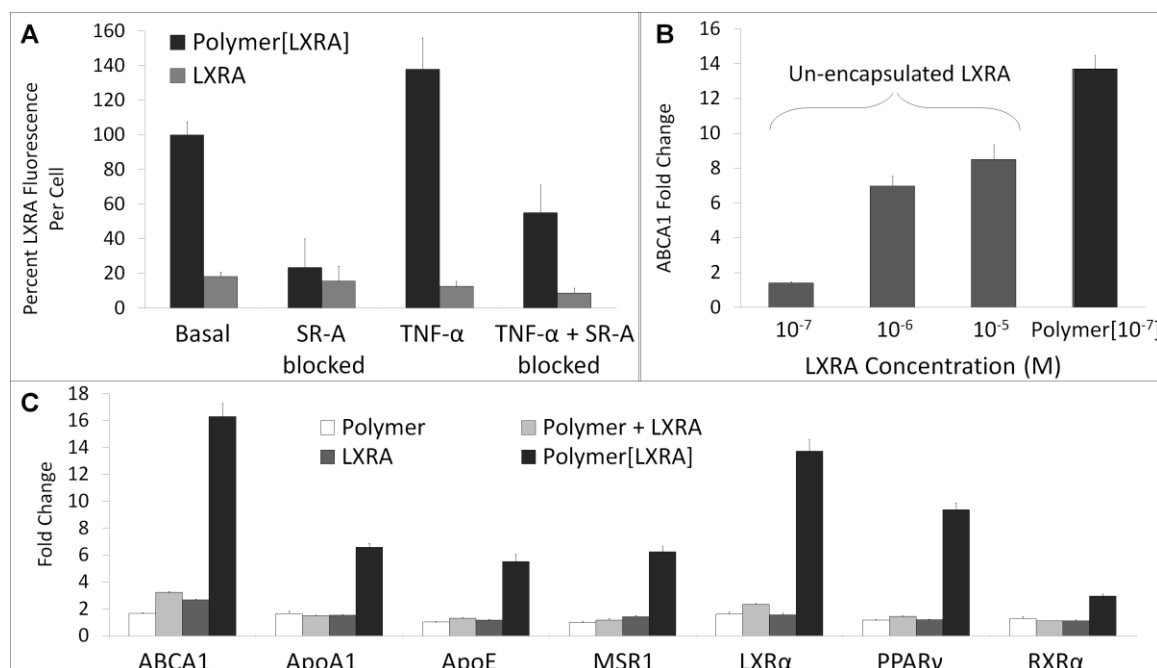


Figure 3.2

LXRA interactions with THP-1 macrophage cells. A) LXRA showed low levels of cellular uptake within both quiescent and activated THP-1 macrophages; this uptake is not mediated by scavenger receptor SR-A. In contrast, polymer-encapsulation of LXRA significantly enhanced the LXRA internalization in quiescent macrophages, and in an even more pronounced manner in activated macrophages. B) Using ABCA1 as a model, gene expression is shown to be upregulated to the greatest extent after cells were exposed to encapsulated polymer[LXRA], drastically more than the same concentration of LXRA without polymer delivery or 10 and 100-fold higher concentration of LXRA alone. C) Among the 7 atherosclerotic genes investigated, the combination of polymer with encapsulated LXRA consistently resulted in greater gene expression than non-encapsulated conditions.

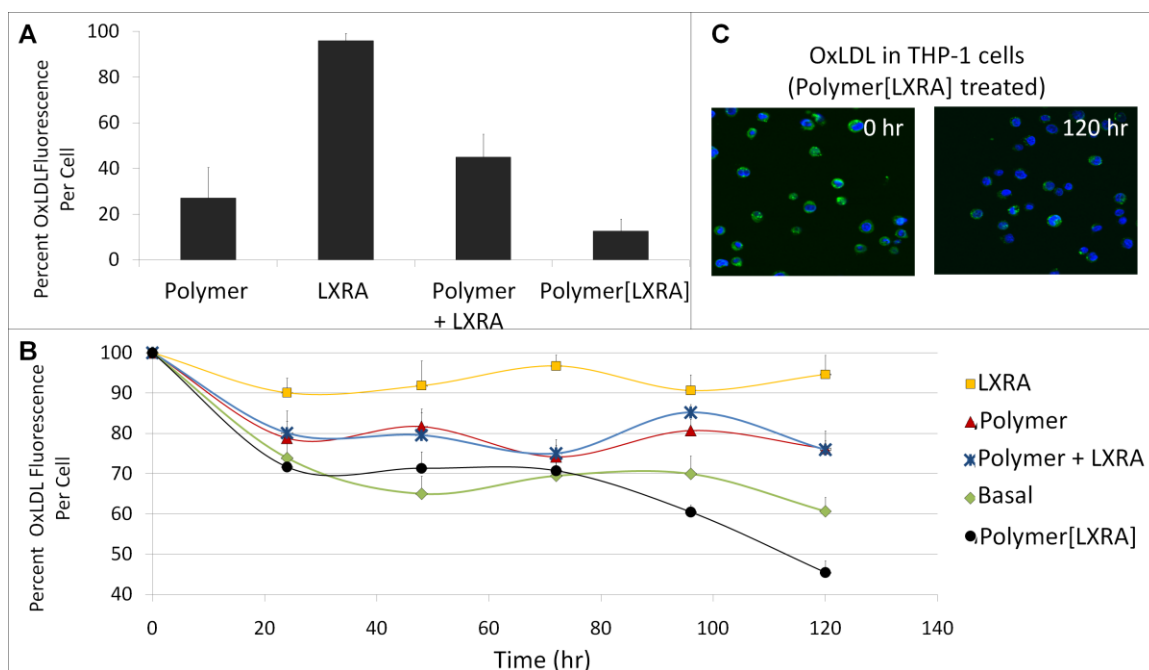


Figure 3.3

Charged amphiphilic polymers, with encapsulated LXRA (Polymer[LXRA]) lowered oxLDL content of THP-1 macrophages. A) OxLDL uptake in THP-1 macrophages: Polymer[LXRA], resulted in a 88% decrease in total oxLDL within cells after a 24 hour incubation period. B) Cells preloaded for 18 hrs were rescued by Polymer[LXRA] over the course of 5 days compared to untreated, oxLDL preloaded cells incubated with media alone (45% compared to 60%). Cell rescue is accomplished through a combination of decreased LDL influx and increased LDL efflux; controlled through polymer attachment and agonist delivery. C) Comparison of cellular oxLDL content after 24 hours and 120 hours of Polymer[LXRA] treatment captured using a 63X objective with a Leica TCS SP2 system (Leica Microsystems Inc).

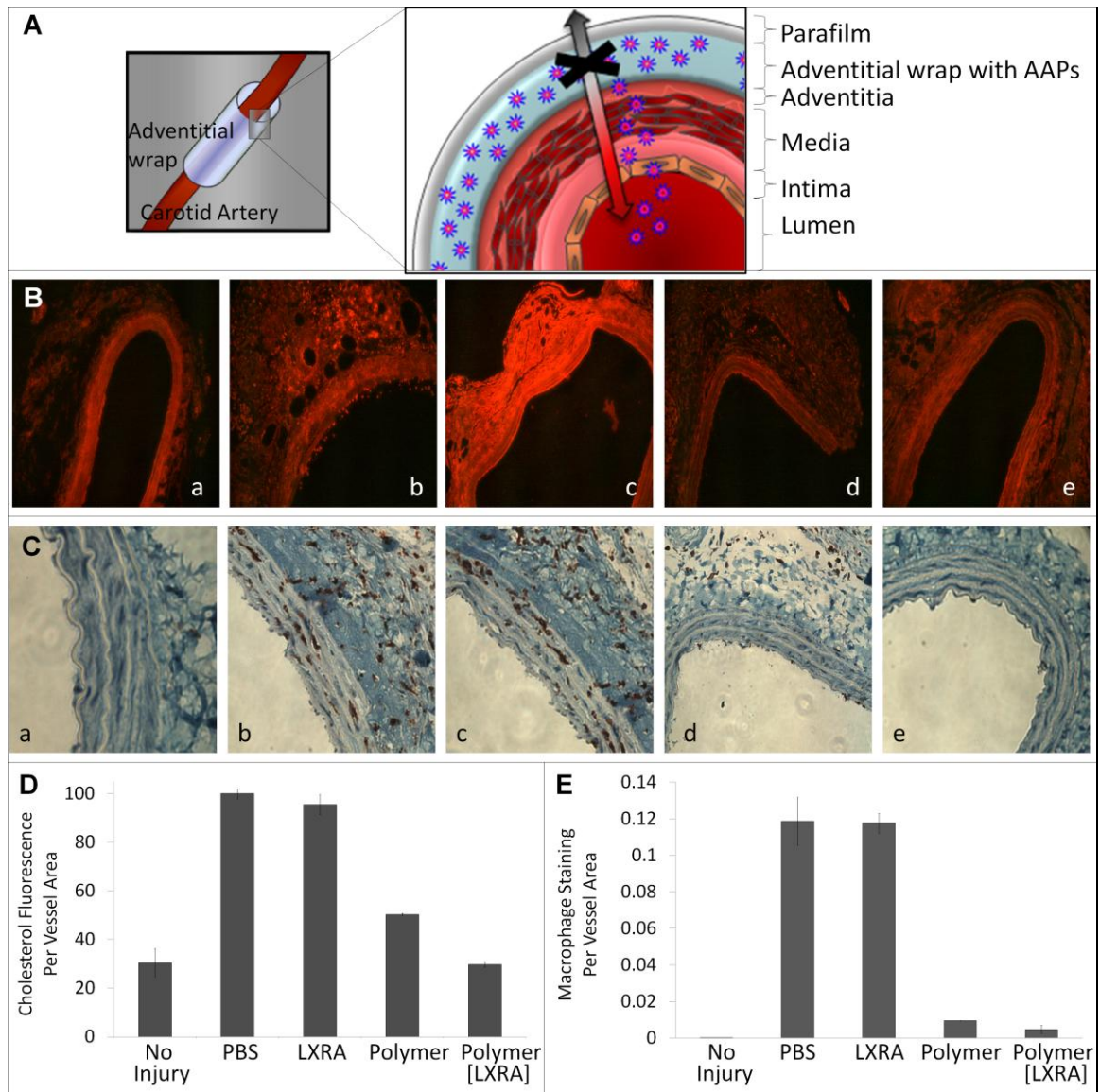


Figure 3.4

The Polymer[LXRA] release from an adventitial wrap significantly altered cholesterol content and macrophage recruitment *in vivo*. A) Polymer is delivered via an adventitial collagen wrap. Polymer diffusion into the vessel wall is encouraged through the use of a parafilm layer surrounding the wrap, preventing external diffusion. B and D) Carotid artery cholesterol content 4 days after crush injury and treatment application through adventitial wrap

placement, Polymer and Polymer[LXRA] decreased cholesterol content by 50% and 70% respectively a) non-injured control b) PBS control c) LXRA d) Polymer e) Polymer[LXRA]. C and E) Macrophage recruitment to the site of injury is greatly reduced by the addition of polymer and to a greater degree with Polymer[LXRA], 92% and 96% respectively a) non-injured control b) PBS control c) LXRA d) Polymer e) Polymer[LXRA].

3.7 Supplemental Material

3.7.1 Supplemental Methods

Ligand Concentration Optimization

The optimal encapsulated LXRA concentration for oxLDL influx inhibition was determined through comparison of oxLDL uptake at 24 hours by THP-1 cells exposed to encapsulated and non-encapsulated ligand at concentrations ranging from 10^{-4} M to 10^{-8} M with **AAP** at 10^{-6} M and in 5% serum containing RPMI-1640.

LDL Efflux

The efflux of oxLDL from macrophage cells was assayed following pre-incubation of fluorescently labeled oxLDL (10 μ g/mL) with cells for 2 hours at 37C and 5% CO₂. The excess oxLDL was then removed from all conditions and the different test conditions were employed and incubated for 5 hours at 37C and 5% CO₂. The different conditions that the cells were exposed to include a control condition with only RMPI-1640 medium, a LXRA and **AAP** condition in which a non-encapsulated ligand at 1×10^{-7} M is delivered to the cells in conjunction with 1×10^{-6} M **AAP**, and an encapsulated ligand condition in which the 1×10^{-7} M LXRA is encapsulated by **AAP** at 1×10^{-6} M. The cells were then washed twice with PBS and imaged. The images were analyzed with Image Pro Plus 5.1 software (Media Cybernetics, San Diego, CA) and fluorescence was

normalized with cell number and compared to the control sample where no **AAP** or LXRA was administered.

Collagen Gel Formation and Diffusion Testing

Polymer and ligand diffusion from a collagen gel was utilized for *in vivo* delivery. The gel was created by sequentially adding HEPES buffer, 10x EMEM, 0.1M NaOH, ligand or polymer in H₂O and type 1 collagen from calf skin (Elastin Polymer Company, Inc Missouri) in PBS before crosslinking in a Spectrolinker XL-1500 UV Crosslinker on a reflective foil surface for 30 min.

Diffusion experiments were performed on a Franz diffusion cell with a diffusion area of 0.64 cm² and reservoir of 1.5 mL. Parafilm was placed on either side of the fluorescently-tagged polymer loaded gel, one side with a whole of 2 mm in the center, before loading into the diffusion cell. A 37 C water bath was utilized to maintain physiological temperature and samples were taken every 24 hours and tested on CytoFluor multiwell plate reader for fluorescent intensity.

3.7.2 Supplemental Results

Ligand Concentration Optimization

Uptake of hoxLDL in THP-1 macrophage cells was significantly inhibited by encapsulated ligand at 10⁻⁷M and higher. When GW3965 was delivered to cells at 10⁻⁸M

it no longer showed hoxLDL inhibition efficacy to a greater extent than the polymer alone.

LDL Efflux

Efflux of hoxLDL from THP-1 cells displayed trends similar to the influx results. Polymer encapsulated ligand caused the most significant efflux, 87%, followed by polymer and polymer with non-encapsulated ligand, 63% and 51% respectively, while ligand alone showed an insignificant efflux of 4%.

Collagen Diffusion Testing

Polymer diffusion from collagen gel showed concentrations above CMC (10^{-7} M) occurred within the first 24 hours and consisted for 14 days.

3.7.3 Supplemental Figures

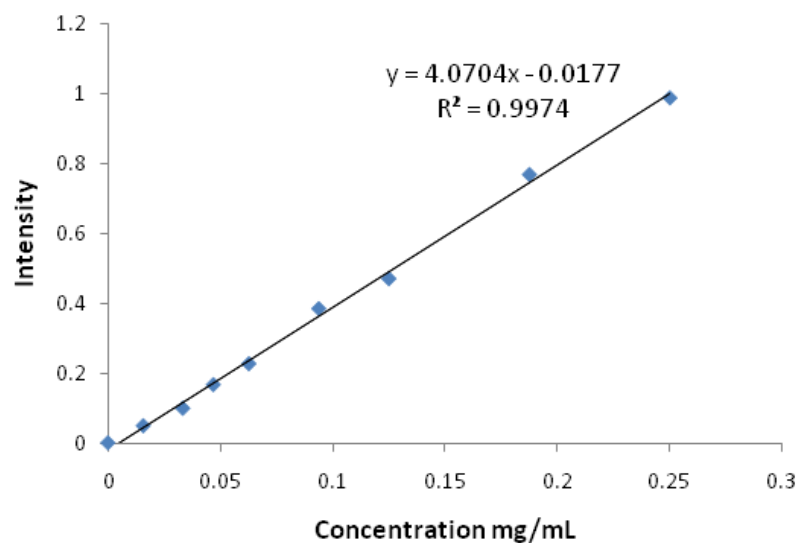


Figure 3.5

Drug encapsulation concentration was analyzed by Jinzhong Wang in Kathryn Uhrich's laboratory at Rutgers University. Standard curve shows equation used to determine the concentration of ligand that was encapsulated within the polymeric micelle, almost 100% efficiency at the 100:1 ligand to polymer ratio was achieved and shown to remain encapsulated for over two weeks.

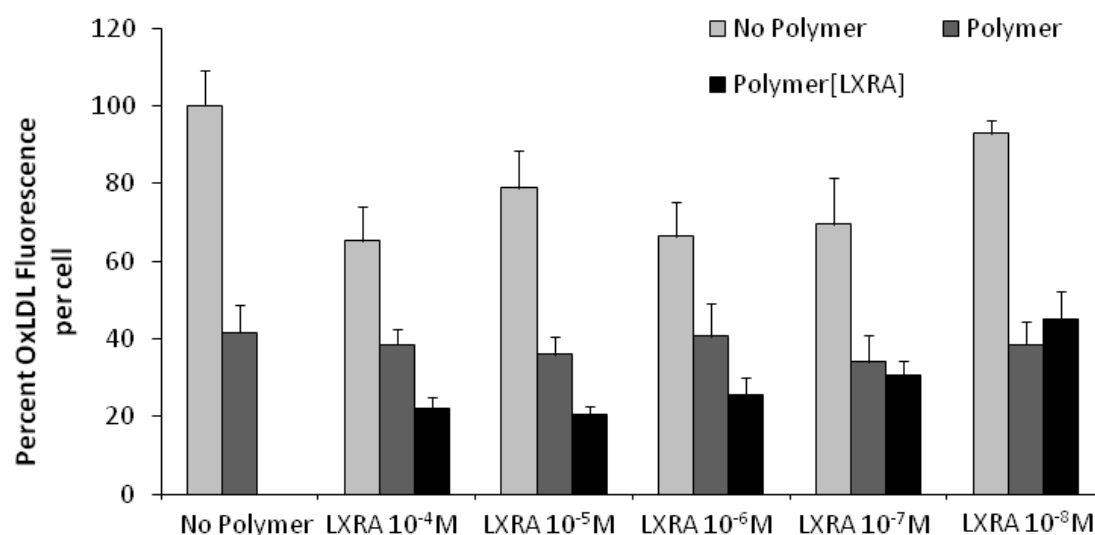


Figure 3.6

The optimal encapsulated GW3965 concentration for oxLDL influx inhibition was determined through comparison of oxLDL uptake at 24 hours by THP-1 cells in RPMI with 5% serum containing encapsulated and non-encapsulated LXRA at concentrations 10^{-4} M - 10^{-8} M with polymer at 10^{-6} M. Uptake of oxLDL in THP-1 macrophage cells was significantly inhibited by encapsulated ligand at 10^{-7} M and higher. When GW3965 was delivered to cells at 10^{-8} M it no longer showed oxLDL inhibition efficacy to a greater extent than the polymer alone.

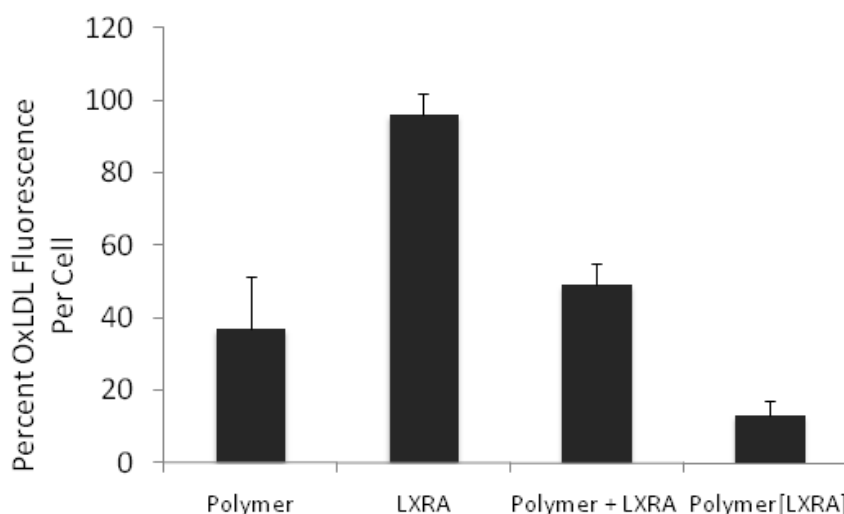


Figure 3.7

The efflux of oxLDL from macrophage cells was assayed following pre-incubation of fluorescently labeled oxLDL (10 $\mu\text{g/mL}$) with cells in 5% serum RPMI 1640 for 2 hours at 37 $^{\circ}\text{C}$ and 5% CO_2 . The excess oxLDL was then removed from all conditions and the different test conditions were incubated for 5 hours at 37 $^{\circ}\text{C}$ and 5% CO_2 . Conditions included a control of medium alone, Polymer (10^{-6}M) and LXRA (10^{-7}M) non-encapsulated, and encapsulated Polymer[LXRA] ($10^{-6}\text{M}/10^{-7}\text{M}$). The cells were washed twice with 1xPBS and imaged using a Nikon Eclipse TE2000-S fluorescent microscope. Images were analyzed with Image Pro Plus 5.1 software (Media Cybernetics, San Diego, CA) and cell associated fluorescence was normalized to cell number and compared to the control. Efflux of oxLDL from THP-1 cells displayed trends similar to the oxLDL influx data (Figure 3a). Encapsulated Polymer[LXRA] caused the most significant efflux, 87%, followed by polymer alone and Polymer + LXRA, 63% and 51% respectively, while LXRA alone showed a trivial efflux of 4%.

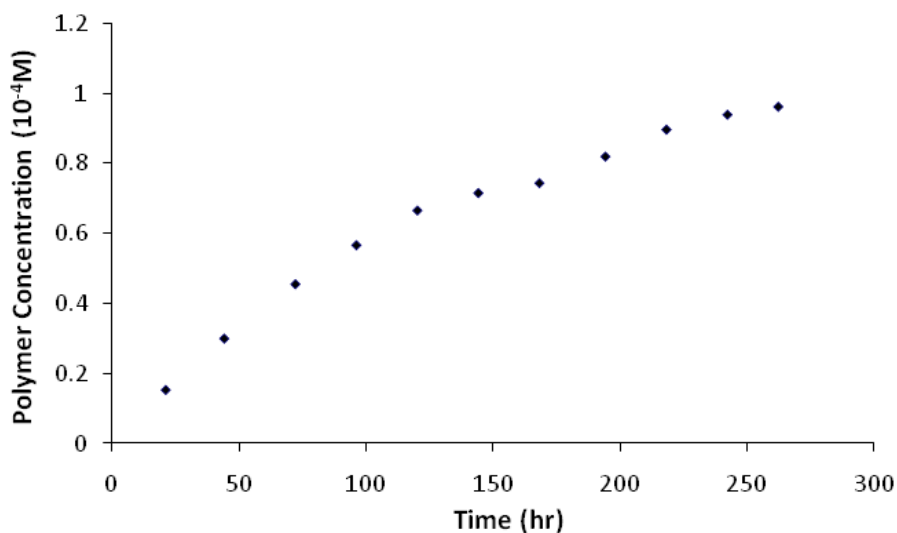


Figure 3.8

Polymer diffusion from a collagen gel was analyzed in order to optimize parameters for *in vivo* delivery of polymer and drug via a collagen adventitial wrap. A Franz diffusion cell with a diffusion area of 0.64 cm^2 and reservoir of 1.5 mL was utilized to determine the concentration of fluorescently tagged polymer released from the gel over 11 days. The gel was created by addition of HEPES buffer, 10x EMEM, 0.1M NaOH, **AAP** in water, and type 1 collagen from calf skin (Elastin Polymer Company, Inc Missouri) in PBS prior to crosslinking in a Spectrolinker XL-1500 UV Crosslinker on a reflective foil surface for 30 min. Parafilm squares, one containing a 2 mm hole and one intact, were placed on either side of the fluorescently-tagged polymer loaded gel before loading into the diffusion cell. A $37\text{ }^{\circ}\text{C}$ water bath was utilized to maintain physiological temperature and samples were taken every 24 hr and analyzed using a CytoFluor multiwell plate reader for fluorescent intensity measurements.

Polymer diffusion from collagen gel showed concentrations above CMC (10^{-7}M) occurred within the first 24 hours and consisted for 14 days.

Chapter 4

Role of Amphiphilic Macromolecules in the Inhibition of Macrophage Inflammatory Responses

4.1 Abstract

The progression of atherosclerosis, the leading cause of death in America, has recently been identified as an inflammatory disease that is not well controlled through current pharmaceuticals. Macrophage cells play a dual role in escalating the progression of atherosclerosis; they trigger atherogenesis through increased lipoprotein uptake and further disease progression through up-regulation and secretion of inflammatory factors. The administration of nanoscale carboxy-terminated amphiphilic polymers to macrophage cells inhibits highly oxidized low density lipoprotein internalization, decreases the activation of matrix metalloproteinase and down-regulates the secretion of inflammatory cytokines. In this study it is shown that the therapeutic effect of the polymers is not solely size, charge or scavenger receptor mediated, but a combination of multiple factors leading to the modulation of macrophage inflammation.

4.2 Introduction

Atherosclerosis, the leading cause of death in America (1), has recently been classified as an inflammatory disease. (27, 158-161) Although the mechanism of inflammation is not fully understood (161), it is established that cytokine secretion, specifically tissue necrosis factor alpha (TNF α) and interleukin 1 beta (IL-1 β), and matrix metalloproteinase (MMP) activation are two important factors in disease progression. (162-164) These macrophage derived cytokines have been shown to correlate with atherosclerosis progression, specifically they have been shown to increase accumulation of cholesterol within cells through increased endothelial cell permeability (165) and decreased adipocyte-derived lipoprotein lipase activity (166); increase white blood cell concentration through altered leukocyte surface adhesion molecule expression (167, 168); increase cell proliferation through up regulation of growth factor production (169); and propagate the inflammatory cycle through further cytokine production (170, 171). Matrix metalloproteinases are believed to promote atherosclerotic plaque rupture by altering and degrading extracellular matrix components, particularly fibrillar collagen, proteoglycan, fibronectin, laminin and elastin. (29, 172) This matrix re-modeling, along with mechanical forces, are the critical instigators of plaque rupture and an acute coronary event. (173-175)

We propose the use of nanoscale carboxy-terminated amphiphilic polymers to down-regulate inflammation by competitively inhibiting the attachment and

internalization of inflammatory mediators by macrophage scavenger receptors. Amphiphilic macromolecules (AMs), composed of a hydrophobic mucic acid backbone and a hydrophilic PEG chain, have been shown to bind to macrophage scavenger receptor A (SR-A) and inhibit binding and internalization of highly oxidized low density lipoprotein (oxLDL). (90, 91) The AMs have also been shown to decrease the accumulation of cholesterol and the recruitment of macrophage cells *in vivo*, two key precursors to the inflammatory cascade, within an injured blood vessel. (145, 146) Due to its proven ability to inhibit oxLDL uptake, it is hypothesized that the addition of AMs will decrease the onset of inflammation by inhibiting small inflammatory particles from attachment and internalization by macrophage cells through SR-A.

4.3 Materials and Methods

4.3.1 Polymer Synthesis and Characterization

1cM

Polymer synthesis was performed by Sarah Sparks in Kathryn Uhrich's laboratory at Rutgers University as previously described. Briefly, mucic acid was acylated with lauroyl chloride in the presence of zinc chloride, which was then esterified with hydroxy-poly (ethylene glycol) (5 kDa) with DCC as the dehydrating reagent and DPTS as the catalyst at room temperature for 48 hours under argon gas. DCU byproduct was removed by vacuum filtration and the filtrate washed with 0.1 N HCl and brine, dried over $MgSO_4$,

and concentrated. The desired product was then precipitated from CH₂Cl₂ by addition of 10-fold diethyl ether and the solid collected by centrifugation. Solvent was removed by decanting and the resulting yellow solid was dried under ambient atmosphere (12 hrs) and under high vacuum (12 hrs). (88)

ocM

Polymer synthesis was performed by Sarah Sparks in Kathryn Uhrich's laboratory at Rutgers University as previously described. 1cM was esterified with N-hydroxysuccinimide with DCC as the dehydrating reagent in anhydrous CH₂Cl₂ and DMF. The reaction was stirred for 24 hours at room temperature under argon gas before DCU byproduct was removed by vacuum filtration and the filtrate washed with 0.1 N HCl and 50:50 brine/H₂O, dried over MgSO₄, and concentrated. The desired product was then precipitated from CH₂Cl₂ by addition of 10-fold diethyl ether and the solid collected by centrifugation. Solvent was removed by decanting and the resulting yellow solid was dried under ambient atmosphere (12 hrs) and under high vacuum (12 hrs). (125)

2cbM

Polymer synthesis was performed by Sarah Sparks in Kathryn Uhrich's laboratory at Rutgers University. The carboxylic acid of 1cM (0.56 g, 0.094 mmol) was activated with SOCl₂ (50 mL) at 90 °C overnight under argon gas. Excess SOCl₂ was removed via rotary evaporation and the yellow oil subsequently dissolved in anhydrous THF (15 mL) and anhydrous pyridine (1 mL). 5-Aminoisophthalic acid (0.14 g, 0.75 mmol) in anhydrous THF

(16 mL) and anhydrous pyridine (2 mL) was then added to the reaction flask and allowed to react for 48 hours at room temperature under argon. THF and pyridine were removed via rotary evaporation and the resulting oil dissolved in CH_2Cl_2 , washed with 1N HCl and brine, dried over MgSO_4 , and concentrated. The desired product was then precipitated from CH_2Cl_2 by addition of 10-fold diethyl ether and the solid collected by centrifugation. Solvent was removed by decanting and the resulting yellow solid was dried under ambient atmosphere (12 hrs) and under high vacuum (12 hrs). Yield: 0.52 g, 91 %. $^1\text{H-NMR}$ (CDCl_3): δ 8.61 (m, 1H, ArH), 8.17 (m, 2H, ArH), 5.70 (m, 2H, CH), 5.20 (m, 2H, CH), 4.24 (m, 2H, CH_2), 3.60 (m, ~ 0.45 kH, CH_2O), 3.38 (s, 3H, CH_3), 2.44 (m, 4H, CH_2), 2.29 (m, 4H, CH_2), 1.60 (m, 8H, CH_2), 1.26 (m, 64H, CH_2), 0.88 (t, 12H, CH_3). $T_m = 56^\circ\text{C}$ GPC: Mw: 6.3 kDa; PDI: 1.09.

4.3.2 Cell Culture

Human THP-1 monocytes (ATCC), were grown in suspension, at a concentration of 100,000 cells/ cm^2 with RPMI medium containing 0.4 mM Ca^{2+} and Mg^{2+} (ATCC) and supplemented with 10 % fetal bovine serum (FBS), in an incubator with 5% CO_2 at 37°C and split every four days through centrifugation. The cells were seeded at a concentration of 100,000 cells/ cm^2 and differentiated from monocytes into adherent macrophage cells by the addition of 16 nM phorbol myristate acetate. (123) Once differentiated, the macrophage cells were not propagated and were used within one week of differentiation.

4.3.3 *LDL Oxidation to hoxLDL*

Highly oxidized LDL (hoxLDL) was prepared by oxidation of LDL within five days of each experiment. BODIPY-labeled human plasma derived LDL (Molecular Probes, OR) was oxidized by incubation with 10 μ M CuSO₄ (Sigma) for 18 hrs at 37 °C with 5% CO₂ before oxidation was stopped with the addition of 0.01% w/v EDTA (Sigma) (13, 14). Characterization of hoxLDL has been previously reported. (91)

4.3.4 *TNF α Cytokine Secretion*

Human THP-1 cells were incubated with lipopolysaccharide (LPS) (100 ng/mL) and test conditions; 2cbM (10⁻⁶M), 1cM (10⁻⁶M), ocM (10⁻⁶M), anti-SRA (10 μ g/mL), Thalidomide (4 μ g/mL), Pluronic (10⁻⁶M), PEG (MW 5000, 10⁻⁶M), PEG-COOH (MW 5000, 10⁻⁶M); for 24 hours in RPMI-1640 with 5% serum. The supernatant was then removed and stored at -20C until testing on TNF-alpha ELISA by Thermo Scientific. Cells were washed and CyQUANT Cell Proliferation Assay by Invitrogen was used to determine cell number per well. Results are quantified as pg TNF α per cell.

4.3.5 *IL-1B Cytokine Secretion*

Human THP-1 cells were incubated with LPS (100 ng/mL) and test conditions; 2cbM (10⁻⁶M), 1cM (10⁻⁶M), ocM (10⁻⁶M), anti-SRA (10 μ g/mL), Thalidomide (4 μ g/mL), β -sitosterol (10⁻⁶M), Pluronic (10⁻⁶M), PEG (MW 5000, 10⁻⁶M), PEG-COOH (MW 5000, 10⁻⁶M); for 48 hours in RPMI-1640 with 5% serum. The supernatant was then removed

and stored at -20°C until testing on IL-1 β ELISA by Thermo Scientific. Cells were washed and CyQUANT Cell Proliferation Assay by Invitrogen was used to determine cell number per well. Results are quantified as pg IL-1 β per cell.

4.3.6 *Matrix Metalloproteinase Secretion*

Human THP-1 cells were incubated with lipopolysaccharide (LPS) (100 ng/mL) and test conditions; 2cbM (10^{-6} M), 1cM (10^{-6} M), ocM (10^{-6} M), anti-SRA (10 μ g/mL), Thalidomide (4 μ g/mL), Pluronic (10^{-6} M), PEG (MW 5000, 10^{-6} M), PEG-COOH (MW 5000, 10^{-6} M); for 24 hours in RPMI-1640 with 5% serum. The supernatant was then removed and stored at -20°C until testing on MMP-9 ELISA by Bender MedSystems. Cells were washed and CyQUANT Cell Proliferation Assay by Invitrogen was used to determine cell number per well. Results are quantified as pg MMP-9 per cell.

4.3.7 *Gene Expression*

The mRNA levels of TNF α were quantified via QRT²-PCR gene expression analysis. The RNA of the samples was extracted with the RNeasy Mini kit from Qiagen. Briefly, cells were lysed with β -mercaptoethanol and QiaShredder before extraction of and purification of the samples. Reverse transcription was performed with a High Capacity cDNA Reverse Transcription Kit from Applied Biosystems. DNA expansion of TNF α was performed with Quantitative RT-PCR conducted on a Roche light cycler 2.0 with β -actin as a housekeeping gene (SA Biosciences, Frederick, MD).

4.3.8 Statistical Analysis

Error bars on graphs indicate standard error of the mean based upon biological triplicate samples in each *in vitro* experiment with three separate experiments for each condition; *in vivo* experiments included two animals per condition with three tissue sections examined per animal. Single factor ANOVA, performed Excel's data package software, was used for statistical analysis. Significance is claimed for differences of $p < 0.05$.

4.4 Results

4.4.1 TNF α Cytokine Secretion

Human macrophage cells incubated with 1cM in conjunction with LPS had significantly lower levels of TNF α secretion (47%) than cells incubated with 2cbM (62%), ocM (123%), anti-SR-A (83%), Thalidomide (70%), and control conditions (Pluronic 125%, PEG 118% and PEG-COOH 99%) in addition to LPS. Refer to fig. 4.1

4.4.2 IL-1 β Cytokine Secretion

Human macrophage cells incubated with 1cM in conjunction with LPS had significantly lower levels of IL-1 β secretion (59%) than cells incubated with 2cbM (76%), ocM (92%), anti-SR-A (92%), Thalidomide (81%), β -Sitosterol (81%) and control conditions (Pluronic 99%, PEG 77% and PEG-COOH 83%) in addition to LPS. Refer to fig. 4.2

4.4.3 Matrix Metalloproteinase Secretion

Human macrophage cells incubated with 1cM in conjunction with LPS had significantly lower levels of MMP-9 secretion (17%) than cells incubated with 2cbM (35%), ocM (45%), anti-SR-A (60%), Thalidomide (80%), and control conditions (Pluronic 69%, PEG 103% and PEG-COOH 123%) in addition to LPS. Refer to fig. 4.3

4.4.4 Gene Expression

The addition of 1cM or 2cbM to inflamed cells caused a two-fold down-regulation of TNF α expression compared to non-treated cells, a significantly greater down regulation than other treatment conditions.

4.5 Discussion

Although inflammation is an integral aspect to the progression of atherosclerosis, the specific mechanism of action is not well understood. (161) Two of the major inflammatory processes of macrophage activation are cytokine secretion and MMP activation. (161-164) We investigated the ability of the nanoscale amphiphilic polymers to modulate macrophage inflammation *in vitro*. The primary goal was to identify the key physiochemical features of the polymers that correlate with enhanced anti-inflammatory effects.

The major finding of this study is that 1cM, a member of a macromolecular library of polymers (see Table 2.1), was most effective at the reduction of both cytokine and MMP-9 secretion in response to LPS stimulation. The 1cM polymer corresponds to a nanoscale carboxy-terminated polymer configuration. The importance of polymer features such as size, amphiphilicity and charge were analyzed. Two PEG chain controls (charged and uncharged) of the same molecular weight as that in 1cM (PEG 5000 Da) were studied and showed that the PEG chain, whether charged or neutral, was not responsible for the inhibitory effects seen with 1cM. A polymer of similar molecular weight and amphiphilicity, Pluronic, was compared to 1cM and it was shown that amphiphilicity alone will not lead to cytokine secretion inhibition. The importance of charge was studied with 2cbM and ocM, polymers from the same library with twice the number of anionic groups and zero anionic groups respectively. The 2cbM was able to significantly inhibit cytokine secretion, but not to the extent of 1cM, while the neutral ocM polymer showed little to no effectiveness in cytokine secretion inhibition. It is therefore determined that a combination of multiple characteristics is responsible for the inhibitory effects of 1cM on cytokine secretion.

It was hypothesized that cytokine secretion would be decreased in the presence of the polymers due to the SR-A binding potential, but in the presence of an SR-A antibody there was not as significant a drop in cytokine secretion as when the 1cM was present. The SR-A antibody did inhibit TNF α secretion by 17% hence it is hypothesized that the SR-A binding capabilities of the polymer are essential, but the additional 36% decrease in TNF α secretion is due to another aspect of 1cM.

The ability of the polymer to inhibit $\text{TNF}\alpha$ and $\text{IL-1}\beta$ secretion was also compared to known anti-inflammatory factors to determine whether the degree of inflammation inhibition was similar. It was shown that the polymer was able to inhibit cytokine secretion more significantly than known anti-inflammatory agents Thalidomide and β -sitosterol, which have been shown to decrease cytokine levels to similar extents as those observed here. (176, 177)

The molecular level to which the polymer inhibits cytokine secretion through blocking gene activation, as opposed to blocking cytokine release from the cells or increasing cytokine digestion, was probed through the quantification of mRNA expression levels. The decrease in $\text{TNF}\alpha$ mRNA shows that the 1cM and 2cbM polymers were capable of inhibiting transcriptional activation of an inflammatory gene related to $\text{TNF}\alpha$ secretion.

Cytokine secretion by macrophage cells is important not only due to its addition to the development and progression of atherosclerosis, but also due to its contribution towards plaque rupture. (178-181) The presence of hoxLDL alone fails to induce MMP-9 secretion by macrophage cells, but the addition $\text{TNF}\alpha$ and hoxLDL together leads to MMP-9 production through a prostaglandin-independent pathway. (182, 183) The AMs provide a two-pronged treatment for MMP-9 secretion; they inhibit macrophage production of $\text{TNF}\alpha$ as well as lowering hoxLDL internalization, (90, 91) down-regulating two essential MMP activating factors.

These findings show that 1cM; through a combination of charge, amphiphilicity, and SR-A binding; significantly decreases $\text{TNF}\alpha$, $\text{IL-1}\beta$ and MMP-9 secretion by human

macrophage cells. Further studies are needed to prove the polymers' efficacy *in vivo*, but *in vitro* data shows the exciting potential of a biocompatible nanoscale anti-inflammatory agent.

4.6 Future Work

Further studies of *in vivo* efficacy are currently underway; a septic shock mouse model is being utilized to examine the role of injected polymers on systemic inflammatory endpoints. The proficiency of 1cM in decreasing lung, liver and arterial tissue damage and cytokine concentration in blood serum will be tested. It is hypothesized that there will be an increase in the time from injury to morbidity in polymer treated mice in comparison to non-treated animals.

4.7 Figures

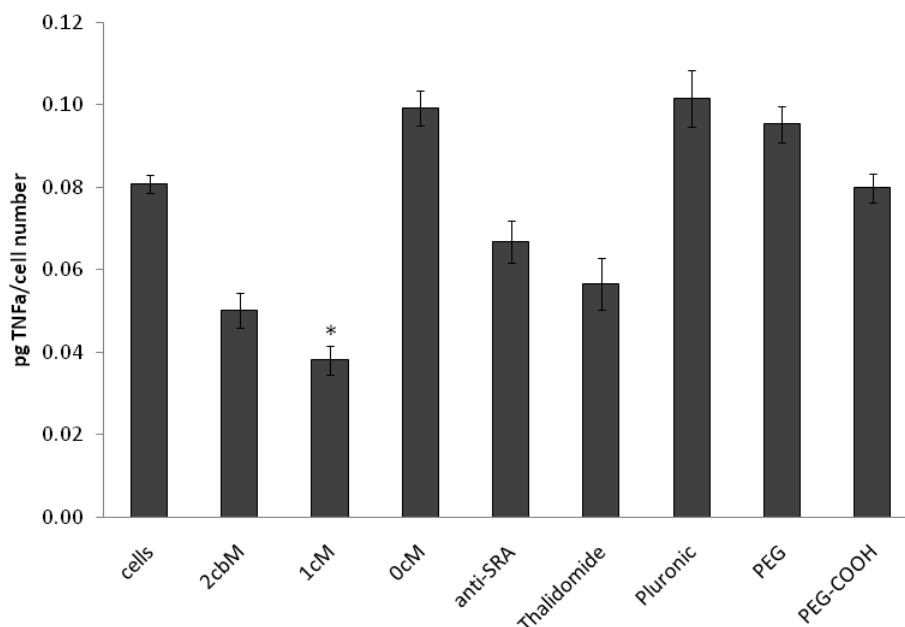


Figure 4.1

Comparative evaluation of the role of nanoscale amphiphilic polymers on tumor necrosis factor-alpha (TNF α) secretion in THP-1 human macrophage cells stimulated with 100 ng/ml LPS in 5% serum and test conditions for 24 hours; 2cbM (10^{-6} M), 1cM (10^{-6} M), 0cM (10^{-6} M), anti-SRA (10 μ g/mL), Thalidomide (4 μ g/mL), Pluronic (10^{-6} M), PEG (MW 5000, 10^{-6} M), PEG-COOH (MW 5000, 10^{-6} M). Cells incubated with 1cM polymer exhibited significantly less TNF α secretion than cells exposed to other treatment and control groups. Conditions not stimulated by LPS did not show detectable TNF α secretion levels and none of the conditions showed significant cell death. Significance is claimed for differences of $p < 0.05$.

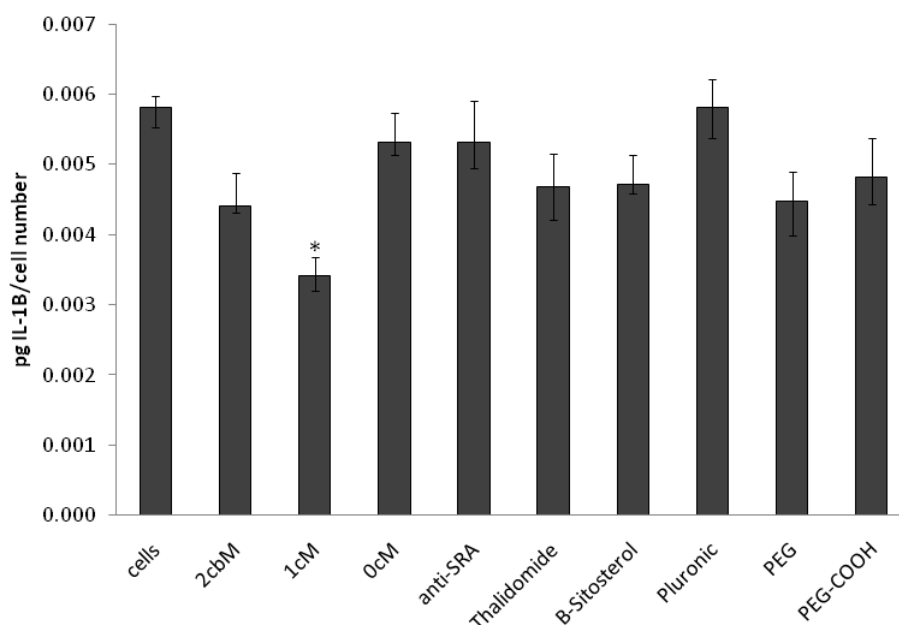


Figure 4.2

Comparative evaluation of the role of nanoscale amphiphilic polymers on interleukin 1 beta (IL-1 β) secretion in THP-1 human macrophage cells stimulated with 100 ng/ml LPS in 5% serum and test conditions for 48 hours; 2cbM (10^{-6} M), 1cM (10^{-6} M), 0cM (10^{-6} M), anti-SRA (10 μ g/mL), Thalidomide (4 μ g/mL), β -sitosterol (10^{-6} M), Pluronic (10^{-6} M), PEG (MW 5000, 10^{-6} M), PEG-COOH (MW 5000, 10^{-6} M). Cells incubated with 1cM polymer exhibited significantly less IL-1 β secretion than cells exposed to other treatment and control groups. Conditions not stimulated by LPS did not show detectable IL-1 β secretion levels and none of the conditions showed significant cell death. Significance is claimed for differences of $p < 0.05$.

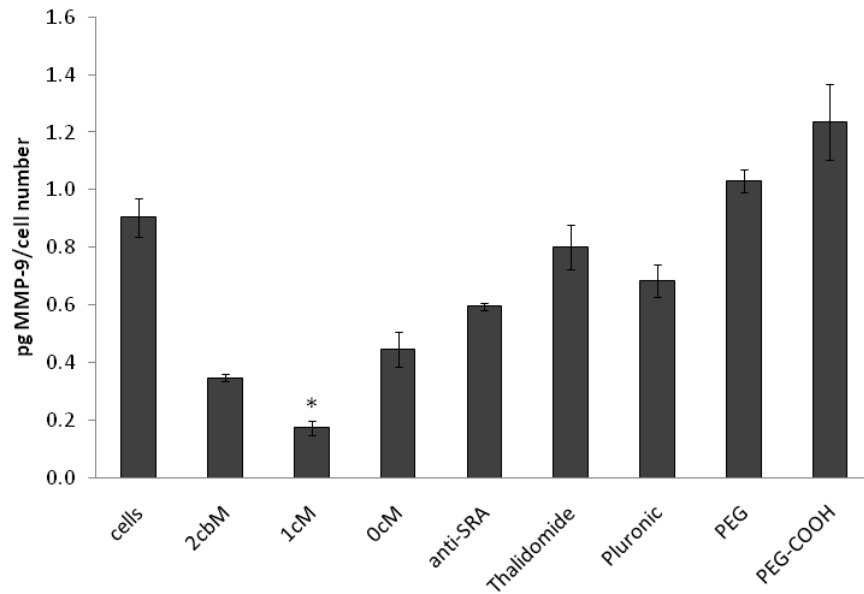


Figure 4.3

Concentration of matrix metalloproteinase secreted from THP-1 human macrophage cells over a 24 hour period of LPS (100 ng/mL) treatment in RPMI-1640 with 5% serum; 2cbM (10^{-6} M), 1cM (10^{-6} M), 0cM (10^{-6} M), anti-SRA (10 μ g/mL), Thalidomide (4 μ g/mL), Pluronic (10^{-6} M), PEG (MW 5000, 10^{-6} M), PEG-COOH (MW 5000, 10^{-6} M). Cells incubated with 1cM polymer exhibited significantly less MMP-9 secretion than cells exposed to other treatment and control groups. Conditions not stimulated by LPS did not show detectable MMP-9 secretion levels and none of the conditions showed significant cell death. Significance is claimed for differences of $p < 0.05$.

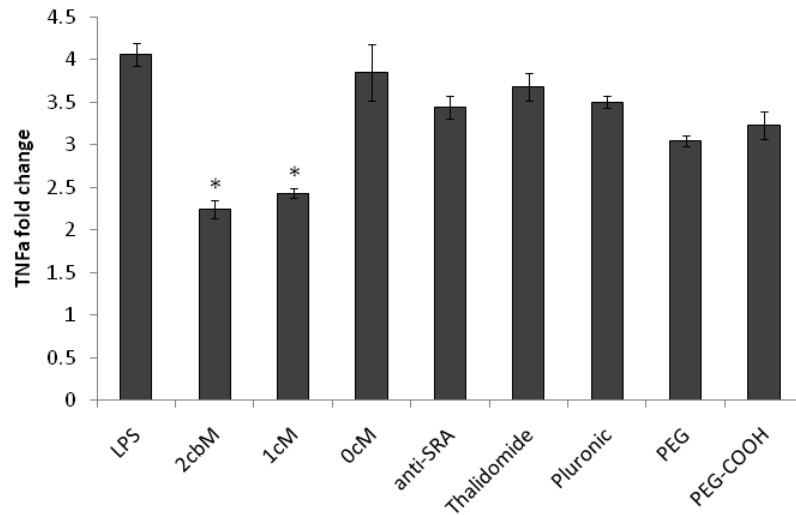


Figure 4.4

TNF α gene expression of human macrophage cells exposed to LPS (100 ng/mL) for 24 hours in RPMI-1640 with 5% serum; 2cbM (10^{-6} M), 1cM (10^{-6} M), ocM (10^{-6} M), anti-SRA (10 μ g/mL), Thalidomide (4 μ g/mL), Pluronic (10^{-6} M), PEG (MW 5000, 10^{-6} M), PEG-COOH (MW 5000, 10^{-6} M); fold change is in comparison to cells not inflamed by LPS with β -actin as the housekeeping gene. Cells incubated with 1cM or 2cbM polymer exhibited significantly less TNF α gene expression than cells exposed to other treatment and control groups. Significance is claimed for differences of $p < 0.05$.

Chapter 5

Conclusions and Future Directions

5.1 Conclusions

This thesis focused on the inhibition of atherosclerotic and inflammatory progression through the administration of nano-scale assembled polymers. The complex confluence of atherogenesis and inflammation poses a major challenge to the treatment of cardiovascular disease.

We investigated the role of nano-assembled polymers in the basic cholesterol dynamics underlying atherosclerosis. Three serial studies were designed. First we investigated the role of multiple polymer compositions on the efficacy of inhibition of hoxLDL uptake in macrophages *in vitro*. Various polymer design parameters included altering the length of the PEG chain, carboxylic acid location, type of anionic charge, number of anionic charges, rotational motion of the anionic group, and PEG architecture, to determine optimal hoxLDL inhibition characteristics. The rigid, hydrophobic carboxylic acid and 5 kDa linear PEG chain polymer 1cM was observed to have the most pronounced effects. Next, we exploited the amphiphilic nature of the polymers and investigated the concerted application of an LXR agonist along with the nanopolymers. The two pronged treatment of atherosclerosis through polymer encapsulated ligand delivery resulted in an 88% inhibition of hoxLDL accumulation within human macrophage cells and the rescue of injured carotid artery tissue to a non-injured physiology. The third phase of this work displayed the *in vitro* inhibition of

inflammatory cytokines and matrix metalloproteinase through the administration of 1cM polymers.

This thesis demonstrates the multifunctional potential of the AM polymers for treatment of vascular atherogenesis and inflammation. Through hoxLDL inhibition, drug delivery and anti-inflammatory activities the polymer can alter multiple aspects of the cardiovascular disease states as well as other inflammatory diseases. Ideas related to these prospective directions are highlighted in this chapter.

5.2 Future Directions

5.2.1 Polymer Mechanism of Action

Although the role of the AM polymers in hoxLDL uptake by macrophage cells was identified, further insights are necessary to establish the specific mechanism of action, particularly with regard to drug delivery and the attenuation of inflammation. The attachment kinetics and internalization behaviors of AMs, mediated largely by scavenger receptors, needs to be further correlated with the chemistry and architecture of the polymers. A possible method to investigate polymer attachment kinetics is to use genetically engineered cells that express only SR-A and measure polymer concentration in solution and on cell surface over time. Techniques such as quantitative fluorometry or total internal reflection fluorescence (TIRF) could be used to quantify the polymer/receptor binding kinetics to cell surfaces. Two possible methods of polymer internalization can also be studied, SR-A attachment and non-specific internalization.

The addition of a fluorescently tagged polymer to SR-A expressing cells followed by the addition of an extracellular quenching agent could show the polymer internalization. The non-specific internalization of polymers, through pinocytosis or clathrin coated pits, can be determined by using non-scavenger receptor expressing cells and tagged polymer. Once internalization kinetics are determined for SR-A binding, additional cell surface receptors can be tested in a similar manner, showing the optimal polymer architecture for different receptors and allowing for the design of polymers for tissue specific delivery. Due to polymer tunability, conjugation of a targeting group to the polymer also provides the opportunity to target specific tissue or cell types (e.g. endothelial cells) and perhaps specific disease states.

5.2.2 *Polymer and Drug Delivery*

Despite the success of our early *in vivo* model; the current *in vivo* delivery methods are not feasible for translation to clinical practice. There are many possible peritoneal methods; catheter placement, drug eluting stent, and injections; but non-invasive methods, including ingestion and inhalation, are much more convenient and lead to better extended use and patient compliance. (184, 185) Effective and advantageous delivery methods can be determined through polymer stability and viability testing. Polymer attachment to cells under flow conditions needs to be tested to determine whether systemic delivery is possible or if the polymer needs to be in a non-flow, purely diffusion driven model to bind to and alter cell function. Two possible ways to test polymer attachment under flow are through the use of quartz crystal

microbalance (QCM) or surface plasmon resonance (SPR). In the current research the polymers have not been challenged with the extremely low pH of gastric acid in the stomach; it is yet to be determined if AM characteristic properties will be altered under these harsh conditions. Another important aspect is polymer clearance from the body. If the liver and kidneys filter large polymer concentrations from the bloodstream, then it will be difficult for an effective dose to reach the area of interest. *In vivo* fluorescent imaging of animals injected with tagged polymers will be necessary (these studies are currently being planned in the Moghe lab) to track the concentration of polymers in different tissues throughout the body. This data combined with the polymer kinetics data will determine whether the polymer is in the bloodstream or tissue of interest for a long enough time period to treat the desired disease.

As candidates for a drug delivery vehicle it is also important that the AM's mechanism of drug delivery to intracellular regions is modeled. By utilizing a pH sensitive tag the encapsulated drug can be monitored within the cell and its pathway determined, either through acidic lysosomes or other vesicles.

5.2.3 Polymer Treatment of Multiple Disease Models

The development of non-invasive delivery mechanisms of the AMs will allow for the treatment of many chronic inflammatory diseases such as rheumatoid arthritis, psoriasis, inflammatory bowel disease and chronic obstructive pulmonary lung disease. The polymers were shown to inhibit three atherosclerosis associated inflammatory factors, but could potentially decrease the progression of other inflammatory

conditions. The anti-inflammation and drug encapsulation capabilities of the polymers could combine to provide a new treatment option for the many non-controlled inflammatory diseases.

This polymer also allows for a disease treatment modality primarily based on its size. Passive targeting of nanoparticles to cancerous tumors due to the gaps found in angiogenic blood vessels (186, 187) is known as the enhanced permeability and retention effect (ERP). (188-191) The poor lymphatic draining system of tumors (187, 192-194) couples with leaky vessels and allows for an accumulation of nano-scale particles within the growing tissue. (195) By encapsulating anti-cancer drugs within these polymers it may be possible to deliver high concentrations of the toxic treatments to tumor cells and have minimal exposure to other healthy tissue.

Appendix

Appendix A

Nanoscale Amphiphilic Macromolecules as Lipoprotein Inhibitors The Role of Charge and Architecture

This chapter was published in the journal International Journal of Nanomedicine, 2(4):697-705. 2007 coauthored by J.Z. Wang, N. Plourde, N. Iverson, P.V. Moghe, and K.E. Uhrich.

A.1 Abstract

A series of novel amphiphilic macromolecules composed of alkyl chains as the hydrophobic block and poly(ethylene glycol) as the hydrophilic block were designed to inhibit highly oxidized low density lipoprotein (hoxLDL) uptake by synthesizing macromolecules with negatively charged moieties (carboxylic acids) located in the two different blocks. The macromolecules have molecular weights around 5,500 g/mol, form micelles in aqueous solution with an average size of 20–35 nm, and display critical micelle concentration values as low as 10^{-7} M. Their charge densities and hydrodynamic size in physiological buffer solutions correlated with the hydrophobic/hydrophilic block location and quantity of the carboxylate groups. Generally, carboxylate groups located in the hydrophobic block destabilize micelle formation more than carboxylate groups in the hydrophilic block. Although all amphiphilic macromolecules inhibited unregulated uptake of hoxLDL by macrophages, inhibition efficiency was influenced by the quantity and location of the negatively charged-carboxylate on the macromolecules. Notably, negative charge is not the sole factor in reducing hoxLDL uptake. The combination of

smaller size, micellar stability and charge density is critical for inhibiting hoxLDL uptake by macrophages.

A.2 Introduction

Atherosclerosis is a process characterized by the buildup of low density lipoproteins (LDL) within the vascular intima and ensuing interactions between macrophages and their extracellular matrix molecules; it is the single leading cause of death in America. (196-199) Recent advances in nanotechnology for cardiovascular health are abundant and include the application of nanosensors to monitor nitro-oxidative species (oxidative stress) produced in the failing heart (200), microarrays or microchips for the study of cardiovascular disease(201), electrospun nanofibers as tissue engineered vascular grafts (202-204), and carbon nanotubes implanted for anticoagulant and antithrombotic properties. (205, 206) In contrast to the implantable devices described above, an avenue of particular interest in nanotechnology is the use of a “nano-blocker” to prevent highly oxidized LDL (hoxLDL) uptake via scavenger receptors. Native LDL uptake is mediated by feedback inhibition, whereas binding of hoxLDL to macrophage scavenger receptors leads to unregulated cholesterol accumulation and foam cell formation. Thus, controlling binding to hoxLDL is an important focus for new atherosclerotic treatments. (19, 140)

Previous work on LDL uptake has focused on synthetic compounds that target and bind scavenger receptors, such as SR-A and CD36 that appear to be of primary importance in atherogenesis. (207-210) For example, phosphocholine as a ligand for CD36 has been shown to inhibit the binding of hoxLDL in CD36-expressing cells. (208) In addition, sulfatide derivatives for targeting SR-A have been shown to reduce

acetylated LDL binding and uptake. (207) Although previous efforts to develop scavenger receptor blockers are encouraging, increased efficiency may be reached through the use of an organized 3D presentation of the targeting groups or a multifunctional particle to simultaneously target several scavenger receptors. (90) To create a multifunctional nano-blocker, one could exploit the fact that all scavenger receptors share an affinity for anionic ligands. (211)

We previously reported a unique series of polymers, amphiphilic scorpion-like macromolecules (AScM), (88) that self-organize into micelles and not only act as a drug delivery system but also decrease hoxLDL's uptake. Previous results show promise for AScMs as a hydrophobic drug carrier in terms of low CMC (critical micelle concentration), low cytotoxicity, high drug loading efficiency, and sustained release. (124, 127) These macromolecules consist of three major components: poly(ethylene glycol) (PEG), mucic acid, and aliphatic acid chains, as seen in Figure 1. (88) These building blocks were chosen because they are naturally occurring or biocompatible compounds, and each component is joined by potentially biodegradable ester bonds. PEG contributes to the hydrophilicity and is used to prevent the non-specific adsorption of proteins, mucic acid is a multi-hydroxylated saccharide providing reaction sites for further modification of the polymer, and aliphatic acid chains control the polymer hydrophobicity.

Previous studies have focused on anionic AScMs that spontaneously form micelles at concentrations above the CMC (10^{-7}M). (88) Each AScM is functionalized with a carboxylic acid, such that the micellar nanoparticle displays anionic charges in an

organized and clustered configuration. The anionic AScMs reduced hoxLDL uptake by up to 80%, and both SR-A and CD36 receptors were involved in the uptake of the polymers and hoxLDL. (89, 90)

In this paper, we present a series of macromolecules that maintain two structural elements as previously described: mucic acid derivatives as the hydrophobic component and PEG as the hydrophilic component. For this investigation, the location and number of carboxylic acid groups were varied with our synthetic design; carboxylate groups can be precisely located in either the hydrophobic or hydrophilic domains, or in both domains (Figure 2).

The inhibition ability of these novel macromolecules for highly oxidized LDL by macrophages were studied as well as their solution properties, including micelle aggregation size, CMC and charge density.

A.3 Methods

A.3.1 Chemical reagents for synthesis

Heterobifunctional poly(ethylene glycol) (HCl·NH₂-PEG-COOH) with molecular weight of 5000 Da was obtained from Nektar (San Carlos, CA). 4-(Dimethylamino) pyridinium *p*-toluenesulfonate (DPTS) was prepared as previously described. Monomethoxy-poly(ethylene glycol) (mPEG) with molecular weights of 5000 Da was purchased from Sigma-Aldrich. All PEG reagents were dried by azeotropic distillation with toluene. β -Glutamic acid, 5-aminoisophthalic acid, 4-hydroxybenzoic acid, N-

hydroxyl succinimide (NHS), triethylamine (99.7%) and 1,3-dicyclohexylcarbodiimide (DCC) in 1 M methylene chloride solution were purchased from Aldrich and used as received. All other reagents and solvents were reagent grade and used as received.

A.3.2 *Macromolecules 1CM, oCM and 1CP*

The macromolecules **1CM**, **oCM** and **1CP** were prepared as previously described. (88, 90)

A.3.3 *Chemical characterization*

Chemical structures and compositions were confirmed by ^1H and ^{13}C NMR spectroscopy with samples (~5–10 mg/mL) dissolved in CDCl_3 solvent on Varian 400 MHz spectrometers, using tetramethylsilane as the reference signal. IR spectra were recorded on a Mattson Series spectrophotometer (Madison Instruments, Madison, WI) by solvent (methylene chloride) casting on a KBr pellet. Negative ion-mass spectra were recorded with a ThermoQuest Finnigan LCQTM_{DUO} System (San Jose, CA) that includes a syringe pump, an optional divert/inject valve, an atmospheric pressure ionization (API) source, a mass spectrometer (MS) detector, and the Xcalibur data system. Meltemp (Cambridge, Mass) was used to determine the melting temperatures (T_m) of all the intermediates.

Gel permeation chromatography (GPC) was used to obtain molecular weight and polydispersity index (PDI). It was performed on Perkin-Elmer Series 200 LC system equipped with PL gel column (5 μm , mixed bed, ID 7.8 mm, and length 300 mm) and

with a Water 410 refractive index detector, Series 200 LC pump and ISS 200 Autosampler. Tetrahydrofuran (THF) was the eluent for analysis and solvent for sample preparation. Sample was dissolved into THF (~5 mg/mL) and filtered through a 0.45 μ m PTFE syringe filter (Whatman, Clifton, NJ) before injection into the column at a flow rate of 1.0 mL/min. The average molecular weight of the sample was calibrated against narrow molecular weight polystyrene standards (Polysciences, Warrington, PA).

A.3.4 Synthesis of 1CM1CP

Mucic acid lauroyl derivative (**1**) was prepared as previously described. (88) Compound **1** (0.47 g, 0.50 mmol) was mixed with thionyl chloride (20 ml, 270 mmol) and heated to reflux temperature for 4 hours. After cooling to room temperature, the excess thionyl chloride was removed by rotary evaporation. The acyl chloride intermediate was dissolved in 5.0 ml anhydrous methylene chloride solution with 2.0 ml pyridine. Heterobifunctional poly(ethylene glycol) (HCl·NH₂-PEG-COOH) (M_w = 5.0 kDa) (0.50 g, 0.10 mmol) in 5.0 ml methylene chloride solution was added drop wise over 2 min. After 24 hours stirring at room temperature, the reaction mixture was acidified by 0.1 N HCl aqueous solution (10 ml \times 2) and washed by brine (10 ml). The organic portion was dried over sodium sulfate, concentrated by rotary evaporator and added into diethyl ether (60 ml) to precipitate the product.

1CM1CP was obtained as white waxy solid. 0.52 g, 86% yield. ¹H NMR (CDCl₃) (δ): 5.59 (d, 1H, CH), 5.62 (d, 1H, CH) 5.21 (m, 1H, CH), 5.02 (m, 1H, CH), 3.64 (m, ~0.4kH, CH₂ on PEG), 2.38 (t, 4H, CH₂), 2.21 (t, 4H, CH₂), 2.57 (t, 2H, CH₂-COOH of

PEG), 1.61 (m, 4H, CH₂), 1.51 (m, 4H, CH₂), 1.25 (m, 48H, CH₂), 0.88 (t, 12H, CH₃). IR (KBr, cm⁻¹): 2911 (C-H), 1754 (C = O), 1250, 1105, (C-O). T_m: 58.0–59.5 °C; GPC: M_w: 5500; PDI: 1.1.

A.3.5 Synthesis of 1BM

Molecule **1** (0.94 g, 1.0 mmol) was mixed with thionyl chloride (20 ml, 270 mmol) and heated to reflux temperature for 4 hours. After cooling to room temperature, the excess thionyl chloride was removed by rotary evaporation. A solution of anhydrous THF (10 ml) and pyridine (5.0 ml) was added to the reaction mixture. 4-Hydroxybenzoic acid (0.55 g, 4.0 mmol) dissolved in THF (5.0 ml) was added drop wise over 2 min at 0 °C. The reaction was warmed to room temperature and stirred for 6 hours. The reaction was quenched by adding 1 N HCl (400 ml) to the reaction mixture. The solid was collected by vacuum filtration and obtained as intermediate product, **2**.

Intermediate **2** was obtained as white solid, 0.89 g, 75% yield. ¹H NMR (CDCl₃) (d): 8.02 (d, 4H, ArH), 6.95 (d, 4H, ArH), 5.59 (m, 2H, CH), 4.94 (m, 2H, CH), 2.32 (m, 8H, CH₂), 1.49 (m, 8H, CH₂), 1.25 (m, 48H, CH₂), 0.86 (t, 12H, CH₃). IR (KBr, cm⁻¹): 2930 (C-H), 1752 (C = O), 1250, 1148 (C-O), 742 (Aromatic C-C). T_m: 154.5–156.5 °C. FW: 1167; MS: 1165.5.

Intermediate **2** (0.59 g, 0.50 mmol), mPEG (M_w = 5.0 kDa, after azeotropic distillation) (0.50 g, 0.10 mmol) and DPTS (0.16 g, 0.50 mmol) were dissolved in methylene chloride (10 ml) and DMF (1.5 ml) solution. 1 M DCC in methylene chloride solution (1.0 ml, 1.0 mmol) was added slowly. After 24 hours stirring at room

temperature, the side product was removed by filtration. The organic solution was washed by 0.1 N HCl aqueous solution (10 ml \times 2) and brine (10 ml). The organic portion was dried over sodium sulfate and concentrated by rotary evaporator. Diethyl ether (15 ml) was added to precipitate the product 1BM. Additional ethyl ether (15 ml \times 2) was used to wash the product.

1BM was obtained as white waxy solid. 0.54 g, 88% yield. ^1H NMR (CDCl_3) (d): 8.00 (d, 4H, ArH), 6.93 (d, 4H, ArH), 5.60 (m, 2H, CH), 4.94 (m, 2H, CH), 2.31 (m, 8H, CH_2), 1.47 (m, 8H, CH_2), 1.25 (m, 48H, CH_2), 0.88 (t, 12H, CH_3). IR (KBr, cm^{-1}): 2956 (C-H), 1755 (C = O), 1258, 1106 (C-O), 733 (Aromatic C-C). T_m : 55.4–56.5 $^\circ\text{C}$. GPC: M_w : 5500; PDI: 1.2.

A.3.6 *Synthesis of 2CM*

Compound 1CM (0.60 g, 0.10 mmol; after azeotropic distillation with toluene) and NHS (0.50 g, 0.43 mmol) were dissolved in 20 ml methylene chloride and DMF (0.8 ml). DCC in methylene chloride (0.50 ml, 0.50 mol) was added drop wise under argon. After 12 h, the side product was removed by vacuum filtration. The isolated solution was directly reacted with β -glutamic acid (0.020 g, 0.43 mmol) in the present of triethylamine (1.0 ml, 7.0 mmol). After 8 hours, the reaction mixture was washed by 0.1 N HCl aqueous solution (10 ml \times 2), brine (10 ml), dried over sodium sulfate and concentrated by rotary evaporator. Diethyl ether (15 ml) was added to precipitate the product 2CM.

2CM was obtained as white waxy solid. 0.43 g, 71% yield. ^1H NMR (CDCl_3) (δ): 5.62 (m, 2H, CH), 5.08 (m, H, CH), 3.66 (m, $\sim 0.4\text{kHz}$, CH_2 on PEG), 2.38 (t, 4H, CH_2), 2.21 (t, 4H, CH_2), 1.61 (m, 4H, CH_2), 1.51 (m, 4H, CH_2), 1.25 (m, 48H, CH_2), 0.88 (t, 12H, CH_3). IR (KBr, cm^{-1}): 2925 (C-H), 1750 (C = O), 1229, 1146 (C-O). T_m : 54.6–55.2 $^\circ\text{C}$. GPC: M_w : 5500; PDI: 1.2.

A.3.7 Synthesis of oBM

Compound 1CM (0.60 g, 0.10 mmol; after azeotropic distillation with toluene), DPTS (0.31 g, 1.0 mmol) and p-phenetidine (0.80 ml, 1.0 mmol) were dissolved in methylene chloride (20 ml). DCC in methylene chloride (0.20 ml, 0.20 mol) was added drop wise under argon. After 12 h, the side product was removed by vacuum filtration. The organic portion was washed by 0.1 N HCl solution (10 ml \times 2), brine (10 ml), dried over sodium sulfate and concentrated under rotary evaporator. Diethyl ether (15 ml) was added to precipitate the product.

oBM was obtained as white waxy solid. 0.56 g, 92% yield. ^1H NMR (CDCl_3) (δ): 7.21 (d, 2H, ArH), 6.71 (d, 2H, ArH), 5.78 (d, 1H, CH), 5.49 (d, 1H, CH), 5.38 (m, 1H, CH), 4.95 (m, 1H, CH), 3.66 (m, $\sim 0.4\text{kHz}$, CH_2 on PEG), 2.38 (t, 4H, CH_2), 2.21 (t, 4H, CH_2), 1.61 (m, 4H, CH_2), 1.51 (m, 4H, CH_2), 1.25 (m, 48H, CH_2), 0.88 (t, 12H, CH_3). IR (KBr, cm^{-1}): 2917 (C-H), 1737 (C = O), 1250, 1120 (C-O), 780 (Aromatic C-C). T_m : 55.5–57.2 $^\circ\text{C}$. GPC: M_w : 5500; PDI: 1.2.

A.3.8 Dynamic light scattering study

Dynamic light scattering (DLS) analyses were performed using a Malvern Instruments Zetasizer Nano ZS-90 instrument (Southboro, MA), with reproducibility being verified by collection and comparison of sequential measurements. Polymer solutions (1.0 wt %) in phosphate buffered aqueous solution (PBS) (pH 7.4) were prepared. Measurements were performed in triplicate at a 90° scattering angle at 25 °C. Z-average sizes and standard deviation of polymers in solution were collected and analyzed.

A.3.9 Fluorescence spectroscopy

Critical micelle concentration (CMC) measurements were carried out on a Spex fluoroMax (Piscataway, NJ) spectro-fluorometer at 25 °C. Using pyrene as the probe molecule, a stock solution at 5.00×10^{-7} M in pH 7.4 PBS solution was prepared. Polymer samples were dissolved in the stock pyrene solutions then diluted to specific concentrations. Excitation was performed from 300 nm to 360 nm, using 390 nm as the emission wavelength. Pyrene maximum absorption shifted from 332 nm to 334.5 nm upon secondary micelle formation. The ratio of absorption of polymer (334.5 nm) to pyrene only (332 nm) was plotted as the logarithm of polymer concentrations. The inflection point of the curves was taken as CMC.

A.3.10 Zeta potential

Charge densities of all polymeric micelle solutions were measured by the zeta potential method using a Malvern Instruments Zetasizer Nano ZS-90 instrument (Southboro, MA), with reproducibility verified by collection and comparison of sequential measurements. Instrument settings and calculation parameters were defined as temperature at 25 °C, dispersant viscosity at 0.89 cP and dielectric constant of 78.5. The viscosity of the samples was estimated to be that of water. All the samples measured were prepared at 10^{-4} M in PBS solution (pH 7.4).

A.3.11 Preparation of micelles for in vitro testing

Micelles were freshly prepared and used within 7 days at 10^{-4} M in serum-free RPMI medium (without FBS). The micelles were then combined with serum-free RPMI and/or hoxLDL to create a final macromolecule concentration of 10^{-6} M.

A.3.12 Lipoprotein model: LDL oxidation

Highly oxidized LDL (hoxLDL) was prepared within five days of each experiment. BODIPY-labeled and unlabeled human plasma derived LDL (Molecular Probes, OR) was oxidized for 18 hours in the presence of 10 μ M CuSO_4 (Sigma) at 37°C and 5% CO_2 . (13, 14) The oxidation was stopped with 0.01% w/v EDTA. Thiobarbituric acid reactive substances (TBARS), lipid hydroperoxide (LPO), conjugated dienes, and electrophoretic mobility (with the help of Dr. Schaich) was performed to ensure accurate and consistent oxidation levels were attained.

A.3.13 LDL internalization

The internalization of hoxLDL by macrophage cells was assayed by incubating fluorescently labeled hoxLDL (10 µg/mL) with IC21 macrophages for 24 hours at 37 °C and 5% CO₂. The cells were then washed twice with serum-free RPMI medium. The cell-associated fluorescence was measured by acquiring images on a confocal microscope (Sun Microsystems, Santa Clara, CA) and quantifying the fluorescence intensity using Image Pro Plus 5.1 software (Media Cybernetics, San Diego, CA) and normalized to cell number.

A.3.14 Cell culture

IC21 macrophages, a well established differentiated murine cell line acquired from ATCC, were used for all studies. The cells have morphology and structure comparable to that of freshly isolated activated mouse peritoneal macrophages, and have demonstrated LDL receptor activity. (212) IC21 cells degrade acetylated LDL and thus an acceptable model for the study of cholesterol and lipoprotein metabolism by macrophages. These cells are an economical alternative to freshly isolated mouse peritoneal macrophages. The cells were propagated with RPMI media containing 0.4 mM Ca²⁺ and Mg²⁺, (ATCC) and supplemented with 10% fetal bovine serum (FBS). The cells were maintained in an incubator with 5% CO₂ at 37 °C and harvested prior to reaching confluence. All cell assays were performed in triplicate.

A.4 Results

A.4.1 *Synthesis of the macromolecules*

Several different amphiphilic macromolecules were synthesized in which the number and location of carboxylate groups were modified (Figure 3).

The 1CM, oCM and 1CP were prepared as described in previous work. (90) The design rationale for each macromolecule is as follows. 1CM1CP probes the combinatorial activity of a carboxylic acid present in both the hydrophilic and hydrophobic blocks of AScMs. It was successfully synthesized by coupling (NH₂-PEG-COOH) with mucic acid acyl derivatives (1) activated as acyl chloride. 1BM was prepared to investigate any differences between aliphatic and aromatic carboxylates, in this molecule, carboxylates are located in the hydrophobic domain. Our first attempt to generate an aromatic carboxylate group was not successful; we attempted to couple molecule 1CM directly with 4-hydroxybenzoic acid. However, the low nucleophilicity of the phenol yielded unacceptably low coupling efficiencies. Instead, we prepared the symmetric intermediate (2), which was easy to purify and then successfully coupled with mPEG-OH (5k) to obtain 1BM. The macromolecule oBM was prepared as a control for 1BM and synthesized through direct esterification of the carboxylate on polymer 1CM. 2CM was designed to study how two carboxylates in the hydrophobic block may synergistically influence hoxLDL uptake. Overall, all coupling reactions were achieved in reasonably high coupling efficiency and high yield. All seven macromolecules displayed a comparable molecular weights (~5500) and melting temperatures (~56 °C).

A.4.2 *Physical properties of the AScMs*

The molecules are similar in size (23–27 nm) in aqueous media (Table 1) except for 2CM, which is slightly larger (~35 nm), and all macromolecules display mono-modal size distributions. The CMC values are in similar range, again with the exception of 2CM, which has the highest CMC value (1.8×10^{-6} M); the CMC values is approximately 7 times larger than the CMC of 1CM, for example.

With respect to charge density, the polymers oCM and oBM are charge neutral yet still register slightly negative zeta potential values (Table 1). 1CM, 1CP and 2CM, display a similar zeta potential value (~ -10mV). Solutions of 1CM1CP display the most negative zeta potential (~ -20 mV), which is double the values for 1CM, 1CP and 2CM.

A.4.3 *Highly-oxidized LDL uptake inhibition studies*

At 24 hours, hoxLDL uptake in macrophages was significantly reduced in the presence of the anionic nano-sized micelles, namely 1CM, 1CP, 1CM1CP, 2CM and 1BM (Figure 4). The degree of uptake was normalized to controls without polymers present; positive controls included the neutral micelles (oCM and oBM). Among the effective hoxLDL uptake inhibitors, the 1CM1CP micelles resulted in the highest inhibition of hoxLDL uptake, reducing hoxLDL internalization more significantly ($p < 0.05$) than all the other polymer micelles.

A.5 Discussion

A.5.1 *Synthesis and solution-based properties*

Micelle formation and nanoscale size are both important in hoxLDL inhibition; our hypothesis about the macrophage receptors is that they are slightly positively charged, such that nanoscale micelles with a high density of negative charges are more accessible via electrostatic interactions.

All seven amphiphilic macromolecules self-organized to form micelles in aqueous solutions, as indicated by the CMC values near 10^{-6} to 10^{-7} M. The critical micelle concentration (CMC) is a crucial parameter that measures the stability of amphiphiles. All amphiphilic macromolecules have relatively low CMC values (from 10^{-6} to 10^{-7} M), a critical characteristic for biological applications as low CMC values indicate higher stability upon dilution in blood plasma. Most of the AScMs have similar CMC values, indicating that a single negative charge does not prevent self-aggregation into micelles at pH 7.4. Notably, molecule 2CM has a relatively higher CMC value compared to the other macromolecules. Two aliphatic carboxylate groups on hydrophobic domain of polymeric micelles appear to slightly inhibit micelle formation, possibly due to the repulsion between adjacent negative charges formed in slightly basic (pH 7.4) solution.

Similar to the CMC data, molecule 2CM displays different behavior than the other macromolecules in terms of size. The micellar sizes of all AScMs, except 2CM, are approximately 20 nm (table 1), indicating that a single negative charge does not change

the micelle aggregation size. In contrast, molecule 2CM is larger in size (35 nm) than the other macromolecules. Compared with the other macromolecules, 2CM is relatively less hydrophobic due to the presence of two carboxylates in the hydrophobic block, resulting in a “looser” aggregation or larger size.

Zeta potential measurements determine the surface charge densities, which are expected to be negative for the carboxylate-containing amphiphilic macromolecules. The neutral macromolecules (oCM and oBM) registered slight negative charges (−3.5 mV and −0.4 mV, respectively). 1BM has a slightly more negative zeta potential than 1CM as benzoic acid is more acidic than the aliphatic carboxylic acid. Notably, 1CM1CP has the most negative value (−20 mV) likely because it contains two carboxylate groups, one in the hydrophobic block and one in the hydrophilic block. Molecule 2CM also bears two negative charges, but both carboxylates reside within the hydrophobic core. As a result, the charge density does not increase in comparison with 1CM.

A.5.2 Inhibition of hoxLDL uptake by amphiphilic nanoparticles

The uncontrollable internalization of hoxLDL by macrophage cells is an essential aspect in atherosclerotic progression. (213) It has previously been proven that 1CM molecules significantly reduce hoxLDL uptake through blockage of SR-A and CD36 scavenger receptors. (90) The mechanism that leads to enhanced hoxLDL internalization with the anionic micelle particles relative to similar neutral polymers is not completely understood; therefore, nanoparticles with anionic groups placed in precise locations were prepared and evaluated.

The key finding in this study is that charge alone does not determine the extent of hoxLDL internalization reduction by macrophage cells. 1CM1CP is the most effective macromolecule in reducing hoxLDL internalization, while the similarly charged 2CM reduced hoxLDL uptake even less than 1CM. We hypothesize that the size of the 2CM might modulate the behavior of nanoparticle binding to the scavenger receptors. Scavenger receptors typically bind to particles and are then internalized through clathrin-coated pits. (214) Previous studies have shown that the increased size of PEGylated nanoparticles, nanoscale iron oxide contrast agents, and colloids can promote their scavenger receptor mediated uptake in macrophages. (215-217) However, consequences for scavenger receptor ligands such as hoxLDL were not evaluated. The exact mechanism for micellar nanoparticle binding in our system is not clear, but we offer two potential mechanisms. For example, the larger 2CM micellar nanoparticles (~35 nm) may promote the internalization of scavenger receptors in relation to the smaller diameter of 1CM1CP micelle (23.1 nm) and cooperatively facilitate hoxLDL uptake through mechanisms not yet clear. Alternately, the larger nanoparticles may interfere with folding and internalization of scavenger receptors. In either case, the major result is that the reduction in hoxLDL internalization is not addressed from charge alone: The 1CM decreases hoxLDL internalization more significantly than 2CM, even though both exhibit similar values of zeta potential (~ -10 mV).

A.6 Conclusion

Several amphiphilic scorpion-like macromolecules were synthesized to investigate how the number and location of carboxylate groups influence hoxLDL inhibition. All macromolecules self-organized into stable nanoscale micelles in an aqueous environment. Carboxylate groups located in the hydrophobic block influenced micelle size and CMC more than carboxylate groups in the hydrophilic block. Overall, molecule 1CM1CP demonstrates several unique characteristics: small size (23.1 nm), low CMC ($\sim 10^{-7}$ M) and high zeta potential (~ -20 mV). The combination of size, nanoparticle stability and charge density appear to be critical for inhibition hoxLDL uptake by macrophages.

Future investigations will focus on identifying the mode of micelle internalization, with a view to support or disprove the hypothesis that micelle diameter affects scavenger receptor occupancy. Mixed micelles will also be tested to determine whether a micelle can be created that will decrease hoxLDL internalization even more significantly than the 1CM1CP alone.

A.7 Tables and Figures

	1CM	0CM	1CP	1CM1CP	1BM	2BM	0BM
Z-average size (nm) at 10⁻⁴M	23.2	27.4	23.6	23.1	23.4	35.1	23.9
CMC (M)	3.2x10 ⁻⁷	5.7x10 ⁻⁷	1.0x10 ⁻⁷	8.8x10 ⁻⁷	7.0x10 ⁻⁷	1.8x10 ⁻⁷	7.8x10 ⁻⁷
Zeta-potential (mV) at 10⁻⁴M	-10.4	-0.47	-9.60	-20.1	-15.3	-9.20	-3.46

Table A.1:

Particle sizes, critical micelle concentrations and zeta-potential values of the amphiphilic macromolecules at pH 7.4

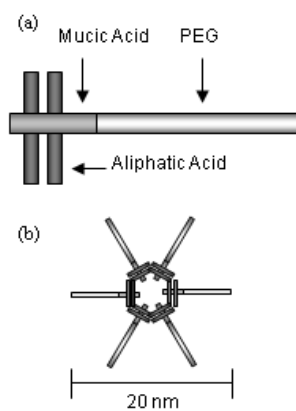


Figure A.1:

Schematic of an amphiphilic macromolecule: at concentrations greater than 10^{-7}M , the unimers in (a) self-aggregate to form micellar nanoparticles (b) with hydrodynamic diameters of $\sim 20\text{ nm}$.

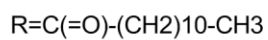
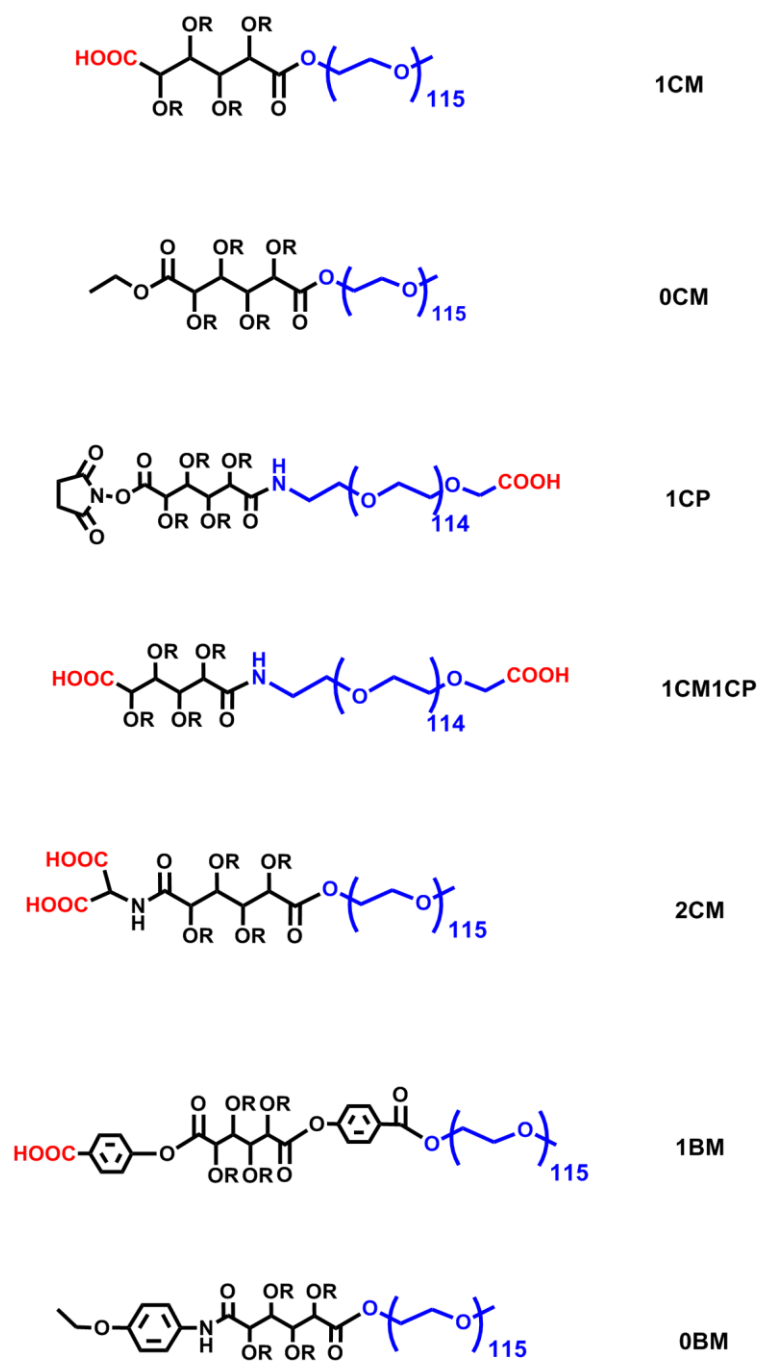


Figure A.2:

Nomenclature for amphiphilic macromolecules, where R in the chemical structures represents a lauroyl carbonyl group

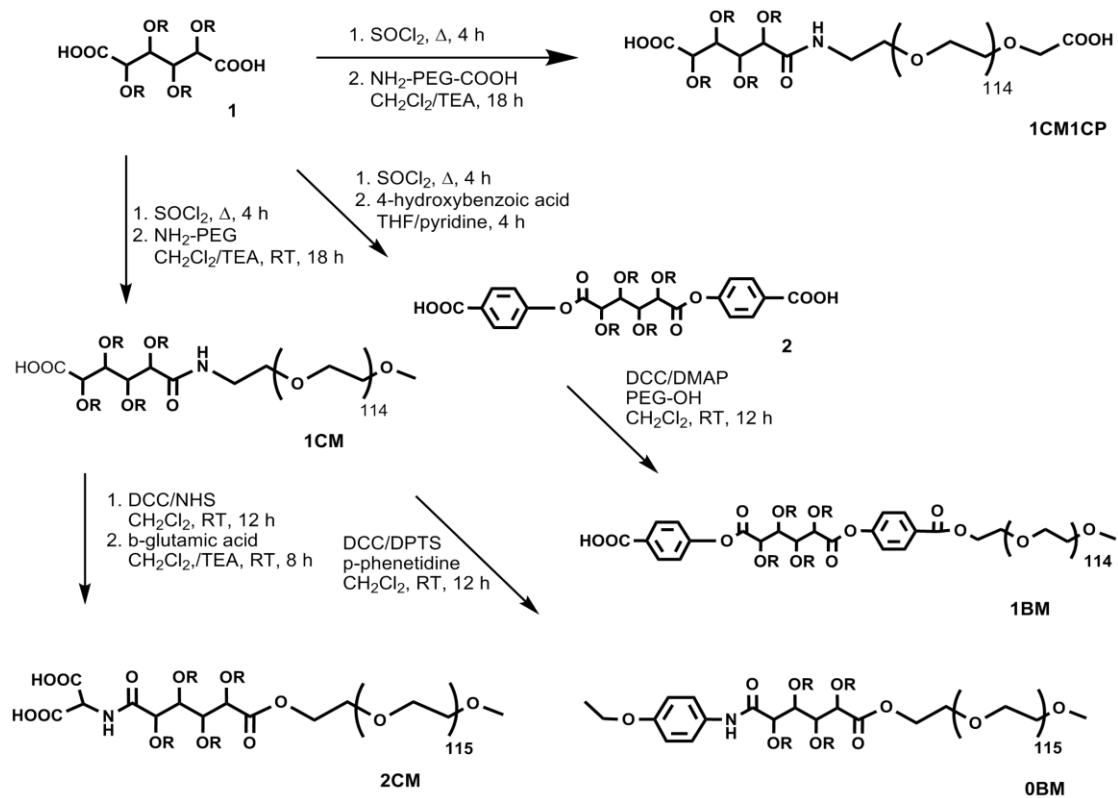


Figure A.3:

Synthetic outline for the amphiphilic macromolecules

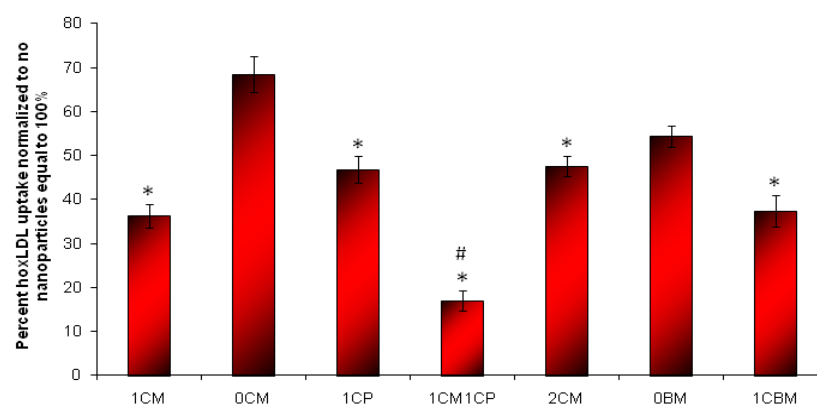


Figure A.4:

After 24 hours, percent of hoxLDL uptake by macrophages in the presence of amphiphilic macromolecules, compared to hoxLDL alone. Macromolecule concentration is 10^{-7} M. * represents a significant decrease ($P < 0.05$) in comparison to hoxLDL alone. # represents a significant decrease ($P < 0.05$) in comparison to hoxLDL with 1BM or 1CM.

Appendix B

Convergence of Nanotechnology and Cardiovascular Medicine Progress and Emerging Prospects

This chapter appeared as a review in the journal BioDrugs, 2008;22(1):1-10, coauthored by N.Iverson, N. Plourde, E. Chnari, G.B. Nackman, and P.V. Moghe.

B.1 Abstract

Advances in the emergence of biological probes, materials, and analytical tools limited to the nanoscale size range, collectively referred to as 'nanotechnology', are increasingly being applied to the understanding and treatment of the major pathophysiological problems in cardiovascular medicine. Analytical techniques based on high-resolution microscopy and molecular-level fluorescence excitation processes capable of detecting nanoscale interactions have been used to elucidate cardiovascular pathology. Nanotechnology has also significantly impacted diagnostic intervention in cardiology, with the use of nanoparticles as contrast agents, for targeted biomedical imaging of vulnerable plaques, for detection of specific pathologic targets signaling the onset of atherosclerosis, and for tracking inflammatory events. Real-time nanoscale biosensors can be used to measure cardiovascular biomarkers, and nanopore sequencing has the potential to speed up the analysis of gene expression in cardiovascular disease. Potential therapeutic applications include the use of nanomaterials in cardiovascular devices, for delivery of drugs and bioactive molecules, or in novel technologies for reducing cholesterol accumulation and for dissolving clots.

B.2 Introduction

A staggering array of emerging technologies are poised for impact on the fields of imaging, drug delivery, diagnostics, biosensors, and regenerative medicine (68, 218-220). Intersecting widely with this broad class of technologies are the areas of nanoscale materials (abbreviated as nanomaterials) and nanoscale imaging, which are collectively referred to as "nanotechnology". Nanomaterials relate to new materials synthesized and manipulated by precisely engineering atoms and molecules to yield new molecular assemblies on the scale of individual cells, organelles, or even smaller components, generally in the range of 5 to 100nm. A more "loose" definition of nanotechnologies extends the size range of materials and processes to 500nm, (221) although the rigorous definition of nanotechnologies defines this range as "sub-microscopic". This review focuses on nanotechnologies related to 5-100 nm size range. The advantage of operating at this size range is that truly nanoscale materials/probes can be engineered to interact with cell features and substrates at a scale that were hitherto impossible to achieve, leading to applications in diagnostics and therapeutics with promising potential. An important area of application is the diagnosis and treatment of cardiovascular disease, the number one cause of deaths in industrialized nations. The role of nanotechnology is steadily increasing in the diagnosis and therapy of cardiovascular diseases. For example, nanoparticles are being widely accepted as biosensors and imaging tools for detection and monitoring of the progression of the disease as well as drug delivery systems for therapeutic purposes. This review is

organized into three broad sections. The first section addresses the emergence of fundamental nanoscale techniques to elucidate cardiovascular pathology *ex vivo* through the use of quantitative approaches for studies of cell-nanosubstrate interactions. The second section provides an overview of nanoscale tools as diagnostics; the final section highlights established and emerging therapeutic modalities based on nanotechnology.

B.3 Nanotechnology as an analytical platform

Recent technological advances in the field of imaging have led to the advancement of the understanding of cardiovascular diseases through the use of techniques and instrumentation capable of detecting nano-scale interactions and phenomena (222). The list of techniques for the study of biological events related to cardiovascular disease is vast; however the limited number of those that can truly be categorized as “nano” technologies are highlighted here. In addition, the application of such devices often requires the use of contrast agents, as in MRI, or sputter coatings, as in scanning electron microscopy. In the following, three methods will be highlighted for their ability to provide nanoscale, sensitive, measurements with little sample perturbation for the most accurate representation of how molecules would interact *in vivo*.

B.3.1 Atomic Force Microscopy (AFM)

Atomic force microscopy (AFM) is based on the attractive and repulsive forces between a probe and a sample that allow for reconstruction and analysis of a sample's surface characteristics. Specifically, the probe is a tip at one end of a microscale cantilever and the attractive or repulsive forces cause a quantifiable deflection of the cantilever, as illustrated in Figure 1a. In addition, AFM is also ideal for analyzing a wide array of biological interactions as it provides a true three dimensional image at the nanoscale with little sample preparation (223). Recently, the technique was used to quantitatively study the structure of C-reactive protein (CRP), a risk factor for both atherosclerotic coronary heart disease and peripheral arterial disease (224, 225), for the future development of CRP sensor chips (226). Atomic force microscopy has been applied to the major challenge of design of a scaffold surface features that supports endothelial cell function in a prosthetic heart valve (227). Another study sought to investigate the topographical features of the native aortic valve endothelial basement membrane for the rational design of a tissue-engineered heart valve (TEHV) (228). In yet another study, the unbinding force and binding activity of the fibronectin (FN)- $\alpha_5\beta_1$ interaction on the surface of up-regulated vascular smooth muscle cells (VSMC) was characterized using AFM (229). These binding events may be important to focal adhesion assembly and mechanotransduction of VSMC and is of particular importance to the escalation of cardiovascular disease (229).

B.3.2 Near-Field Scanning Optical Microscopy (NSOM)

Unlike the AFM, Near-field scanning optical microscopy (NSOM) allows for the imaging of live, unperturbed cells, which opens the door for novel biological studies. The NSOM, described in Figure 1b, employs a sub-wavelength light source as a scanning probe which is capable of resolving both the topographic and optical properties of a sample with resolutions of 40-100nm (230). In this sense, the NSOM is a true "nanoscale" technique and it overcomes the limitations of confocal and two-photon microscopes, whose spatial resolution is limited to hundreds of microns. The NSOM technique was employed to investigate the nanoscale distribution of voltage-gated L-type Ca^{2+} channels, which regulate cardiac myocyte contractions (231). In addition, traditional NSOM can be modified to study living samples immersed in media. The dynamics of beating cardiac myocytes in culture were elucidated with acute vertical sensitivity below the nanometer range (232). Methods such as this could be applied to numerous vascular cell lines and tissues to visualize and understand phenomenon with a high resolution that was previously unachievable.

B.3.3 Resonance Energy Transfer (FRET and BRET)

Fluorescence Resonance Energy Transfer (FRET) relies on the transfer of energy from a donor fluorescent molecule to an acceptor that are separated by 2-6 nm (233). This short range energy transfer allows for highly sensitive measurements of intermolecular distances and conformations, as seen in Figure 1c. It has been documented that the heart could potentially be protected under metabolic stress

through activation of ATP-sensitive potassium (K_{ATP}) (234, 235) and FRET analysis has been used to aid in illuminating the molecular basis and mechanism of the K_{ATP} channels in mitochondria. In this very recent FRET study, it was found that protein kinase C (PKC) activation caused insertion of K_{ATP} channels into the mitochondrial inner membrane (236). Other FRET studies have suggested that a recombinant antibody-based protein (PLN-Ab) mimics the effects of phospholamban phosphorylation, which can inhibit the calcium pump (237). This is of importance due to the fact that changes in intracellular calcium handling, for example a reduction of the sarcoplasmic reticulum calcium pump (SERCA), can contribute to contractile dysfunction. A similar technique, BRET (bioluminescence resonance energy transfer), exploits energy transfer between a bioluminescent donor protein and a fluorescent acceptor protein (238). Using this technology, Prinz et al. (239) have been able to intracellularly monitor subunit interactions of protein kinase A (PKA), an intracellular effector of cardiovascular disease (240).

B.4 Nanotechnology as a diagnostic modality

B.4.1 Imaging/detection using nanotechnology

Advances in nanoparticles have significantly impacted the area of biomedical imaging, particularly for the targeting of pathogenesis and functional imaging. For example, deposited fibrin lies at the core of a growing plaque and is an early determinant of plaque erosion and rupture (221). Nanoparticles functionalized with

antibody fragments specific to the cross-linked fibrin peptide domains, were successfully used to image vulnerable plaques with ultrasound or paramagnetic MR contrast agents, see figure 2 (218, 241). Angiogenesis, which also plays an important role in plaque growth and rupture, (242, 243) was similarly imaged through the use of $\alpha_v\beta_3$ -integrin targeted paramagnetic nanoparticles and MRI (244).

The bimolecular specificity of nanoparticles can also be harnessed to detect specific targets in patients, including detecting specific types of cells, such as smooth muscle cells (245), and targeted pathologic cells, such as cells undergoing apoptosis (246). For example, atherosclerotic lesion formation (247) has been detected through the application of i) technetium-labeled annexin, which binds to exposed phosphatidyl serine epitopes of apoptotic cell membranes, (248) or ii) magnetofluorescent nanoparticles conjugated to a short peptide chain that binds specifically to vascular cell adhesion molecule VCAM-1. (249)

Another approach proposed to detect the early onset of atherosclerosis involves the use of nanoscale particles of iron oxide, which can be rapidly internalized by plaque-resident macrophages (250). Once such plaques are identified, subsequent monitoring can establish the efficacy of therapies on inhibiting plaque expansion and thus, possibly preventing plaque destabilization and rupture. In addition to iron oxides, quantum dots, a family of fluorescent semiconductors have recently received a lot of attention for intracellular imaging, as they can be excited over a broad range while emitting at very specific wavelengths (66, 251, 252). As depicted in figure 2 the high fluorescence intensity of quantum dots can potentially allow for the tracking of cells throughout the

body, particularly even following cell division (66). A wide spectrum of quantum dot based approaches is expected to be useful in tracking inflammatory events such as macrophage cell infiltration into arterial tissue or angiogenesis and vascular remodeling, including the rejuvenation of the endothelial lining of the intima after cardiovascular procedures have damaged the vasculature.

B.4.2 Biosensors

There are many possibilities for nanotechnology to improve diagnostics through the use of real time biosensors. In vivo sensors could potentially monitor signaling cascades and detect the response of surrounding tissue to inflammation or cardiac events (66), although the clinical "integration" and realization of this promise from the standpoint of real-time intervention is challenging. The nanowires that are currently utilized in computer components could be used to detect small alterations in biological or chemical components, allowing for the smallest of changes in a patient to be considered with treatment options (253). Quantum dots could also be used as biosensors that can detect specific proteins or DNA sequences to conduct high-throughput screening for many medical conditions (220). Other biosensors have been primarily employed in "ex vivo" applications. For example, molecular beacons have the ability to target nucleic acids with high specificity and high signal-to-background ratios for disease detection applications (254-256). Molecular beacons consist of a single-stranded oligonucleotide which naturally forms a hairpin so that the fluorescent reporter and quencher, which are conjugated to opposite ends of the strand, will

interact. The loop of the hairpin contains a probe sequence situated between two short complementary sequences that create the stem. When the beacon comes in contact with and binds to a strand containing the target sequence a conformational change separates the fluorescent probe from the quencher and the beacon fluoresces (256). Mutations in genes such as methylenetetrahydrofolate reductase (MTHFR), which is linked to an increased risk of cardiovascular disease, have been detected via molecular beacon assays which are able to rapidly screen blood samples (257). Surface plasmon resonance (SPR)-based sensors can provide label-free real-time data *ex vivo* or *in vitro* on specific biochemical binding reactions between strategic ligands and receptors. Detection relies on the surface plasmon resonance phenomenon that occurs when polarized light is reflected on the underside of a metal film. At a critical angle of incident light, surface plasmons are generated at the surface, which results in a decrease in the intensity of reflected light. The angle depends on the refractive index near the surface, which changes with surface binding. Recently, a method has been developed by Masson, et al, for measurement of biomarkers in undiluted serum samples via SPR (258). The group quantified two myocardial infarction biomarkers, cardiac troponin I (cTnI) and myoglobin (MG), without the need of sample treatment or dilution, thus reducing the processing and time associated with analyzing samples.

B.4.3 DNA sequencing

DNA sequencing is a modern diagnostic tool that can be used to investigate gene expression patterns that may be characteristic of cardiovascular disease

expression and progression. Nanopore sequencing, a new technique that involves drawing a DNA strand through an α -hemolysin protein complex and determining each base by the current and time profile, is an interesting new approach to high-throughput DNA morphology detection. This technology can sequence more than 1000 base pairs per second and can determine single nucleotide polymorphisms. (219, 259) The more commonly used technique of DNA comparisons through microarrays is a diagnostic tool that allows researchers to investigate gene expression patterns, genes involved in monogenetic and complex physiological conditions, genes linked in cellular pathways, effects of drugs and possible generation of new drug pathways as well as many other areas of interest (260). The speed of nanopore sequencing could lead to its prominence and a decrease in researchers' dependence on current sequencing technology which is slower, more expensive and less accurate (261-263). Expression profiling has proven to be beneficial towards determining the molecular basis of complex traits; specifically it has shed light on some of the complexities involved in cardiovascular disease (264, 265).

B.5 Nanotechnology as a therapeutic modality

Two classes of therapeutic applications are reviewed here: established cardiovascular therapies and emerging technologies with translational potential.

B.5.1 Established cardiovascular therapies enabled via nanotechnology

B.5.1.1 Carbon Nanotubes

Carbon nanotubes are biologically inert, electrically conductive rolled graphite sheets of pure carbon atoms with the strongest tensile strength of any synthetic fiber. (266-269). Due to their extraordinary electrical, physical and structural characteristics, carbon nanotubes have been utilized in a variety of fields including biosensors, diagnostics and imaging (270-272). Meng et al. have created a multiwalled carbon nanotube and polyurethane composite that considerably increased the strength and elasticity of polyurethane while reducing the incidence of red blood cell disruption and platelet activation typically found on polyurethane matrices (206). Despite the promise of carbon nanotubes, several concerns regarding their usage remain. Li et al. have found that hypercholesterolemic (ApoE^{-/-}) mice experienced an increase in the percentage of aortic arch covered by plaque after in administration of single walled carbon nanotubes in comparison to vehicle treated controls (273, 274). It is believed that the plaque formation was due to an inflammatory response in the lungs or circulatory system initiated by the carbon nanotubes (273, 274).

B.5.1.2 Cardiovascular Stents

Coronary stents represent one of the most rapidly growing applications of implantable cardiovascular biomaterials (275). Stents have been shown to reduce restenosis in comparison to balloon angioplasty, but in-stent restenosis (re-narrowing

within the confines of the stent) is also a problem, occurring in ten to sixty percent of patients (55-58). The placement of the stent is able to smooth the luminal surface following creation of an arterial dissection following angioplasty and to prevent elastic recoil leading to the suboptimal expansion of the flow lumen. The stent leads to "positive remodeling" which increases overall diameter of the vessel. However, as a result of the initial injury, neointima hyperplasia frequently results and is the primary cause of the restenosis phenomena, or "negative remodeling" causing a decrease in the diameter of the flow lumen. (59, 60). The restenosis after stent placement is associated with the migration of smooth muscle cells into the neointima. The smooth muscle cells ultimately produce significant amounts of matrix protein leading to a mostly collagen containing lesion and neointimal thickening (61). Initial studies have shown that coating stents with drugs such as paclitaxel or sirolimus, may result in a 70 to 80% reduction in necessity of repeat procedures for restenosis (63). However, these drug eluting stents aimed at inhibiting the cell cycle also inhibit the normal remodeling of the vessel that results in the stent becoming implanted in the vascular wall. As a result of this, the exposed stents are prone to thrombus formation and patients must be given anti-platelet drugs to prevent clotting. Additionally, there are several other stent coatings currently under investigation, including polytetrafluoroethylene, 7-hexanolytaxol and rapamycin-eluting microporous stents (276-278). Nanotextured stent coatings (hydroxyapatite and titania) are currently under development with an aim to enhance vascular cell attachment and proliferation (to promote re-endothelialization of the vessel wall) (65). An innovative alternative to the problem of neointima formation after

balloon injury was proposed by Wong et al. based on the use of submicroscopic spheres to provide a sustained release of elastase that creates a chemoattractant gradient across arterial walls directing smooth muscle cell migration away from the lumen (64). It is also possible that this technology can be utilized to direct cell migration in other areas, such as to injury sites for repair purposes (66) or away from injury to decrease macrophage infiltration.

B.5.1.3 Drug delivery

Nanoparticles and microscale particles can also be used for encapsulation and localized delivery of drugs and bioactive molecules. Most systemically introduced drugs circulate through the entire body, leading to difficulty in maintaining an optimal concentration in disease specific areas due to metabolism and excretion of drugs as well as toxicity in non-related tissues (66). By encapsulating drugs in nanospheres (67), erodible self-assembled structures (68) or $\alpha_v\beta_3$ -integrin targeted paramagnetic nanoparticles concurrently used for imaging (69) specificity in drug release can be introduced. This technology can deliver drugs to diseased areas without causing toxicity to healthy tissue as well as allowing for a prolonged release period of the drug.

B.5.2 Novel nano technologies as potential therapies

Apart from the advances of nanotechnology in traditional areas of cardiovascular therapies, novel technologies have been developed with a potential for use as treatments for cardiovascular disease. This review focuses on two novel

technologies, in particular, clot-dissolving bubbles combined with low-frequency ultrasound (Sonolysis) and micellar nanoparticles (NanoLipoBlockers – NLBs) that control the metabolism of oxidized lipoproteins, with potential to reduce cholesterol accumulation and foam cell formation.

B.5.2.1 Sonothrombolysis

The removal of blood clots from arteries and veins remains a challenge. Standard techniques such as use of a balloon catheter result in the injury of the endothelial cell lining. The use of thrombolytic drugs, although less physically damaging to the vessel wall, are associated with a risk of bleeding. Low-frequency ultrasound is a technique that has recently been developed in an effort to destroy clots in thrombosed arteries and veins. Not only are the bubbles used to generate higher resolution ultrasound images, but the addition of micro/nanoscale bubbles seems to enhance the lytic activities of ultrasound, even in the absence of thrombolytic drugs, as well as increasing thrombolytic drug effectiveness and allowing lower, safer doses (279, 280). The mechanism of action of the bubbles involves their adherence to the clot and application of ultrasound that causes their fragmentation and subsequent mechanical erosion of the adjacent clot, as demonstrated in Figure 3. (281) This therapeutic method is called sonothrombolysis (SonoLysis Therapy) and has applications in acute thrombosis following plaque rupture that leads to occlusion of critical blood vessels and in deep vein thrombosis that affects thousands of people in the US and may lead to death due to pulmonary embolism (282).

Clinical trials are currently underway on a SonoLysis technology utilizing perfluoropropane-filled nanobubbles (MRX-815) for acute ischemic stroke (283, 284). The MRX-815 bubbles have been previously tested and described as microbubbles with mean diameters of 1.0-1.8 μm (285, 286). It is not clear that traditional sonolytic approaches operate under nanoscale regimen. While the bubbles are frequently referred to as “microbubbles”, acoustic analyses have shown that nanobubbles may populate a substantial fraction of microbubble suspensions (287), suggesting that selected sonolytic regimen may fall under the class of nanotechnologies. Recent modifications of these techniques are inspired by the possible integration of microbubble-based sonolysis with truly nanoscale drug-carrying particles. For example, contrast agent microbubbles have been used to selectively permeabilize tissue for the enhanced transport of intravascular nanoparticles via ultrasound (288). Chappell et al found that ultrasound combined with microbubbles resulted in an increase of nanoparticle deposition 4.5 times more than ultrasound alone and 152 times more than with microbubbles alone in arterially occluded mouse hindlimb (289). Studies such as these open the door for the development of drug-loaded nanoparticles for noninvasive delivery and controlled release (289).

B.5.2.2 Nanolipoblockers (NLBs)

NanoLipoBlockers (NLBs) are a class of anionic amphiphilic drug-encapsulating polymers that approach the problem of excessive accumulation of low density lipoproteins (LDL) within blood vessel walls (intima) in a novel way (119). NLBs do not

deal with cholesterol through the liver or systemic vasculature as many other cholesterol drugs do (statins, resins and niacin) (290-295) but attempt to treat the problem in a more localized fashion. The NLBs are spontaneously formed micelles (when concentration of unimers is above the critical micelle concentration) consisting of unimers created by PEG, mucic acid and alkyl chains (88). There are multiple configurations of NLBs currently in the testing stage, both anionic as well as neutral controls, many of which can be seen the table 1.

The NLBs are able to interact with LDL in two main ways. Anionic NLBs interact with neutral (nLDL) and mildly oxidized LDL (moxLDL), potentially preventing their entrapment by glycosaminoglycans, thus inhibiting further oxidation of the LDL particles. The nLDL and moxLDL can then be internalized by the macrophage cells and metabolized in a controlled way (88, 89). The highly oxidized LDL (hoxLDL) does not directly interact with the NLBs, but hoxLDL uptake fate is still influenced by NLB presence. NLBs competitively bind to scavenger receptors (involved in the uncontrolled uptake of hoxLDL) and therefore block hoxLDL binding and internalization by scavenger receptors (88, 89). Specific configurations of NLBs that presented anionic charged groups at the hydrophobic termini were able to inhibit 75% of hoxLDL internalization in IC21 macrophages, primarily through SR-A and CD-36 scavenger receptor blocking (90). This reduction in hoxLDL internalization led to significantly less cholesterol accumulation in macrophage cells and a substantial decrease in the number of foam cells formed (90). The same configuration of NLBs

were also able to attenuate tumor necrosis factor alpha (TNF- α) release by macrophages. Figure 4 depicts the possible mechanisms of action for NLBs and LDL.

NLBs have shown great promise *in vitro* and have begun the *in vivo* testing phase. These nanoparticles hold the promise of not only a system to inhibit scavenger receptor mediated oxLDL internalization by macrophage cells, but also a drug delivery system (allowing for a direct delivery of drugs to cells affected by oxLDL). By decreasing the oxLDL internalization, the NLBs can inhibit vascular wall injury triggered by macrophage inflammatory response and potentially reduce matrix remodeling and intimal hyperplasia associated with cells' uptake of oxLDL (90, 296-300).

B.6 Conclusion

The role of nanotechnology in analytical, diagnostic and therapeutic modalities related to cardiovascular pathologies and processes was reviewed in this article. With the continued innovations in imaging, biomaterials, tissue targeted nanoparticles, biosensors and personalized medicine, nanotechnology has potential to offer cardiologists and vascular surgeons new ways to improve patient care and diagnose, monitor, and treat cardiovascular events more efficiently and effectively. Emerging nanotechnology-based therapies can potentially help manage the escalation of atherosclerosis and prevent severe cardiovascular episodes.

B.7 Figures

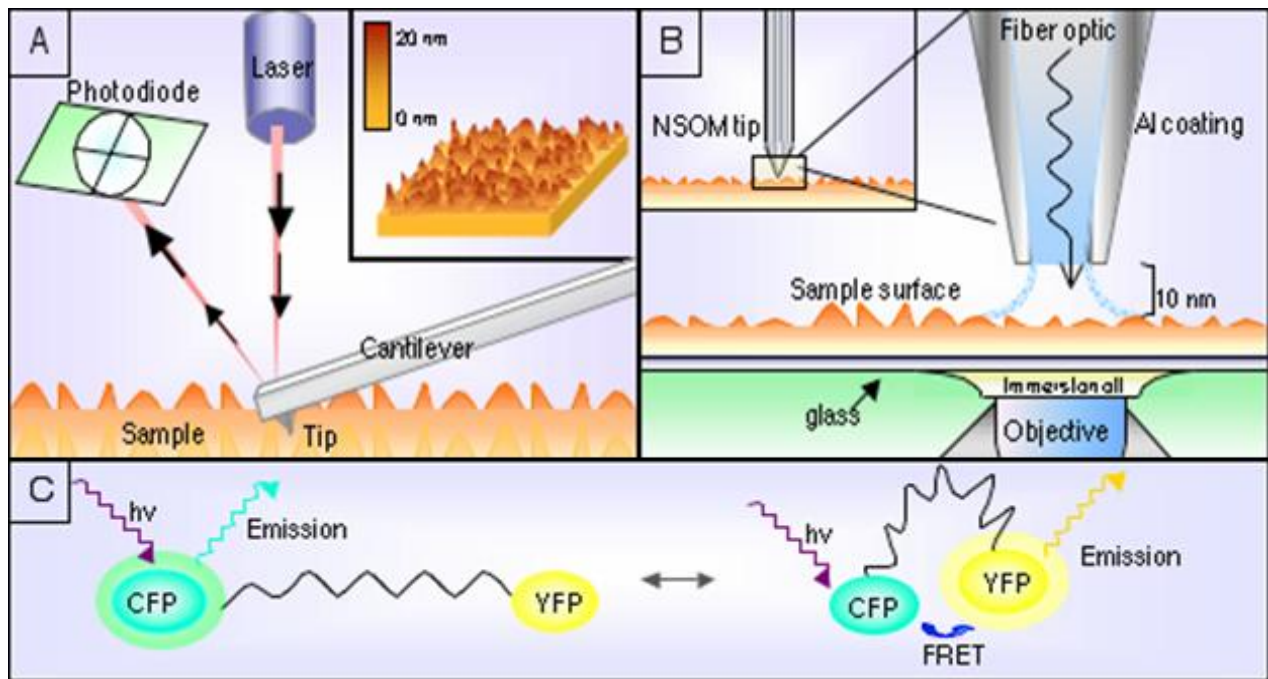


Figure B.1:

Selected analytical methods based on nanotechnology that have been applied to studies of cardiovascular phenomena: A) Atomic force microscopy (AFM): When the tip is brought near the sample surface the forces between the two result in a deflection of the cantilever. The cantilever deflection is recorded by a photodiode which is sensitive to laser light reflected off the cantilever backside. The result is a sensitive topographical map of the sample surface. B) Near-Field Scanning Optical Microscopy (NSOM): The NSOM tip consists of a fiber optic cable coated with metal, usually aluminum. Optical signals pass through the sub-wavelength diameter aperture while the tip scans over the sample surface, which allows for the resolving both the topographic and optical properties. C) Fluorescence Resonance Energy Transfer (FRET) describes an energy transfer

between two chromophores. A common pair is cyan fluorescent protein (CFP) and yellow fluorescent protein (YFP). In FRET, a donor is excited at its specific fluorescence excitation wavelength and when within a few nanometers of an acceptor molecule, some of the emitted energy is transferred to the second molecule.

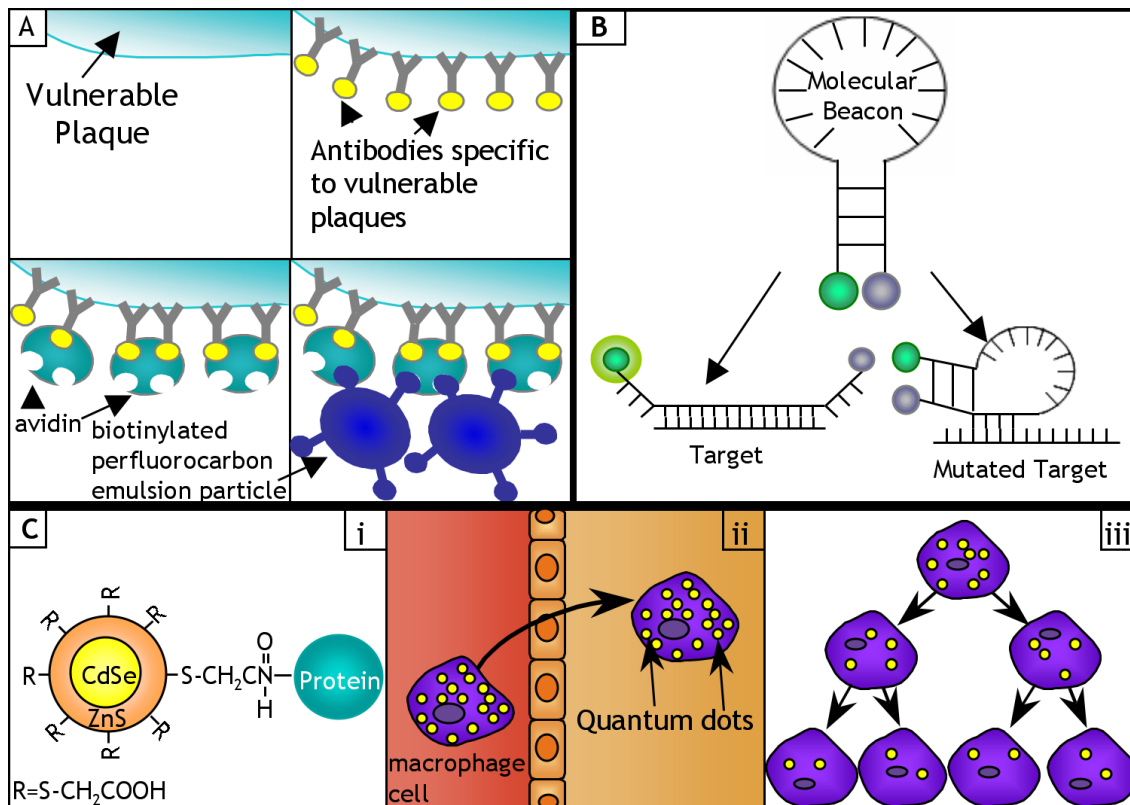


Figure B.2:

Applications of nanotechnology to diagnostic modalities in cardiovascular medicine. (A) Diagnostic Imaging: Antibody fragments specific for cross-linked fibrin domains can be introduced followed by the addition of avidin which binds to and cross-links the antibodies. Biotinylated perfluorocarbon emulsion particles are then bound to the antibody avidin complex. The complex with its greatly increased acoustic reflectivity makes the vulnerable plaques discernable under ultrasound imaging (218, 241). (B) Molecular beacons are designed from a single-stranded oligonucleotide which forms a hairpin with a fluorescent reporter and quencher conjugated to opposite ends of the strand. The loop is a probe sequence between two short complementary sequences, the stem. When

the beacon comes in contact with a complimentary sequence, the fluorescent probe and quencher are separated, and the signal can be detected. (C) Varied quantum dot configurations can be used to target and image cells/tissues. i) Chen and Nei utilized a ZnS-capped protein coupled CdSe quantum dot which is 20 times brighter and 100 times more stable than organic dyes (251). Quantum dots can be used to ii) track cells in the body (such as macrophage cell infiltration into arterial tissue) and iii) observe cell proliferation (such as the re-endothelialization of the vasculature wall) (66, 252).

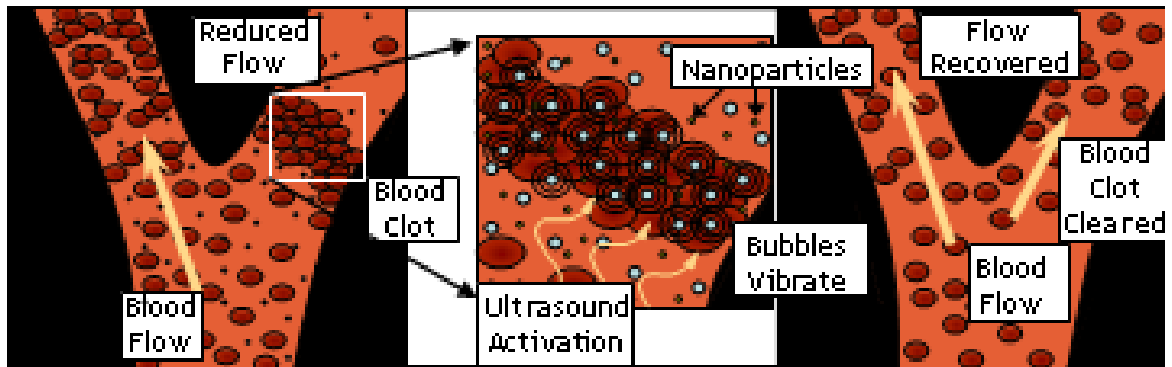


Figure B.3:

Emerging therapeutic application of nanotechnology: Sonothrombolysis. When a blood clot reduces or blocks the flow of blood through a vessel, SonoLysis bubbles can be introduced to the blood stream. The bubbles infiltrate the clot and can destabilize the clot upon ultrasound activation. This can further clear the vessel for recovered flow. (281) When nanoparticles are introduced to the blood stream in conjunction with microbubbles there is a 4.5-fold increase in nanoparticle deposition, which holds promise in controlled release and non-invasive delivery applications (301).

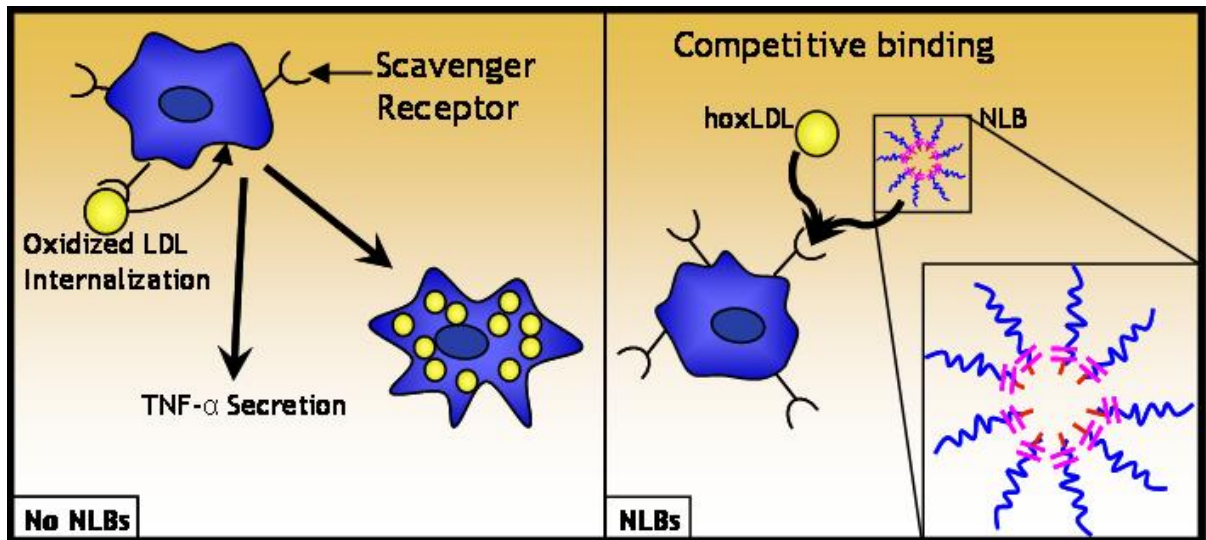


Figure B.4:

Emerging therapeutic approaches in nanotechnology: NanoLipoBlockers (NLBs). Nanoscale assemblies, NLBs have been designed to bind to scavenger receptors on macrophages, which can inhibit the accumulation of highly oxidized LDL (90, 91). NLBs introduced at the site of growing atherosclerotic plaques can serve as a basis to potentially de-escalate foam cell formation and cytokine secretion in vivo. (89)

References

1. Lloyd-Jones D, et al. (2009) Heart disease and stroke statistics--2009 update: a report from the American Heart Association Statistics Committee and Stroke Statistics Subcommittee *Circulation* 119:480-486.
2. Yusuf S, Reddy S, Ounpuu S, et al (2001) Global burden of cardiovascular diseases part I: general considerations, the epidemiologic transition, risk factors, and impact of urbanization *Circulation* 104:2746-2753.
3. Daniels TF, Killinger KM, Michal JJ, Jr. RWW, Jiang Z (2009) Lipoproteins, cholesterol homeostasis and cardiac health *International Journal of Biological Sciences* 5:474-488.
4. Stamler J, Daviglus ML, Garside DB, et al (2000) Relationship of baseline serum cholesterol levels in 3 large cohorts of younger men to long-term coronary, cardiovascular, and all-cause mortality and to longevity *JAMA* 284:311-318.
5. (NCEP) NCEP (2001) Executive Summary of The Third Report of The NCEP Expert Panel on Detection, Evaluation, And Treatment of High Blood Cholesterol In Adults (Adult Treatment Panel III) *JAMA* 285:2486-2497.
6. Blanchette-Mackie E (2000) Intracellular cholesterol trafficking: role of the NPC1 protein *Biochimica et Biophysica Acta* 1486:171-183.
7. Kannel W, Castelli W, Gordon T (1979) Cholesterol in the prediction of arteriosclerotic disease *Ann Intern Med* 90:85-91.
8. Castelli W (1984) Epidemiology of coronary heart disease: the Framingham study *Am J Med* 76:4-12.
9. Kruth H (2001) Lipoprotein Cholesterol and Atherosclerosis *Current Molecular Medicine* 1:633-653.
10. Oorni K, Pentikainen MO, Ala-Korpela M, Kovanen PT (2000) Aggregation, fusion, and vesicle formation of modified low density lipoprotein particles: molecular mechanisms and effects on matrix interactions. *J. Lipid Res.* 41:1703-1714.
11. Camejo G, Hurt-Camejo E, Wiklund O, Bondjers G (1998) Association of apo B lipoproteins with arterial proteoglycans: Pathological significance and molecular basis. *Atherosclerosis* 139:205-222.
12. Cardoso LE, Mourao PA (1994) Glycosaminoglycan fractions from human arteries presenting diverse susceptibilities to atherosclerosis have different binding affinities to plasma LDL. *Arterioscler. Thromb.* 14:115-124.
13. Oorni K, Pentikainen MO, Annala A, Kovanen PT (1997) Oxidation of low density lipoprotein particles decreases their ability to bind to human aortic proteoglycans. Dependence on oxidative modification of the lysine residues. *J. Biol. Chem.* 272:21303-21311.
14. Chang M, Potter-Perigo S, Wight T, Chait A (2001) Oxidized LDL bind to nonproteoglycan components of smooth muscle extracellular matrices *J. Lipid Res.* 42:824-833.

15. Auerbach BJ, Bisgaier CL, Wolle J, Saxena U (1996) Oxidation of low density lipoproteins greatly enhances their association with lipoprotein lipase anchored to endothelial cell matrix. *J. Biol. Chem.* 271:1329-1335.
16. Kaplan M, Aviram M (2001) Retention of Oxidized LDL by Extracellular Matrix Proteoglycans Leads to its Uptake by Macrophages: An Alternative Approach to Study Lipoproteins Cellular Uptake *Arterioscler Thromb Vasc Biol* 21:386-393.
17. Steinberg D (1997) A critical look at the evidence for the oxidation of LDL in atherogenesis *Atherosclerosis* 131:S5-7.
18. Esterbauer H, Ramos P (1996) Chemistry and pathophysiology of oxidation of LDL *Rev. Physiol. Biochem. Pharmacol.* 127:31-64.
19. Steinberg D (1997) Low density lipoprotein oxidation and its pathobiological significance *Journal of Biological Chemistry* 272:20963-20966.
20. Virella G, et al. (1995) Activation of human monocyte-derived macrophage by immune complexes containing low density lipoprotein *Clin. Immunol. Immunopathol.* 75:179-189.
21. Bevilacqua MP PJ, Majeau GR, Cotran RS, Gimbrone MA Jr. (1984) Interleukin 1 induces biosynthesis and cell surface expression of procoagulant activity in human vascular endothelial cells. *J Exp Med.* 160:618-623.
22. Luscinskas FW BA, Arnaout MA, Grimbone MA. (1989) Endothelial leukocyte adhesion molecule-1-dependent and leukocyte (CD11/CD18)-dependent mechanisms contribute to polymorphonuclear leukocyte adhesion to cytokine-activated human vascular endothelium. *J Immunol.* 142:2257-2263.
23. Raines EW DS, Ross R. (1989) Interleukin-1 mitogenic activity for fibroblasts and smooth muscle cells is due to PDGF-AA. *Science* 243:393-396.
24. Nagase H, Woessner JJ (1999) Matrix metalloproteinases *J Biol Chem* 274:21491-21494.
25. Birkedal-Hansen H (1995) Proteolytic remodeling of extracellular matrix *Curr Opin Cell Biol* 7:728-735.
26. Galis Z, Khatri J (2002) Matrix metalloproteinases in vascular remodeling and atherogenesis: the good, the bad, and the ugly *Circ Res* 90:251-262.
27. Ross R (1999) Atherosclerosis: an inflammatory disease *New England Journal of Medicine* 340:115-126.
28. Galis Z, Sukhova, GK, Kranzhoefer, R, Clark, S, Libby, P (1995) Macrophage foam cells from experimental atheroma constitutively produce matrixdegrading proteinases *Proc Natl Acad Sci U S A* 92:402-406.
29. Galis Z, Sukhova G, Lark M, Libby P (1994) Increased expression of matrix metalloproteinases and matrix degrading activity in vulnerable regions of human atherosclerotic plaques *J Clin Invest* 94:2493-2503.
30. Nikkari S, et al. (1995) Interstitial collagenase (MMP-1) expression in human carotid atherosclerosis *Circulation* 92:1398-1408.
31. Halpert I, et al. (1996) Matrilysin is expressed by lipid-laden macrophages at sites of potential rupture in atherosclerotic lesions and localizes to areas of versican deposition, a proteoglycan substrate for the enzyme *Proc Natl Acad Sci U S A* 93:9748-9753.

32. Brown D, Hibbs M, Kearney M, Loushin C, Isner J (1995) Identification of 92-kD gelatinase in human coronary atherosclerotic lesions: association of active enzyme synthesis with unstable angina *Circulation* 91:2125-2131.
33. Thomas B, et al. (2000) The ACAT Inhibitor Avasimibe Reduces Macrophages and Matrix Metalloproteinase Expression in Atherosclerotic Lesions of Hypercholesterolemic Rabbits *Arteriosclerosis Thrombosis Vascular Biology* 20:70-79.
34. Gotto AM (2002) Statins: Powerful Drugs for Lowering Cholesterol *Circulation* 105:1514-1516.
35. Verma S, et al. (2004) Off-Pump Coronary Artery Bypass Surgery Fundamentals for the Clinical Cardiologist *Circulation* 109:1206-1211.
36. Yusuf S, et al. (1994) Effect of coronary artery bypass graft surgery on survival: Overview of 10-year results from randomised trials by the Coronary Artery Bypass Graft Surgery Trialists Collaboration *Lancet* 344:563-570.
37. Hultgren H, Peduzzi P, Detre K, et al. and the Study Participants. (1985) The 5 year effect of bypass surgery on relief of angina and exercise performance *Circulation* 72:79-83.
38. Blumenthal J, Mark D (1994) Quality of life and recovery after cardiac surgery *Psychosom Med* 56:213-215.
39. Bradshaw P, Jamrozik K, Le M, Gilfillan I, Thompson P (2002) Mortality and recurrent cardiac events after coronary artery bypass graft: Long term outcomes in a population study *Heart* 88:488-494.
40. Rahimtoola S, Fessler C, Grunkemeier G, et al. (1993) Survival 15 to 20 years after coronary artery bypass surgery for angina *J Am Coll Cardiol* 21:151-157.
41. Boylan M, et al. (1994) Surgical treatment of isolated left anterior descending coronary stenosis. Comparison of left internal mammary artery and venous autograft at 18 and 20 years of follow-up *J Thorac Cardiovasc Surg* 107:657-662.
42. Jones R, Kesler K, Phillips H, et al. (1996) Long-term survival benefits of coronary artery bypass grafting and percutaneous transluminal angioplasty in patients with coronary artery disease *J Thorac Cardiovasc Surg* 111:1013-1025.
43. Sergeant P, Blackstone E, Meyns B (1998) Does arterial revascularization decrease the risk of infarction after coronary artery bypass grafting? *Ann Thorac Surg* 66:1-11.
44. Myers W, Blackstone E, Davis K, et al. (1999) CASS registry long term surgical survival. Coronary artery surgery study *J Am Coll Cardiol* 33:488-498.
45. Cameron A, Davis K, Rogers W (1995) Recurrence of angina after coronary artery bypass surgery: Predictors and prognosis *J Am Coll Cardiol* 4:895-899.
46. Herlitz J, et al. (1998) Predictors of death during 5 years after coronary artery bypass grafting *Int J Cardiol* 64:15-23.
47. Domanski M, Borkowf C, Campeau L, et al. and the Post CABG Trial Investigators (2000) Prognostic factors for atherosclerosis progression in saphenous vein grafts. The Post coronary Artery Bypass Graft (Post-CABG) Trial *J Am Coll Cardiol* 36:1877-1883.

48. Herlitz J (2004) Secondary prevention after coronary artery bypass grafting - what do we know? *Scand Cardiovasc J* 38:69-74.
49. Wilson J, Ferguson J (1995) Revascularization therapy for coronary artery disease. Coronary artery bypass grafting versus percutaneous transluminal coronary angioplasty *Texas Heart Institute Journal* 22:145-161.
50. Detre K, et al. (1990) Incidence and consequences of periprocedural occlusion: The 1985-1986 National Heart, Lung and Blood Institute Percutaneous Transluminal Coronary Angioplasty Registry *Circulation* 82:739-750.
51. Serruys P, et al. (1988) Incidence of restenosis after successful coronary angioplasty: a time-related phenomenon. A quantitative angiographic study in 342 consecutive patients at 1, 2, 3, and 4 months *Circulation* 77:361-371.
52. Mintz G, Popma J, Pichard A, et al. (1996) Arterial remodeling after coronary angioplasty: a serial intravascular ultrasound study *Circulation* 94:35-43.
53. Schwartz R, Huber K, Murphy J, et al. (1992) Restenosis and the proportional neointimal response to coronary artery injury: results in a porcine model *J Am Coll Cardiol* 19:267-274.
54. Sigwart U, Puel J, Mirkovitch V, et al. (1987) Intravascular stents to prevent occlusion and restenosis after transluminal angioplasty *N Engl J Med* 316:701-706.
55. Serruys P, de Jaeger P, Kiemeneij F et al. for the Benestent Study Group (1994) A comparison of balloon-expandable-stent implantation with balloon angioplasty in patients with coronary heart disease *N Engl J Med* 331:489-495.
56. Fischman D, Leon M, Baim D, et al. for the Stent Restenosis Study Investigators. (1994) A randomized comparison of coronary-stent placement and balloon angioplasty in treatment of coronary artery disease. *N Engl J Med* 331:496-501.
57. Till F, et al. (1996) Real life stenting: a comparison of target vessel revascularization in Benestent-Stress lesions to non Benestent-Stress lesions *Circulation* 94:1-332.
58. Fenton S, Fischman D, Savage M, et al. (1994) Long-term angiographic and clinical outcome after implantation of balloon expandable stents in aortocoronary saphenous vein grafts *Am J Cardiol* 74:1187-1191.
59. Hoffmann R, Mintz G, Dussaillant G, et al. (1996) Patterns and mechanisms of in-stent restenosis: A serial intravascular ultrasound study *Circulation* 94:1247-1254.
60. Mudra H, Regar E, Klauss V, et al. (1997) Serial follow-up after optimized ultrasound-guided deployment of Palmaz-Schatz stents *Circulation* 95:363-370.
61. Hehrlein C, Dönges K, Metz J, Riessen R, Fehsenfeld P, von Hodenberg E, Kübler W (1995) Low-Dose Radioactive Endovascular Stents Prevent Smooth Muscle Cell Proliferation and Neointimal Hyperplasia in Rabbits *Circulation* 92:1570-1575.
62. Yui Y, Kawai C, Hosoda S (1995) Pravastatin (mevalotin) restenosis trial after percutaneous transluminal coronary angioplasty. Cholesterol reduction rate determines the restenosis rate *Annals of the N Y Academy of Sciences* 748:208-216.

63. Babapulle M, Joseph L, Belisle P, et al. (2004) A hierarchical Bayesian meta-analysis of randomised clinical trials of drugeluting stents *Lancet* 364:583– 591.
64. Wong A, Waugh JM, Amabile PG et al. (2002) In vivo vascular engineering: directed migration of smooth muscle cells to limit neointima. *Tissue Engineering* 8:189–199.
65. Caves J, Chaikof EL (2006) The evolving impact of microfabrication and nanotechnology on stent design *J Vasc Surg* 44:1363-1368.
66. Buxton DB, Lee, S.C., Wickline, S.A., Ferrari, M., and Working Group Members (2003) Recommendations of the National Heart, Lung, and Blood Institute Nanotechnology Working Group *Circulation* 108:2737-2742.
67. Kolodgie F, John, M, Khurana, C, et al. (2002) Sustained reduction of in-stent neointimal growth with the use of a novel systemic nanoparticle paclitaxel *Circulation* 106:1195–1198.
68. Finkelstein A, McClean, D, Kar, S, et al. (2003) Local drug delivery via a coronary stent with programmable release pharmacokinetics *Circulation* 107:777–784.
69. Winter P, Neubauer AM, Caruthers SD, et al. (2006) Endothelial alpha-(nu)-beta 3 integrin-targeted fumagillin nanoparticles inhibit angiogenesis in atherosclerosis *Arteriosclerosis Thrombosis Vascular Biology* 26:2103-2109.
70. Lodish H, et al. (2000) *Molecular Cell Biology* (W H Freeman and Company, New York).
71. Torchilin V, Trubetskoy V (1995) Which polymers can make nanoparticulate drug carriers long-circulating? *Adv. Drug Delivery Rev* 16:141-155.
72. Torchilin V (2001) Structure and design of polymeric surfactant-based drug delivery systems *Controlled Release* 73:137-172.
73. Nishikawa M, Takakura Y, Hashida M (1996) Pharmacokinetic evaluation of polymeric carriers *Adv. Drug Delivery Rev* 21:135-155.
74. Takakura Y, Mahato R, Nishikawa M, Hashida M (1996) Pharmacokinetic evaluation of polymeric carriers *Adv. Drug Delivery Rev.* 19:377-399.
75. Hodoshima N, et al. (1997) Lipid nanoparticles for delivering antitumor drugs *Int. J. Pharm.* 146:81-92.
76. Junping W, Takayama K, Nagai T, Maitani Y (2003) Pharmacokinetics and antitumor effects of vincristine carried by microemulsions composed of PEG-lipid, oleic acid, vitamin E and cholesterol *Int J. Pharm.* 251:13-21.
77. Ratner BD, Hoffman AS, Schoen FJ, Lemons JE (1996) *Biomaterials Science An Introduction to Materials in Medicine* (Academic Press, San Diego).
78. Israelachvili J (1997) The different faces of poly(ethylene glycol). *Proc. Natl. Acad. Sci. USA* 94:8378-8379.
79. Uhrich KE, Cannizzaro SM, Langer R, Shakesheff K (1999) Polymeric systems for controlled drug release. *Chem. Rev.* 99:3181-3198.
80. Zalipsky S (1995) Functionalized Poly(ethylene glycols) for Preparation of Biologically Relevant Conjugates *Bioconj. Chem.* 6:150-165.
81. Langer R (1990) New methods of drug delivery. *Science* 249:1527-1533.
82. Kwon JSO, T. (1996) Polymeric micelles as new drug carriers. *Adv. Drug Delivery Rev.* 21:107-116.

83. Miele E, Spinelli GP, Miele E, Tomao F, Tomao S (2009) Albumin-bound formulation of paclitaxel (Abraxane® ABI-007) in the treatment of breast cancer *Int J Nanomedicine* 4:99-105.
84. Rowinsky E, Cazenave L, Donehower R (1990) Taxol: a novel investigational antimicrotubule agent *J Natl Cancer Inst* 82:1247-1259.
85. Weiss R, Donehower R, Wiernik P, et al (1990) Hypersensitivity reactions from Taxol *J Clin Oncol* 8:1263-1268.
86. Gelderblom H, Verweij J, Nooter K, Sparreboom A (2001) Cremophor EL: the drawbacks and advantages of vehicle selection for drug formulation *European Journal of Cancer* 37:1590-1598.
87. Lorenz W, Reimann H, Schmal A, et al (1977) Histamine release in dogs by Cremophor EL and its derivatives: Oxethylated oleic acid is the most effective constituent *Agents Actions* 7:63-67.
88. Tian L, Yam L, Zhou N, Tat H, Uhrich KE (2004) Amphiphilic Scorpion-like Macromolecules: Design, Synthesis, and Characterization *Macromolecules* 37:538-543.
89. Chnari E, Lari H, Tian L, Uhrich K, Moghe P (2005) Nanoscale anionic macromolecules for selective retention of low-density lipoproteins *Biomaterials* 26:3749-3758.
90. Chnari E, Nikitczuk J, Wang J, Uhrich K, Moghe P (2006) Engineered Polymeric Nanoparticles for Receptor-Targeted Blockage of Oxidized Low Density Lipoproteins Uptake and Atherogenesis in Macrophages *Biomacromolecules* 7:1796-1805.
91. Chnari E, Nikitczuk J, Uhrich K, Moghe P (2006) Nanoscale anionic macromolecules can inhibit cellular uptake of differentially oxidized LDL *Biomacromolecules* 7:597-603.
92. Kataoka K, Kwon G, Yokoyama M, Okano T, Sakurai Y (1993) Block copolymer micelles as vehicles for drug delivery *Journal of Controlled Release* 24:119-132.
93. Divchev D, Schieffer B (2008) The secretory phospholipase A2 group IIA: a missing link between inflammation, activated renin-angiotensin system, and atherogenesis? *Vasc Health Risk Manag* 4:597-604.
94. Kudo I, Murakami M (2002) Phospholipase A2 enzymes *Prostaglandins Other Lipid Mediat.* 68-69:3-58.
95. Six D, Dennis E (2000) The expanding superfamily of phospholipase A2 enzymes: classification and characterization *Biochimica et Biophysica Acta* 1488:1-19.
96. Kockx M, Jessup W, Kritharides L (2008) Regulation of Endogenous Apolipoprotein E Secretion by Macrophages *Arteriosclerosis Thrombosis Vascular Biology* 28:1060-1067.
97. Gafencu A, et al. (2007) Inflammatory signaling pathways regulating ApoE gene expression in macrophages *J Biol Chem* 282:21776-21785.
98. Singh N, Ramji D (2006) Transforming growth factor-beta-induced expression of the apolipoprotein E gene requires c-Jun N-terminal kinase, p38 kinase, and casein kinase 2 *Arteriosclerosis Thrombosis Vascular Biology* 26:1323-1329.

99. Galetto R, Albajar M, Polanco J, Zakin M, Rodriguez-Rey J (2001) Identification of a peroxisome-proliferator-activated-receptor response element in the apolipoprotein E gene control region *Biochem J* 357:521-527.
100. Laffitte B, et al. (2001) LXRs control lipid-inducible expression of the apolipoprotein E gene in macrophages and adipocytes *Proceedings of the National Academy of Science U S A* 98:507-512.
101. Geyeregger R, Zeyda M, Stulnig TM (2006) Liver X receptors in cardiovascular and metabolic disease *Cell Mol Life Sci* 63:524-39.
102. Aravindhan K, et al. (2006) Assessing the effects of LXR agonists on cellular cholesterol handling: a stable isotope tracer study *J. Lipid Res.* 47:1250-1260.
103. Tangirala R, Bischoff, ED, Joseph, SB, Wagner, BL, Walczak, R, Laffitte, BA, et al. (2002) Identification of macrophage liver X receptors as inhibitors of atherosclerosis *Proc Natl Acad Sci USA* 2002 99:11896-11901.
104. Tontonoz P, and Mangelsdorf, DJ (2003) Liver x receptor signaling pathways in cardiovascular disease *Mol Endocrinol* 17:985-993.
105. Glass C, Witztum J (2001) Atherosclerosis: the road ahead *Cell* 104:503-516.
106. Bradley MN, et al. (2007) Ligand activation of LXR β reverses atherosclerosis and cellular cholesterol overload in mice lacking LXR α and apoE *J. Clin. Invest.* 117:2337-2346.
107. Lusis AJ (2000) Atherosclerosis *Nature* 407:233-241.
108. Gimbrone MA, Jr (1999) Endothelial dysfunction, hemodynamic forces, and atherosclerosis *Thromb. Haemostasis* 82:722-726.
109. Goldstein J, Ho Y, Basu S, Brown M (1979) Binding site on macrophages that mediates uptake and degradation of acetylated low density lipoprotein, producing massive cholesterol deposition *Proc. Natl. Acad. Sci. U. S. A.* 76:333-337.
110. Loughed M, et al. (1997) High affinity saturable uptake of oxidized low density lipoprotein by macrophages from mice lacking the scavenger receptor class A type I/II *Journal of Biological Chemistry* 272:12938-12944.
111. Berliner J, Heinecke J (1996) The role of oxidized lipoproteins in atherogenesis *Free Radical Biology & Medicine* 20:707-727.
112. Ramprasad M, Terpstra V, Kondratenko N, Quehenberger O, Steinberg D (1996) Cell surface expression of mouse macrosialin and human CD68 and their role as macrophage receptors for oxidized low density lipoprotein *Proceedings of the National Academy of Science U S A* 93:14833-14838.
113. Hiltunen T, Yla-Herttuala S (1998) Expression of lipoprotein receptors in atherosclerotic lesions *Atherosclerosis* 137:S81-S88.
114. de Winther M, van Dijk K, Havekes L, Hofker M (2000) Macrophage scavenger receptor class A: A multifunctional receptor in atherosclerosis *Arterioscler., Thromb., Vasc. Biol.* 20:290-297.
115. Podrez E, et al. (2000) Macrophage scavenger receptor CD36 is the major receptor for LDL modified by monocyte-generated reactive nitrogen species *Journal of Clinical Investigation* 105:1095-1108.

116. Zaman A, Helft G, Worthley S, Badimon J (2000) The role of plaque rupture and thrombosis in coronary artery disease *Atherosclerosis* 149:251-266.
117. Nicholson A, Han J, Febbraio M, Silverstein R, Hajjar D (2001) Role of CD36, the macrophage class B scavenger receptor, in atherosclerosis. *Annals of the N Y Academy of Science* 947:224-228.
118. Yoshimoto T, et al. (2002) Growth simulation and epidermal growth factor receptor induction in cyclooxygenase-overexpressing human colon carcinoma cells *Advances in Experimental Medicine and Biology* 507:403-407.
119. Wang J, Plourde NM, Iverson N, Moghe PV, Uhrich KE (2007) Nanoscale amphiphilic macromolecules as lipoprotein inhibitors: the role of charge and architecture *International Journal of Nanomedicine* 2:697-705.
120. Plourde NM, Kortagere S, Welsh W, Moghe PV (2009) Structure-activity relations of nanolipoblockers with the atherogenic domain of human macrophage scavenger receptor A *Biomacromolecules* 10:1381-1391.
121. Harmon A, Uhrich K (2009) In vitro evaluation of amphiphilic macromolecular nanocarriers for systemic drug delivery *Journal of Bioactive and Compatible Polymers* 24:185-197.
122. Wang J, LS del Rosario, B Demirdirek, A Bae, and KE Uhrich (2009) Comparison of PEG chain length and density on amphiphilic macromolecular nanocarriers: Self-assembled and unimolecular micelles *Acta Biomaterialia* 5:883-892.
123. Tsuchiya S, et al. (1980) Establishment and characterization of a human acute monocytic leukemia cell line (THP-1) *Int J Cancer* 26:171-176.
124. Djordjevic J, Barch M, Uhrich K (2005) Polymeric micelles based on amphiphilic scorpion-like macromolecules: novel carriers for water-insoluble drugs *Pharmaceutical research* 22:24-32.
125. Djordjevic J, del Rosario L, Wang J, Uhrich K. (2008) Amphiphilic scorpion-like macromolecules as micellar nanocarriers *Journal of Bioactive and Compatible Polymers* 23:532-551.
126. Steege K, Wang J, Uhrich K, Castner Jr. E (2007) Local Polarity and Microviscosity in the Hydrophobic Cores of Amphiphilic Star-like and Scorpion-like Macromolecules *Macromolecules* 40:3739-3748.
127. Tao L, Uhrich KE (2006) Novel amphiphilic macromolecules and their in vitro characterization as stabilized micellar drug delivery systems *J. Colloid Interface Sci.* 298:102-110.
128. Fontana G, Licciardi M, Mansueto S, Schillaci D, Giammona G (2001) Amoxicillin-loaded polyethyl cyanoacrylate nanoparticles: Influence of PEG coating on the particle size, drug release rate and phagocytic uptake *Biomaterials* 22:2857-2865.
129. Zahr A, Davis C, Pishko M (2006) Macrophage Uptake of Core-Shell Nanoparticles Surface Modified with Poly(ethylene glycol) *Langmuir* 22:8178-8185.
130. Ogris M, Brunner S, Schuller S, Kircheirs R, Wagner E (1999) PEGylated DNA/transferrin-PEI complexes: reduced interaction with blood components,

- extended circulation in blood and potential for systemic gene delivery *Gene Therapy* 6:595-605.
131. Yang Z, Sahay G, Sriadibhatla S, Kabanov A (2008) Amphiphilic Block Copolymers Enhance Cellular Uptake and Nuclear Entry of Polyplex-Delivered DNA *Bioconjugate Chem.* 19:1987-1994.
 132. Tian Y, Bromberg L, Lin S, Alan Hatton T, Tam K (2007) Complexation and release of doxorubicin from its complexes with pluronic P85-b-poly(acrylic acid) block copolymers *Journal of Controlled Release* 121:137-145.
 133. Patel S, Datta A (2005) pH effect on the binding of chlorin derivatives with Cremophor EL, a potential drug delivery vehicle. *Chemical Physics Letters* 413:31-35.
 134. Alberts B, et al. (2002) *Molecular Biology of The Cell* (Garland Science, New York).
 135. Yoshiizumi K, Nakajima F, Dobashi R, Nishimura N, Ikeda S (2002) Studies on scavenger receptor inhibitors. Part 1: synthesis and structure-activity relationships of novel derivatives of sulfatides *Bioorganic & Medicinal Chemistry* 10:2445-2460.
 136. Fee C (2007) Size comparison between proteins PEGylated with branched and linear poly(ethylene glycol) molecules *Biotechnology and Bioengineering* 98:725-731.
 137. DeNoon DJ (2002) in *WebMD Health News*.
 138. McKenney JM (2001) Lipid Management: Tools for Getting to the Goal *Am. J. Man. Care* 7:S299-S306.
 139. Kunjathoor V, et al. (2002) Scavenger receptors class A-I/II and CD36 are the principal receptors responsible for the uptake of modified low density lipoprotein leading to lipid loading in macrophages *J. Biol. Chem.* 277:49982-49988.
 140. Brown MS, Goldstein JL (1983) Lipoprotein metabolism in the macrophage: implications for cholesterol deposition in atherosclerosis *Annu. Rev. Biochem.* 52:223-261.
 141. Babaev V, et al. (2000) Reduced atherosclerotic lesions in mice deficient for total or macrophage specific expression of scavenger receptor-A *Arterioscler., Thromb., Vasc. Biol.* 20:2593-2599.
 142. Febbraio M, et al. (2000) Targeted disruption of the class B scavenger receptor CD36 protects against atherosclerotic lesion development in mice *J. Clin. Invest.* 105:1095-1108.
 143. Fujiwara Y, et al. (2007) Esculeogenin A, a New Tomato Sapogenol, Ameliorates Hyperlipidemia and Atherosclerosis in ApoE-Deficient Mice by Inhibiting ACAT *Arterioscler., Thromb., Vasc. Biol.* 27:2400-2406.
 144. Manning-Tobin JJ, et al. (2009) Loss of SR-A and CD36 Activity Reduces Atherosclerotic Lesion Complexity Without Abrogating Foam Cell Formation in Hyperlipidemic Mice *Arterioscler., Thromb., Vasc. Biol.* 29:19-26.
 145. Ross R (1995) Cell biology of atherosclerosis *Annu. Rev. Physiol.* 57:791-804.

146. Yamakawa T, et al. (2009) Effect of Dehydroepiandrosterone on Atherosclerosis in Apolipoprotein E-Deficient Mice *J. Atheroscler. Thromb.* 16:501-508.
147. Oorni K, et al. (1997) Oxidation of low density lipoprotein particles decreases their ability to bind to human aortic proteoglycans. Dependence on oxidative modification of the lysine residues. *Journal of Biological Chemistry* 272:21303-11.
148. Mani (2006) Feasibility of In Vivo Identification of Endogenous Ferritin with Positive Contrast MRI in Rabbit Carotid Crush Injury Using GRASP *Magnetic Resonance in Medicine* 56:1096-1106.
149. Krieger M (1997) The other side of scavenger receptors: pattern recognition for host defense *Curr. Opin. Lipidol.* 8:275-280.
150. Chnari E, Nikitzuk JS, Wang J, Uhrich KE, Moghe PV (2006) Engineered polymeric nanoparticles for receptor-targeted blockage of oxidized low density lipoprotein uptake and atherogenesis in macrophages *Biomacromolecules* 7:1796-805.
151. Geng YJ, et al. (1995) Expression of the macrophage scavenger receptor in atheroma. Relationship to immune activation and the T-cell cytokine interferon-gamma *Arterioscler Thromb Vasc Biol* 15:1995-2002.
152. Luoma J, et al. (1994) Expression of alpha 2-macroglobulin receptor/low density lipoprotein receptor-related protein and scavenger receptor in human atherosclerotic lesions *J Clin Invest* 93:2014-21.
153. Platt N, Gordon S (2001) Is the class A macrophage scavenger receptor (SR-A) multifunctional? - The mouse's tale *J Clin Invest* 108:649-54.
154. Joseph SB, et al. (2002) Synthetic LXR ligand inhibits the development of atherosclerosis in mice *Proc. Natl. Acad. Sci. U. S. A.* 99:7604-7609.
155. Joseph SB, and Tontonoz P (2003) LXRs: new therapeutic targets in atherosclerosis? *Curr Opin Pharmacol* 3:192-197.
156. Albers M, et al. (2006) A Novel Principle for Partial Agonism of Liver X Receptor Ligands *J. Biol. Chem.* 281:4920-4930.
157. Hansson GK (2001) Immune mechanisms in atherosclerosis *Arterioscler., Thromb., Vasc. Biol.* 21:1876-1890.
158. Hansson G (2001) Regulation of immune mechanisms in atherosclerosis *Ann N Y Acad Sci* 947:157-165.
159. Libby P (2000) Changing concepts of atherogenesis *J Intern Med* 247:349-358.
160. Blake G, Ridker P (2001) Inflammatory mechanisms in atherosclerosis: from laboratory evidence to clinical application *Ital Heart J* 2:796-800.
161. Khanna AK (2009) Enhanced susceptibility of cyclin kinase inhibitor p21 knockout mice to high fat diet induced atherosclerosis *Journal of Biomedical Science* 16:
162. Hansson G (2005) Inflammation, atherosclerosis and coronary artery disease *N Engl J Med* 352:1685-1695.
163. Schreyer SA, Peschon JJ, LeBoeuf RC (1996) Accelerated Atherosclerosis in Mice Lacking Tumor Necrosis Factor Receptor p55 *The Journal of Biological Chemistry* 271:26174-26178.
164. Dinarello C (1996) Biologic basis for interleukin-1 in disease *Blood* 87:2095-2147.

165. Stolpen A, Guinan E, Fiers W, Pober J (1986) Recombinant Tumor Necrosis Factor and Immune Interferon Act Singly and in Combination to Recognize Human Vascular Endothelial Cell Monolayers *Am J Pathol* 123:16-24.
166. Kawakami M, Pekala P, Lane M, Cerami A (1982) Lipoprotein lipase suppression in 3T3-L1 cells by an endotoxin-induced mediator from exudate cells *Proc Natl Acad Sci USA* 79:912-916.
167. Pober J, Cotran R (1991) What can be learned from the expression of endothelial adhesion molecules in tissues? *Lab. Invest.* 64:301-305.
168. Cotran R, Pober J (1990) Cytokines and endothelial cell biology *J Am Soc Nephrol* 1:225-235.
169. Yoshizumi M, et al. (1992) Tumor necrosis factor increases transcription of the heparin-binding epidermal growth factor-like growth factor gene in vascular endothelial cells *J Biol Chem* 267:9467-9469.
170. Koeffler H, Gasson J, Tobler A (1988) Transcriptional and posttranscriptional modulation of myeloid colony-stimulating factor expression by tumor necrosis factor and other agents *Mol Cell Biol* 8:3432-3437.
171. Marucha P, Zeff R, Kreutzer D (1991) Cytokine-induced IL-1 beta gene expression in the human polymorphonuclear leukocyte: transcriptional and post-transcriptional regulation by tumor necrosis factor and IL-1 *J Immunol* 147:2603-2608.
172. Yukihiro H, et al. (2000) Matrix Metalloproteinase-1 Expression by Interaction between Monocytes and Vascular Endothelial Cells *J Mol Cell Cardiol* 32:1459-1468.
173. Richardson P, Davies M, Born G (1989) Influence of plaque configuration and stress distribution on fissuring of coronary atherosclerotic plaques *Lancet* 2:941-944.
174. Cheng G, Loree H, Kamm R, Fishbein M, Lee R (1993) Distribution of circumferential stress in ruptured and stable atherosclerotic lesions *Circulation* 87:1179-1187.
175. Falk E, Shah P, Fuster V (1995) Coronary plaque disruption *Circulation* 92:657-671.
176. Ding Y, Nguyen HT, Kim SI, Kim HW, Kim YH (2009) The regulation of inflammatory cytokine secretion in macrophage cell line by the chemical constituents of *Rhus sylvestris* *Bioorganic & Medicinal Chemistry* 19:3607-3610.
177. Sampaio EP, Sarno EN, Galilly R, Cohn ZA, Kaplan G (1991) Thalidomide Selectively Inhibits Tumor Necrosis Factor ac Production by Stimulated Human Monocytes *J Exp Med* 173:699-703.
178. Sukhova G, et al. (1999) Evidence for increased collagenolysis by interstitial collagenases-1 and -3 in vulnerable human atheromatous plaques *Circulation* 99:2503-2509.
179. Xu X, et al. (1999) Oxidized low-density lipoprotein regulates matrix metalloproteinase-9 and its tissue inhibitor in human monocyte-derived macrophages *Circulation* 99:993-998.

180. Libby P, Galis Z (1995) Cytokines regulate genes involved in atherogenesis *Ann N Y Acad Sci* 748:158-168.
181. Libby P, Sukhova G, Lee R, Galis Z (1995) Cytokines regulate vascular functions related to stability of the atherosclerotic plaque *J Cardiovasc Pharmacol* 25:S9-S12.
182. Zhang Y, McCluskey K, Fujii K, Wahl L (1998) Differential Regulation of Monocyte Matrix Metalloproteinase and TIMP-1 Production by TNF- α , Granulocyte-Macrophage CSF, and IL-1 β Through Prostaglandin-Dependent and Independent Mechanisms *The Journal of Immunology* 161:3071-3076.
183. Ardans JA, Economou AP, Jr. JMM, Zhou M, Wahl LM (2002) Oxidized low-density and high-density lipoproteins regulate the production of matrix metalloproteinase-1 and -9 by activated monocytes *Journal of Leukocyte Biology* 71:1012-1018.
184. Agu R, Ugwoke M, Armand M, Kinget R, Verbeke N (2001) The lung as a route for systemic delivery of therapeutic proteins and peptides *Respir Res* 2:198-209.
185. Siekmeier R, Scheuch G (2008) Systemic Treatment by Inhalation of Macromolecules - Principles, Problems and Examples *Journal of Physiology and Pharmacology* 59:53-79.
186. Allen T, Cullis P (2004) Drug delivery systems: entering the mainstream *Science* 303:1818-1822.
187. Edens H, Levi B, Jaye D, et al. (2002) Neutrophil transepithelial migration: evidence for sequential, contact-dependent signaling events and enhanced paracellular permeability independent of transjunctional migration *J Immunol* 169:476-486.
188. Gao X, Cui Y, Levenson R, et al (2004) In vivo cancer targeting and imaging with semiconductor quantum dots *Nat Biotechnol* 22:969-976.
189. Jain T, Morales M, Sahoo S, et al (2005) Iron oxide nanoparticles for sustained delivery of anticancer agents *Mol Pharm* 2:194-205.
190. Pelicano H, Martin D, Xu R, Huang P (2006) Glycolysis inhibition for anticancer treatment *Oncogene* 25:4633-4646.
191. Deryugina E, Quigley J (2006) Matrix metalloproteinases and tumor metastasis *Cancer Metastasis Rev* 25:9-34.
192. Brannon-Peppas L, Blanchette J (2004) Nanoparticle and targeted systems for cancer therapy *Adv. Drug Delivery Rev* 56:1649-1659.
193. Sledge Jr. G, Miller K (2003) Exploiting the hallmarks of cancer: the future conquest of breast cancer *Eur J Cancer* 39:1668-1675.
194. Jain R (1987) Transport of molecules across tumor vasculature *Cancer Metastasis Rev* 6:559-593.
195. Cuenca A, Jiang H, Hochwald S, et al (2006) Emerging implications of nanotechnology on cancer diagnostics and therapeutics *Cancer* 107:459-466.
196. Williams K, Tabas I (1995) The response-to-retention hypothesis of early atherogenesis *Arteriosclerosis Thrombosis Vascular Biology* 15:551-61.
197. Olsson U, Ostergren-Lunden G, Moses J (2001) Glycosaminoglycan-lipo-protein interaction *Glycoconj J* 18:789-797.

198. Camejo G, Olsson U, Hurt-Camejo E, Baharamian N, Bondjers G (2002) The extracellular matrix on atherogenesis and diabetes-associated vascular disease *Atherosclerosis Suppl* 3:3-9.
199. Thom T, Haase N, Rosamond W, et al. (2006) Heart Disease and Stroke Statistics – 2006 Update: A Report From the American Heart Association Statistics Committee and Stroke Statistics Subcommittee *Circulation* 113:e85-e151.
200. Malinski T (2005) Understanding nitric oxide physiology in the heart: a nanomedical approach *Am J Cardiol* 96:13i-24i.
201. Carella M, Volinia S, Gasparini P (2003) Nanotechnologies and microchips in genetic diseases *Journal of Nephrology* 16:597-602.
202. He W, Yong T, Teo W, et al (2005) Fabrication and endothelialization of collagen-blended biodegradable polymer nanofibers: potential vascular graft for blood vessel tissue engineering *Tissue Eng* 11:1574-1588.
203. He W, Ma Z, Yong T, et al (2005) Fabrication of collagen-coated biodegradable polymer nanofiber mesh and its potential for endothelial cells growth *Biomaterials* 26:7606-7615.
204. Ma Z, He W, Yong T, et al. (2005) Grafting of gelatin on electrospun poly(caprolactone) nanofibers to improve endothelial cell spreading and proliferation and to control cell Orientation *Tissue Eng* 11:1149-1158.
205. Endo M, Koyama S, Matsuda Y, et al (2005) Thrombogenicity and blood coagulation of a microcatheter prepared from carbon nanotube-nylon-based composite *Nano Lett* 5:
206. Meng J, et al. (2005) Improving the blood compatibility of polyurethane using carbon nanotubes as fillers and its implications to cardiovascular surgery *J Biomed Mater Res* 74A:208–214.
207. Yoshiizumi K, Nakajima F, Dobashi R, et al. (2004) 2,4-Bis(octadecanoyl amino)benzenesulfonic acid sodium salt as a novel scavenger receptor inhibitor with low molecular weight *Bioorganic & Medicinal Chemistry Letter* 14:2791-2795.
208. Boullier A, Friedman P, Harkewicz R, et al (2005) Phosphocholine as a pattern recognition ligand for CD36 *J Lipid Res* 46:969-976.
209. Broz P, Benito S, Saw C, et al (2005) Cell targeting by a generic receptor-targeted polymer nanocontainer platform *J Control Release* 102:475-488.
210. Guaderrama-Diaz M, Solis C, Velasco-Loyden G, et al (2005) Control of scavenger receptor-mediated endocytosis by novel ligands of different length *Mol Cell Biochem* 271:123-132.
211. Krieger M, Acton S, Ashkenas J, et al (1993) Molecular Flypaper, Host Defense, and Atherosclerosis: structure, binding properties, and functions of macrophage scavenger receptors *J Biol Chem* 268:4569-4572.
212. Traber M, Defendi V, Kayden H. (1981) Receptor activities for low-density lipoprotein and acetylated low-density lipoprotein in a mouse macrophage cell line (IC21) and in human monocyte-derived macrophages *J Exp Med* 154:1852-1867.

213. Patel R, Moellering D, Murphy-Ullrich J, et al. (2000) Cell signaling by reactive nitrogen and oxygen species in atherosclerosis *Free Radical Biol. Med.* 28:1780-1794.
214. Platt N, Siamon G (2001) Is the class A macrophage scavenger receptor (SR-A) multifunctional? - the mouse's tale *J. Clin. Invest.* 108:649-654.
215. Moghimi S, Szebeni J (2003) Stealth liposomes and long circulating nanoparticles: critical issues in pharmacokinetics, opsonization, and protein-binding properties *Prog Lipid Res* 42:463-478.
216. Raynal I, Prigent P, Peyramaure S, et al. (2004) Macrophage endocytosis of superparamagnetic iron oxide nanoparticles: mechanisms and comparison of ferumoxides and ferumoxtran-10 *Investig Radiology* 39:56-63.
217. Vonarbourg A, Passirani C, Saulnier P, et al. (2006) Evaluation of pegylated lipid nanocapsules versus complement system activation and macrophage uptake *J Biomed Mater Res* 78A:620-628.
218. Lanza G, Wickline SA (2001) Targeted ultrasonic contrast agents for molecular imaging and therapy *Prog Cardiovasc Dis* 44:13-31.
219. Chen CM, and Peng, E. H. (2003) Nanopore sequencing of polynucleotides assisted by a rotating electric field *Appl. Phys. Lett.* 82: 1308–1310.
220. Han M, Gao, X, Su, JZ, et al. (2001) Quantum-dot-tagged microbeads for multiplexed optical coding of biomolecules *Nat Biotechnol* 19:631–635.
221. Wickline SA, Neubauer, A.M., Winter, P., Caruthers, S., Lanza, G. (2006) Applications of Nanotechnology to Atherosclerosis, Thrombosis, and Vascular Biology *Arteriosclerosis, Thrombosis, and Vascular Biology* 26:435-441.
222. Tsien RY (2003) Imagining imaging's future *Nat Rev Mol Cell Biol Suppl*:S516-21.
223. Gadegaard N (2006) Atomic force microscopy in biology: technology and techniques *Biotech Histochem* 81:87-97.
224. Blake GJ, Rifai N, Buring JE, Ridker PM (2003) Blood pressure, C-reactive protein, and risk of future cardiovascular events *Circulation* 108:2993-9.
225. Volanakis JE (2001) Human C-reactive protein: expression, structure, and function *Mol Immunol* 38:189-97.
226. Lin S, et al. (2006) Measurement of dimensions of pentagonal doughnut-shaped C-reactive protein using an atomic force microscope and a dual polarisation interferometric biosensor *Biosens Bioelectron* 22:323-7.
227. Flanagan TC, Pandit A (2003) Living artificial heart valve alternatives: a review *Eur Cell Mater* 6:28-45; discussion 45.
228. Brody S, et al. (2006) Characterizing nanoscale topography of the aortic heart valve basement membrane for tissue engineering heart valve scaffold design *Tissue Eng* 12:413-21.
229. Sun Z, et al. (2005) Mechanical properties of the interaction between fibronectin and $\alpha_5\beta_1$ -integrin on vascular smooth muscle cells studied using atomic force microscopy *Am J Physiol Heart Circ Physiol* 289:H2526-35.
230. Pohl DW, Denk W, Lanz M (1984) Optical stethoscopy: image recording with a resolution of $\lambda/20$ *Appl Phys Lett* 44:651-653.

231. Ianoul A, et al. (2004) Near-field scanning fluorescence microscopy study of ion channel clusters in cardiac myocyte membranes *Biophys J* 87:3525-35.
232. Micheletto R, Deyner M, Scholl M, Nakajima A (1999) Observation of the dynamics of live cardiomyocytes through a free-running scanning near-field optical microscopy setup *Appl Opt* 38:6648-6652.
233. Clegg R (1996) in *Fluorescence Imaging Spectroscopy and Microscopy* (John Wiley & Sons, New York, NY), pp. 179-251.
234. Gross GJ, Peart JN (2003) KATP channels and myocardial preconditioning: an update *Am J Physiol Heart Circ Physiol* 285:H921-30.
235. Murry CE, Jennings RB, Reimer KA (1986) Preconditioning with ischemia: a delay of lethal cell injury in ischemic myocardium *Circulation* 74:1124-36.
236. Garg V, Hu K (2007) Protein kinase c isoform-dependent modulation of ATP-sensitive K⁺ channels in mitochondrial inner membrane *Am J Physiol Heart Circ Physiol*
237. Meyer M, et al. (2004) A recombinant antibody increases cardiac contractility by mimicking phospholamban phosphorylation *Faseb J* 18:1312-4.
238. Xu Y, Piston DW, Johnson CH (1999) A bioluminescence resonance energy transfer (BRET) system: application to interacting circadian clock proteins *Proc Natl Acad Sci U S A* 96:151-6.
239. Prinz A, Diskar M, Erlbruch A, Herberg FW (2006) Novel, isotype-specific sensors for protein kinase A subunit interaction based on bioluminescence resonance energy transfer (BRET) *Cell Signal* 18:1616-25.
240. Tasken K, Aandahl EM (2004) Localized effects of cAMP mediated by distinct routes of protein kinase A *Physiol Rev* 84:137-67.
241. Lanza G, Wallace KD, Scott MJ, Cacheris WP, Sheehan CK, Abendschein DR, Christy DH, Sharkey AM, Miller JG, Gaffney PJ, Wickline SA (1996) A novel site-targeted ultrasonic contrast agent with broad biomedical application *Circulation* 95:3334-3340.
242. Moulton K, Heller E, Konerding MA, Flynn E, Palinski W, Folkman J (1999) Angiogenesis inhibitors endostatin or TNP-470 reduce intimal neovascularization and plaque growth in apolipoprotein E-deficient mice *Circulation* 99:1726-1732.
243. Tenaglia A, Peters KG, Sketch MH Jr, Annex BH (1998) Neovascularization in atherectomy specimens from patients with unstable angina: implications for pathogenesis of unstable angina *Am Heart J* 135:10-14.
244. Winter P, Morawski AM, Caruthers SD, Fuhrhop RW, Zhang HY, Williams TA, Allen JS, Lacy EK, Robertson JD, Lanza GM, Wickline SA (2003) Molecular imaging of angiogenesis in early-stage atherosclerosis with alpha(v)beta(3)-Integrin-targeted nanoparticles *Circulation* 108:2270-2274.
245. Lanza G, Yu, X, Winter, PM, et al. (2002) Targeted antiproliferative drug delivery to vascular smooth muscle cells with a magnetic resonance imaging nanoparticle contrast agent: implications for rational therapy of restenosis *Circulation* 106:2842-2847.

246. Zhao M, Beauregard, DA, Loizou, L, et al. (2001) Non-invasive detection of apoptosis using magnetic resonance imaging and a targeted contrast agent *Nat Med* 7:1241–1244.
247. Walsh K, Smith RC, Kim HS (2000) Vascular Cell Apoptosis in Remodeling, Restenosis, and Plaque Rupture *Circ Res* 87:184-188.
248. Blankenberg F, Strauss HW (2001) Noninvasive strategies to image cardiovascular apoptosis *Cardiol Clin.* 19:165–172.
249. Nahrendorf M, Kelly K, Sosnovik D, et al. (2006) Noninvasive vascular cell adhesion molecule-1 imaging identifies inflammatory activation of cells in atherosclerosis *Circulation* 114:1504-1511.
250. Ruehm S, Corot C, Vogt P, et al. (2001) Magnetic resonance imaging of atherosclerotic plaque with ultrasmall superparamagnetic particles of iron oxide in hyperlipidemic rabbits *Circulation* 103:415–422.
251. Chan WC, Nie S (1998) Quantum dot bioconjugates for ultrasensitive nonisotopic detection *Science* 281:2016-8.
252. Dubertret B, Skourides, P., Norris, D.J., et al. (2002) In vivo imaging of quantum dots encapsulated in Phospholipid micelles *Science* 298:1759–1762.
253. Cui Y, Wei, Q, Park, H, et al. (2001) Nanowire nanosensors for highly sensitive and selective detection of biological and chemical species *Science* 293:1289–1292.
254. Bonnet G, Tyagi S, Libchaber A, Kramer FR (1999) Thermodynamic basis of the enhanced specificity of structured DNA probes *Proc Natl Acad Sci U S A* 96:6171-6.
255. Tyagi S, Bratu DP, Kramer FR (1998) Multicolor molecular beacons for allele discrimination *Nat Biotechnol* 16:49-53.
256. Tyagi S, Kramer FR (1996) Molecular beacons: probes that fluoresce upon hybridization *Nat Biotechnol* 14:303-8.
257. Giesendorf BA, et al. (1998) Molecular beacons: a new approach for semiautomated mutation analysis *Clin Chem* 44:482-6.
258. Masson JF, Battaglia TM, Khairallah P, Beaudoin S, Booksh KS (2007) Quantitative measurement of cardiac markers in undiluted serum *Anal Chem* 79:612-9.
259. Jia SZ, Sun, H. Y., and Wang, Q. L. (2002) Nanopore technology and its applications *Prog. Biochem. Biophys.* 29:202–205.
260. Carella M, Volinia, S, Gasparini, P (2003) Nanotechnologies and chirochips in genetic diseases *Journal of Nephrology* 16:597-602.
261. Smith L, Sanders JZ, Kaiser RJ, Hughes P, Dodd C, Connell CR, Heiner C, Kent SBH, and Hood LE (1986) Fluorescence detection in automated DNA sequence analysis *Nature (London)* 321:674-679.
262. Sanger F, Nicklen S, and Coulson AR (1977) DNA Sequencing with Chain-Terminating Inhibitors *Proc. Natl. Acad. Sci. USA* 74:5463-5467.
263. Marziali A, and Akeson M (2001) New DNA sequencing methods *Annu. Rev. Biomed. Eng.* 3:195-223.

264. Flint J, Mott, R (2001) Finding the molecular basis of quantitative traits: successes and pitfalls *Nat Rev Genet* 2:437-45.
265. Barrans J, Stamatiou D, Liew C (2001) Construction of a human cardiovascular cDNA microarray: portrait of the failing heart *Biochem Biophys Res Commun* 280:964-969.
266. Lam C, James JT, McCluskey R, Arepalli S, Hunter RL (2006) A Review of Carbon Nanotube Toxicity and Assessment of Potential Occupational and Environmental Health Risks *Critical Reviews in Toxicology* 36:189-217.
267. Meng J, Kong H, Xu HY, Song L, Wang CY, Xie SS (2005) Improving the blood compatibility of polyurethane using carbon nanotubes as fillers and its implications to cardiovascular surgery *J Biomed Mater Res* 74A:208-214.
268. Yang P, Huang N, Leng YX, Chen JY, Fu RK, Kwok SCH, Leng Y, Chu PK (2003) Activation of platelets adhered on amorphous hydrogenated carbon (a-C:H) films synthesized by plasma immersion ion implantation-deposition(PIII-D) *Biomaterials* 24:2821-2829.
269. Smalley RE (1999) Nanotechnology. Prepared written statement and supplemental material of R. E. Smalley, Rice University, June 22, 1999 *U.S. House of Representatives Committee on Science, Basic Research Subcommittee Hearings, U.S. Government, Washington, DC* 1.
270. Sotiropoulou S, Chaniotakis NA (2003) Carbon Nanotube Array-based Biosensor *Analytical and Bioanalytical Chemistry* 375:103-105.
271. Star A, Tu E, Niemann J, Gabriel JCP, Joiner CS, Valcke C (2006) Label-free detection of DNA hybridization using carbon nanotube network field-effect transistors *PNAS* 103:921-926.
272. Li X, Peng Y, Qu X (2006) Carbon nanotubes selective destabilization of duplex and triplex DNA and inducing B-A transition in solution *Nucleic Acids Res* 34:3670-3676.
273. Li Z, Salmen, R., Huldermen, T., Kisin, E., Shvedova, A., Luster, M.I., and Simeonova, P.P. (2005) Pulmonary exposure to carbon nanotubes induces vascular toxicity *The Toxicologist CD—An Official Journal of the Society of Toxicology* 84:213.
274. Li ZJ, Chapman, R., Hulderman, T., Salmen, R., Shvedova, A., Luster, M.I., and Simeonova, P.P. (2006) Relationship between pulmonary exposure to multiple doses of single wall carbon nanotubes and atherosclerosis in ApoE -/- mouse model *The Toxicologist—Supplement to Toxicological Sciences* 90:213.
275. Bittl J (1996) Medical progress: advances in coronary angioplasty *New England Journal of Medicine* 335:1290-1302.
276. Wessely R, Hausleiter J, Michaelis C, Jaschke B, Vogeser M, Milz S, Behnisch B, Schratzenstaller T, Renke-Gluszko M, Stöver M, Wintermantel E, Kastrati A, Schömig A (2005) Inhibition of Neointima Formation by a Novel Drug-Eluting Stent System That Allows for Dose-Adjustable, Multiple, and On-Site Stent Coating *Arteriosclerosis, Thrombosis, and Vascular Biology* 25:748-753.
277. Sangiorgi G, Arbustini E, Lanzarini P, del Bello B, Maestri M, Gaspari A, Solcia M, Virmani R, Inglese L (2001) Nonbiodegradable Expanded

- Polytetrafluoroethylene-Covered Stent Implantation in Porcine Peripheral Arteries: Histologic Evaluation of Vascular Wall Response Compared with Uncoated Stents *Cardiovascular & Interventional Radiology* 24:260-270.
278. Honda Y, Grube E, de la Fuente LM, Yock PB, Stertzer SH, Fitzgerald PJ (2001) Novel Drug-Delivery Stent Intravascular Ultrasound Observations From the First Human Experience With the QP2-Eluting Polymer Stent System *Circulation* 104:380-383.
 279. Chaux A, H. Luo, et al. (1998) Noninvasive in vivo clot dissolution without a thrombolytic drug: recanalization of thrombosed iliofemoral arteries by transcutaneous ultrasound combined with intravenous infusion of microbubbles *American Journal of Cardiology* 81:229-231.
 280. Xie F, K. Kilzer, et al. (1996) Thrombolytic enhancement with perfluorocarbon-exposed sonicated dextrose albumin microbubbles *Journal of the American Society of Echocardiography* 9(6): 779-86.:779-786.
 281. Culp W, et al. (2003) Microbubble-augmented ultrasound declotting of thrombosed arteriovenous dialysis grafts in dogs *Journal of Vascular & Interventional Radiology* 14:343-347.
 282. Unger EC, T. Porter, et al. (2004) Therapeutic applications of lipid-coated microbubbles *Advanced Drug Delivery Reviews* 56:1291-314.
 283. Bardsley-Elliot A (2006) Biotechnology Industry Organization-- BIO 2006: Annual International Convention; 9-12 April, 2006; Chicago, Illinois, USA *BioDrugs* 20:181-90.
 284. Unger E (2006) Treatment of ischemic stroke with nanobubbles and ultrasound *The Journal of the Acoustical Society of America* 119:3437.
 285. Stieger SM, et al. (2006) Ultrasound assessment of angiogenesis in a matrigel model in rats *Ultrasound Med Biol* 32:673-81.
 286. Tsutsui JM, et al. (2006) Treatment of deeply located acute intravascular thrombi with therapeutic ultrasound guided by diagnostic ultrasound and intravenous microbubbles *J Ultrasound Med* 25:1161-8.
 287. Chin CT, Burns PN (2000) Predicting the acoustic response of a microbubble population for contrast imaging in medical ultrasound *Ultrasound Med Biol* 26:1293-300.
 288. Chappell JC, Price RJ (2006) Targeted therapeutic applications of acoustically active microspheres in the microcirculation *Microcirculation* 13:57-70.
 289. Price R, Chappell J., Song J., Klibanov A. (2006) Nanoparticle delivery into biological tissues by ultra sonic microbubble destruction *Nanomedicine: Nanotechnology, Biology and Medicine* 2:269-312.
 290. Shepherd J, Packard CJ, Bicker S, Lawrie TD, Morgan HG (1980) Effect of cholestyramine on low-density lipoproteins *N Engl J Med* 303:943 – 944.
 291. Stamler J, Wentworth D, Neaton JD (1986) Is relationship between serum cholesterol and risk of premature death from coronary heart disease continuous and graded? Findings in 356,222 primary screenees of the Multiple Risk Factor Intervention Trial (MRFIT) *JAMA* 256:2823-2828.

292. Shepherd J, Cobbe SM, Ford I, Isles CG, Lorimer AR, MacFarlane PW, McKillop JH, Packard CJ (1995) Prevention of coronary heart disease with pravastatin in men with hypercholesterolemia *N Engl J Med* 333:1301-1317.
293. Mabuchi H, Sakai T, Sakai Y, Yoshimura A, Watanabe A, Wakasugi T, et al (1983) Reduction of serum cholesterol in heterozygous patients with familial hypercholesterolemia: Additive effects of compactin and cholestyramine *N Engl J Med* 308:609 – 613.
294. Altschul R, Hoffer A, Stephen JD (1955) Influence of nicotinic acid on serum cholesterol in man *Arch Biochem* 54:558-559.
295. Carlson L, Oro L (1962) The effect of nicotinic acid on the plasma free fatty acid; demonstration of a metabolic type of sympathicolysis *Acta Med Scand* 172:641-645.
296. Takahashi Y, et al. (2002) Growth stimulation and epidermal growth factor receptor induction in cyclooxygenase-overexpressing human colon carcinoma cells *Advanced Experimental Medical Biology* 507:403-407.
297. Weissberg P, Bennett M, Boyle J (2002) Human macrophage-induced vascular smooth muscle cell apoptosis requires NO enhancement of Fas/Fas-L interactions *Arteriosclerosis, Thrombosis, and Vascular Biology* 22:1624-1630.
298. Wada Y, Sugiyama A, Yamamoto T, Naito M, Noguchi N, Yokoyama S, Tsujita M, Kawabe Y, Kobayashi M, Izumi A, Kohro T, Tanaka T, Taniguchi H, Koyama H, Hirano K, Yamashita S, Matsuzawa Y, Niki E, Hamakubo T, Kodama T (2002) Lipid accumulation in smooth muscle cells under LDL loading is independent of LDL receptor pathway and enhanced by hypoxic conditions *Arteriosclerosis, Thrombosis, and Vascular Biology* 22:1712-1719.
299. Absood A, Furutani A, Kawamura T, Graham L (2002) Differential PDGF secretion by graft and aortic SMC in response to oxidized LDL *Am. J. Physiol.-Heart Circ. Physiol.* 283:H725-732.
300. Absood A, Furutani A, Kawamura T, Graham L (2004) A comparison of oxidized LDL-induced collagen secretion by graft and aortic SMCs: role of PDGF *Am. J. Physiol.-Heart Circ. Physiol.* 287:H1200-1206.
301. Price R, Chappell J, Song J, Klibanov A (2006) Nanoparticle delivery into biological tissues by ultra sonic microbubble destruction *Nanomedicine: Nanotechnology, Biology and Medicine* 2:269-312.

CURRICULUM VITA

NICOLE M IVERSON

Iverson@rutgers.edu

EDUCATION

RUTGERS, THE STATE UNIVERSITY OF NEW JERSEY, Piscataway, NJ
Doctorate of Philosophy in Biomedical Engineering: Degree Received May 2010

UNIVERSITY OF MINNESOTA, Minneapolis, MN
Bachelor of Science in Biomedical Engineering: Degree Received May 2003

EXPERIENCE

BIOMEDICAL ENGINEERING DEPARTMENT, RUTGERS UNIVERSITY
Piscataway, NJ 2003 – present
Graduate Researcher
Teaching Assistant

MAYO CLINIC
Rochester, MN 2006
Research Intern

PUBLICATIONS

Nicole Iverson, Nicole Plourde, Sarah Sparks, Gary Nackman, Kathryn E Uhrich and Prabhas V Moghe, Anti-Atherogenic Polymers for Coordinated Rescue of Cholesterol Dynamics in Activated Macrophages. *PNAS In Preparation*.

Nicole Iverson, Sarah Sparks, Kathryn E Uhrich and Prabhas V Moghe, Controllable Inhibition of Cellular Uptake of Oxidized Low Density Lipoprotein: Structure-Property Relationships for Nanoscale Amphiphilic Macromolecules. *Acta Biomaterialia Accepted*.

Nicole Iverson, Nicole Plourde, Evangelia Chnari, Gary Nackman, and Prabhas V Moghe, Convergence of Nanotechnology and Cardiovascular Medicine: Progress and Emerging Prospects. *BioDrugs* 22(1) 2008 1-10.

Jinzhong Wang, Nicole Plourde, **Nicole Iverson**, Prabhas Moghe, and Kathryn Uhrich, Design of nanoscale macromolecules for differential display of anionic groups toward inhibition of cellular uptake of oxidized low density lipoproteins. *Int. J. Nanomed* 2 (4) 2007 697-705.

Jianyi Zhang, Guangrong Gong, Yun Ye, Tao Guo, Abdul Mansoor, Qingsong Hu, Koichi Ochiai, Jingbo Liu, Xiaohong Wang, Yarong Cheng, **Nicole Iverson**, Joseph Lee, Arthur HL From, Kamil Ugurbil, and Robert J Bache. Nitric Oxide Regulation of Myocardial O₂ Consumption and HEP Metabolism. American Journal of Physiology, Heart and Circulatory Physiology 288: H310-H316 2005.